PARAMETRIC DESIGN ANALYSIS OF HYBRID RHEX ROBOT

HİBRİT RHEX ROBOTUN PARAMETRİK TASARIM ANALİZİ

Mustafa Yiğithan BAŞER

ASSIST. PROF. DR. ING. Emir KUTLUAY

Supervisor

Submitted to

Graduate School of Science and Engineering of Hacettepe University

as a Partial Fulfillment to the Requirements

for the Award of the Degree of Master of Science

in Mechanical Engineering

Juanuary 2024

ismini aldığım ve gururla taşıdığım dedem ***Mustafa BAŞER'e***

canım kardeşim ***Hatice Leyra'ya***

itafen

ABSTRACT

PARAMETRIC DESIGN ANALYSIS OF HYBRID RHEX ROBOT

Mustafa Yiğithan BAŞER

Master of Science, Departmant of Mechanical Engineering

Supervisor: Assist. Prof. Dr. Ing. Emir KUTLUAY

January 2024, 110 pages

In recent years, the use of unmanned autonomous wheeled, tracked or insect-legged unmanned ground vehicles has become increasingly widespread, and studies on the development of these ground vehicles are increasingly carried out by scientists and engineers. The works are generally small-sized designs and are carried out on concepts such as wheels, crawlers or insect legs. However, the small size of the designs and especially the leg shapes designed accordingly have problems in overcoming various types of obstacles, especially high surfaces. As a matter of fact, the fact that each different driving surface has different positive and negative aspects can be shown as the reason for this. For example; While robots with wheeled driving surfaces move faster on a flat road, robots with insect-legged driving surfaces can be more effective in climbing and energy saving. In recent years, robots that can both walk and make short flights have been designed in order to reduce these negative aspects of driving surfaces. In this way, robots that are more effective in overcoming obstacles or moving forward are being tried to be created. In this thesis, mathematical modeling will be presented for the insect-legged RHex robot, which can both walk and make short flights, in order to eliminate the limitations that may arise from driving surfaces. Afterwards, walking and short flight models will be transitioned between each other. The resulting general model (walking

and short flight) will be tested with specified task simulations and the simulation results of the RHex robot in this field will be revealed. Task simulations were determined as first crossing a puddle and then overcoming a steep obstacle of a certain size. In this way, the behavior of the hybrid RHex robot will be seen mathematically with the information obtained as a result of the tests.

Keywords: Unmanned ground vehicle, short flight, simulation, RHEX robot

ÖZET

HİBRİT RHEX ROBOTUN PARAMETRİK TASARIM ANALİZİ

Mustafa Yiğithan BAŞER

Yüksek Lisans, Makina Mühendisliği Bölümü

Tez Danışmanı: Dr. Ing. Emir KUTLUAY

Ocak 2024, 110 sayfa

Son yıllarda insansız otonom tekerlekli, paletli veya böcek bacaklı insansız kara araçlarının kullanımı giderek yaygınlaşmakta olup bahse konu kara araçlarının geliştirilmesine yönelik çalışmalar bilim insanları ve mühendisler tarafından artarak sürdürülmektedir. Çalışmalar genellikle küçük boyutta tasarımlar olup tekerlek, paletli veya böcek bacağı gibi konseptler üzerinden yürütülmektedir. Ancak tasarımların boyutlarının küçüklüğü ve özellikle buna bağlı olarak tasarlanan bacak şekilleri başta yüksek yüzeyler olmak üzere değişik türden engelleri aşmada problemler yaşamaktadır. Nitekim her bir farklı sürüş yüzeyinin birbirinden farklı pozitif ve negatif yönlerinin bulunması bunun nedenleri olarak gösterilebilir. Örneğin; tekerlekli sürüş yüzeyine sahip robotlar düz bir yolda daha hızlı ilerler iken böcek bacaklı sürüş yüzeyine sahip robotlar ise tırmanma ve enerji tasarrufu kısmında daha etkili olabilmektedir. Son yıllarda sürüş yüzeylerinin bu negatif yönlerini azaltmak amacıyla hem yürüyebilen hem de kısa uçuş yapabilen robotlar tasarlanmaktadır. Böylelikle engelleri aşmada veya düz ilerlemede daha etkili robotlar ortaya çıkartılmaya çalışılmaktadır. Bu tezde, sürüş yüzeylerinden kaynaklanabilecek kısıtlamaları ortadan kaldırmak amacıyla hem yürüyebilen hem de kısa uçuş yapabilen böcek bacaklı RHex robot için matematiksel modellemeler ortaya konacaktır. Daha sonrasında ise yürüme ve kısa uçuş modellemelerinin birbiri arasında

geçişi sağlanacaktır. Elde edilen genel modelin (yürüme ve kısa uçuş) belirlenen görev simülasyonları ile test edilerek RHex robotun bu alanda simülasyon sonuçları ortaya konacaktır. Görev simülasyonları ilk olarak su birikintisi geçme ve daha sonra belli boyuttaki dik bir engeli aşma olarak belirlenmiştir. Bu sayede testlerin sonucunda elde edilecek bilgiler ile matematiksel olarak hibrit RHex robotun davranışı görülecektir.

Anahtar Kelimeler: İnsansız kara aracı, kısa uçuş, simülasyon, RHEX robot

ACKNOWLEDGEMENTS

I would like to express my deep appreciation and sincere gratitude to my esteemed supervisor Dr. Ing. Emir Kutluay for his continuous support, encouragement, and great leadings. He has been a light to my path and guidancein the dark.

I would like to thank the committee members, Dr. Ing.Okan Görtan, Dr. Mehmet Nurullah Balcı, Dr. Hakan Doğan and Dr. Ali Emin, for their valuable feedbackand contributions to the thesis.

I would also like to thank my dear friend Ahmet Can Özgren, who supported me in writing the thesis, and my dear friend Volkan Aydıngül, who supported me in starting my master's degree. Also, many thanks to Esra Çakırtaş, who stood by me with her endless support.

I would also like to special thanks Mr. Volkan Kargın, who gave me the engineering perspective and thought and was the main enabler of my ability to write this thesis.

Finally but most importantly, this study could not have existed without my great family members, my father Murat Başer, my mother Rabia Başer, and my dear sister Hatice Leyra Başer, for their unwavering help and support throughout my life and my master's degree.

CONTENTS

FIGURES

TABLES

ABBREVIATIONS

EOM : Equation Of Motion

COM : Center Of Mass

DOF : Degree Of Freedom

$\boldsymbol{L}$: Length of the body (from rear leg joint to front leg joint)

$\boldsymbol{L_f}$: Distance between front leg joint and body center of mass

$\boldsymbol{L_m}$: Distance between middle leg joint and body center of mass

$\boldsymbol{L_r}$: Distance between rear leg joint and body center of mass

$\boldsymbol{R_f}$: Distance between front leg joint and front leg center of mass

$\boldsymbol{R_m}$: Distance between rear leg joint and middle leg center of mass

$\boldsymbol{R_r}$: Distance between rear leg joint and rear leg center of mass

$\boldsymbol{m_b}$: Mass of the Body

$\boldsymbol{m_l = m_r = m_m = m_f}$: Mass of a rear, middle and front leg

$\boldsymbol{I_{b,z}}$: Body inertia around centroidal z-axis

$\boldsymbol{I_{b,y}}$: Body inertia around centroidal y-axis

$\boldsymbol{I_{l,y}}$: Leg inertia around centroidal z-axis

$\boldsymbol{\theta}$: Angle(Pitch Angle) between fixed ground frame x-axis and body longitudinal axis.

$\boldsymbol{\varphi}$: Angle(Heading Angle) between fixed ground frame and body longitudinal axis.

$\boldsymbol{\theta_f}$: Front leg angle according to body center line

$\boldsymbol{\theta_m}$: Middle leg angle according to body center line

$\boldsymbol{\theta_r}$: Rear leg angle according to body center line

$\boldsymbol{r_b}$: Body center of mass position vector

$\boldsymbol{r_f}$: Front leg center of mass position vector

$\boldsymbol{r_m}$: Middle leg center of mass position vector

$\boldsymbol{r_r}$: Rear leg center of mass position vector

$\boldsymbol{v_b}$: Body center of mass velocity vector

$\boldsymbol{v_f}$: Front leg center of mass velocity vector

$\boldsymbol{v_m}$: Middle leg center of mass velocity vector

$\boldsymbol{v_r}$: Rear leg center of mass velocity vector

$\boldsymbol{a_b}$: Body center of mass acceleration vector

$\boldsymbol{a_f}$: Front leg center of mass acceleration vector

$\boldsymbol{a_m}$: Middle leg center of mass acceleration vector

$\boldsymbol{a_r}$: Rear leg center of mass acceleration vector

$\boldsymbol{T}$: Total thrust created by thruster acting to body

$\boldsymbol{\tau}$: Total torque created by thruster acting to body

$\boldsymbol{T_f}$: Torque of front leg

$\boldsymbol{T_m}$: Torque of middle leg

$\boldsymbol{T_r}$: Torque of rear leg

$\boldsymbol{F_D}$: Drag Force

1. INTRODUCTION

In this thesis, the hybrid model and parametric design of a legged rhex robot capable of short flights are discussed. Rhex robot studies with short flight capabilities have been previously studied in the literature. Gültekin's thesis delves into the flight dynamics of a hybrid robot with four legs, analyzing its short-flight capabilities utilizing a imaginary thrust system located at its center of mass[1]. The study demonstrates that the robot can execute short flights with controllable legs in air. However, the determination of the hybrid model and the propulsion system to be used is discussed in this thesis as a new issue.

Nowadays, many studies are being carried out on legged robots. In many ways, legged robots are efficient to use. Their ability to move, especially in difficult ground conditions, and their high energy efficiency have made legged robots stand out among land robots. For these reasons, many studies have been and are being carried out on legged robots. However, despite the essential features of legged robots, they need help in crossing difficult obstacles and deep water. Different concepts have been put forward for legged robots to overcome such obstacles. The most important of these is to integrate short flight capability into the legged robot and create a hybrid legged robot that moves both in the air and on land. In this thesis, modeling and testing of this idea for the Rhex robot will be carried out.

Legged robots have many advantages in ground dynamics. These advantages are that it has the ability to move on difficult ground and at the same time it can reach significant speeds with high efficiency. However, although the legged rhex robot has high mobility, it has difficulty in crossing steep obstacles or deep water. Different approaches are put forward to help the Rhex robot overcome or pass these obstacles. The most important of these is to give the rhex robot short flight capability. In order to provide short flight capability, a propulsion system that will lift the rhex robot into the air must be integrated into the robot. In this thesis, it will be tried to find the most suitable propulsion system for the rhex robot with short flight capability. Simulations will be made with the flight model created to select the appropriate propulsion system. After selecting the appropriate propulsion system, a hybrid model will be created by combining the land model and flight

model. Simulation results of the determined tasks will be obtained with the hybrid model and appropriate propulsion system.

1.1. Scope of the Thesis

The central theme of this dissertation pertains to the exploration of parametric design analysis for the hybrid RHex robot.This thesis focuses on parametric design evaluation for the rhex robot. To fulfill this focus, both ground and flight dynamics will first be modeled mathematically. Afterward, simulations will be made on the flight model to select the appropriate propulsion system. Once the optimal propulsion system has been identified, the next phase of the research will involve conducting mission simulations using the hybrid model, which will be created by integrating the ground and flight models.

1.2. Organization

The organization of the thesis is as follows:

- Chapter 1 introduce the this thesis and focus of the subject.
- Chapter 2 literature survey of the topic and find the missing of the hybrid legged robots.
- Chapter 3 modelling ground model and flight model, also select the recomenned setup for propulsion system. Lastly creating hybrid model with using ground model and flight model.
- Chapter 4 making two mission simulation with selected setup using hybrid model. Additionaly analyzing the results of the mission simulations.
- Chapter 5 to state the results of the thesis and to indicate future works that are thought to be appropriate to do.

2. LITERATURE SURVEY

2.1. Introduction

In this section, a literature study is conducted for this thesis. Along with this literature study, the sources of inspiration for this thesis are shared. By showing the studies carried out, it better reveals the purpose of the thesis. In Section 2.2, studies on the Rhex robot will be discussed, leading to a better understanding of the Rhex robot. In Section 2.3, the advantages of hybrid movement will be highlighted by examining robot studies with hybrid use. The last section will explain the propulsion system and investigations required for the hybrid system.

2.2. Rhex Robot

Nowadays, studies on legged robots are frequently carried out. Energy efficiency increases with legged robots and offers the opportunity to move in terrains where the mobility of wheeled robots is limited. Due to these features, studies on legged robots are increasing. Rhex robot, classified as a legged robot, offers high efficiency and mobility. Studies are being carried out on different subjects and topics for Rhex robots. Saranli et al. showed that the Rhex robot passed obstacles higher than its body span and locomoted at a speed equal to the length of the Rhex robot in one second [2]. This study also indicates that the robot makes locates robust and quick. The Rhex robot in this study has six c-shaped legs, and each leg is rotated independently of each other with an actuator.

Figure 2.1. First Exprimentel Rhex Robot [2]

The RHex robot dynamic configuration created using the SLIP(Spring Loaded Inverted Pendulum) model provides both forward and backward movement capabilities and specific behaviors such as jumping and climbing stairs. The hexapod design that provides this structure is given in figure 2.2. It is stated in this article that in future studies, efforts should be made to develop a rhex robot with an air phase modeled with 6 degrees of freedom.

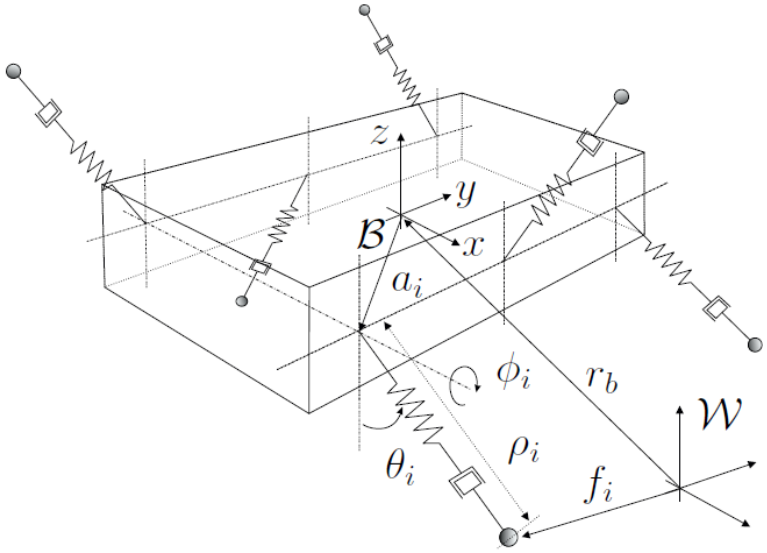

Figure 2.2. The compliant hexapod design[2]

D. Campbell and M. Buehler studied the bounding performance of the RHex robot[3]. This paper showed that bounding is more efficient. The same design for the RHex robot was used in this work. Dynamic modeling has been made for jumping with a c-shaped 6-legged design. This study revealed different options other than straight walking. Thus, both increased performance and extra mobility on rough terrains are demonstrated. With this article, different approaches are considered with the RHex robot. It has also been observed that efficiency and mobility on rough terrains increase with different approaches. The bounding movement obtained in this study is shown in figure 2.3.

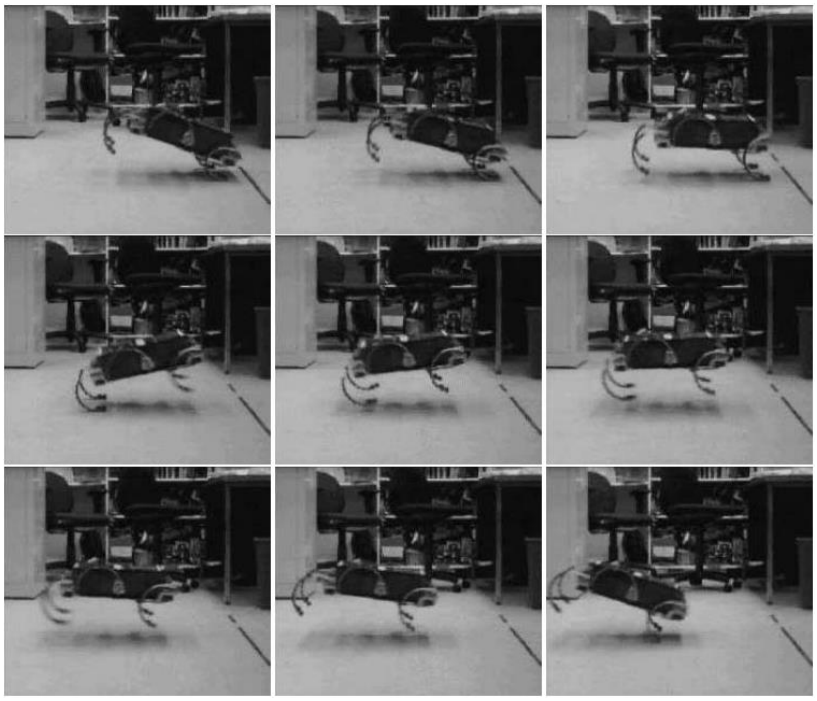

Figure 2.3. Bounding motion of RHex [3]

E. Z. Moore et al. worked on stair climbing of a simple RHex robot[4]. The study examined and researched the stair climbing ability of the rhex robot. Research shows that the Rhex robot successfully climbs normal-sized stairs. However, his leg length allows RHex to climb all kinds of stairs. Additionally, it consumes a lot of energy while climbing stairs. Due to physical limitations and energy problems, adding a short flight phase for climbing the stairs would be better. The stair climbing image of the RHex robot is shown in Figure 2.4.

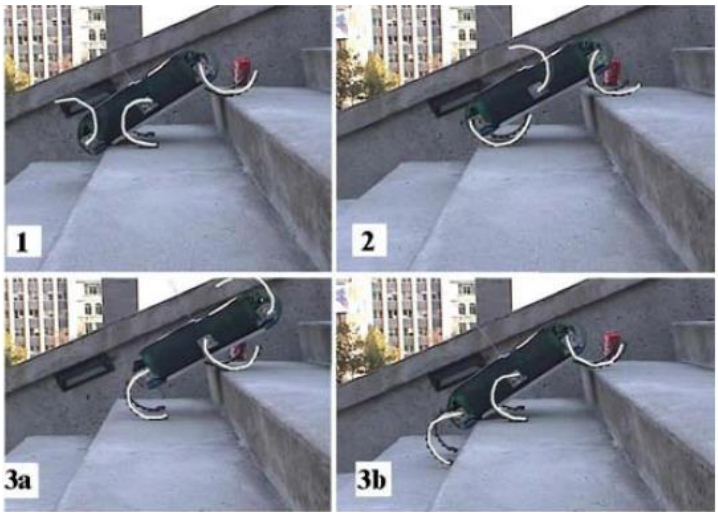

Figure 2.4. Stair climbing of Simple RHex [4]

In the study published by Altendorfer et al., a running RHex robot was shown[5]. In this study, this running action was inspired by the running of a cockroach. Thus, a c-legged robot that can reach high speeds was designed. "SLIP" model is used for Rhex dynamics in the article. Graphs containing the SLIP model and experimental results are shown in figure 2.5. With this thesis, a robot compatible with nature, stable, energy efficient, and capable of moving under challenging terrains has emerged. Because of these capabilities, RHex will be a robot that will help us explore the Earth and other planets..

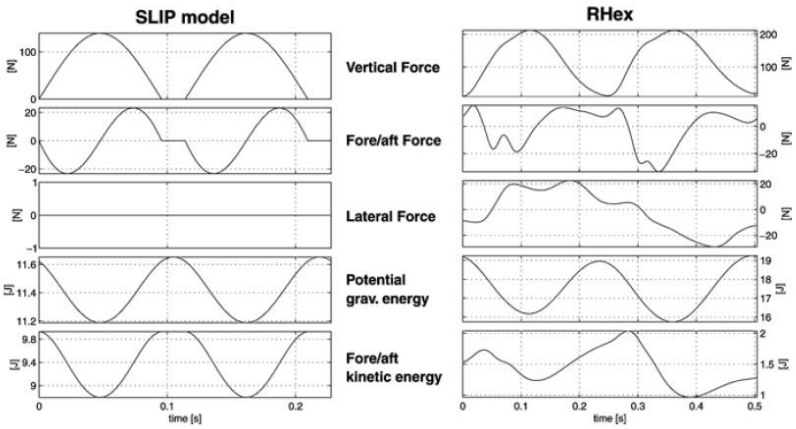

Figure 2.5. Comparison of RHex and SLIP model [5]

C. Georgiades et al. developed a robot called AQUA that can move in water using the Rhex infrastructure[6]. With this study, a robot capable of moving in another environment with the features and infrastructure of the RHex robot was developed. A robot has been built that can quickly enter rocks that humans cannot enter and collect data to conduct surveys in the water. The image of the robot moving underwater with Rhex infrastructure is given in Figure 2.6. This study gained inspiration and courage for a rhex robot that will move in the short flight phase.

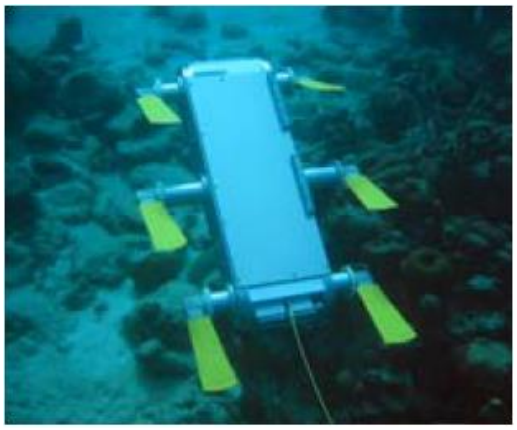

Figure 2.6. AQUA robot in water [6]

2.3. Walking Robots With Flying Capabilities

Currently, engineers and scientists are working on hybrid systems. Robots are one of the areas where hybrid system mechanisms are intensively used. In particular, studies are being carried out on robots that can move both on the ground and in the air. With these studies, many tasks are completed by robots with hybrid movement features. Thanks to hybrid systems, these tasks are performed efficiently. In 2016, researchers named Christopher J. Pratt and Kam K. Leang developed a system called DUCK, which can both walk and fly by adding passive legs to a quadrocopter[7]. The photo showing the walking and flying ability of the DUCK robot is given in figure 2.7.

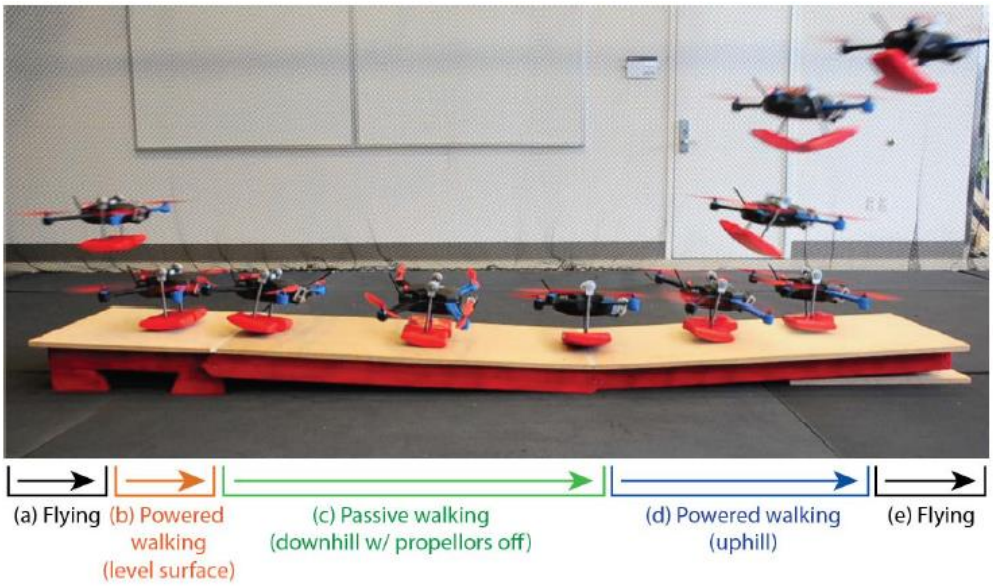

Figure 2.7. Sequence shot for the DUCK[7]

Significant energy savings have been achieved with passive walking movement. It also performed tasks with high mobility on complex surfaces and obstacles. With this approach, the importance of hybrid systems in terms of energy has been seen.

Kevin Peterson and Ronald S. Fearing worked on a tiny hybrid robot called BOLT[8]. As a result of these studies, he developed a hybrid robot that has the ability to move both on land and in the air, even at petite sizes. It also succeeded in overcoming obstacles that were proportionately higher than its size. The BOLT robot is shown in figure 2.8.

Figure 2.8. BOLT Robot [8]

Koji Kawasaki et al. studied a hybrid robot they named MUWA[9]. This robot has a wheel-like structure with four propellers and plastic covering them on the y-axis. The picture of MUWA is shown in figure 2.9. In this study, it has been shown that the robot can move on land as a wheel by using the torque forces of the propellers. Due to this movement capability, it has successfully performed tasks in highly challenging environments and obstacles. Although the MUWA robot is approximately 1 meter in size, it has successfully applied its hybrid operating logic.

Figure 2.9. MUWA robot in different environment [9]

Christopher J. Dudley et al. developed a hybrid robot by adding an exoskeleton to a quadcopter [10]. High maneuverability was achieved by covering the entire quadcopter with a thin, lightweight exoskeleton. The image of this robot, named ATR, is given in figure 2.10. Thanks to the exoskeleton, this robot has the ability to roll on the ground. Thus, this study shows that hybrid systems show high energy savings. In particular, the rolling motion can travel approximately 2 km. This shows that it travels a very long distance compared to its size. In addition, ATR can overcome obstacles thanks to its flying ability.

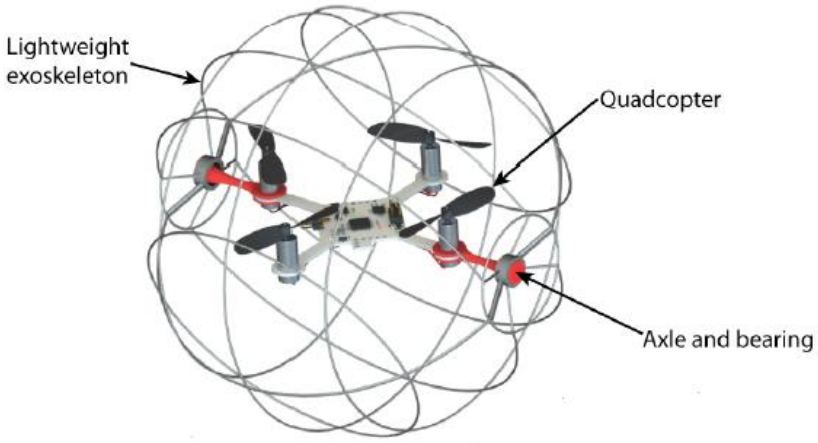

Figure 2.10. ATR robot sketch [10]

Oğuzhan Gültekin wrote a thesis on short-term flight modeling and control for legged robots in 2022 [1]. This thesis demonstrated flight capability with the propulsion system added to a RHex robot using the RHex robot infrastructure. It has also been shown that pitch angle control can be achieved by using legs in the air. Thus, the foundations of a RHex robot capable of short flights in the air were laid. In the thesis, it has been observed that the 4-legged Rhex robot takes off in a simulation environment when sufficient thrust is provided. This was pioneering work for an RHex robot with short-flight capability. Figure 2.11 shows the free-body diagram created for the 4-legged RHex. The effects of the propulsion system, which will be used as an unstudied area in the thesis, on the robot have not been observed. It did not answer questions such as what this propulsion system should be or how it should be positioned..

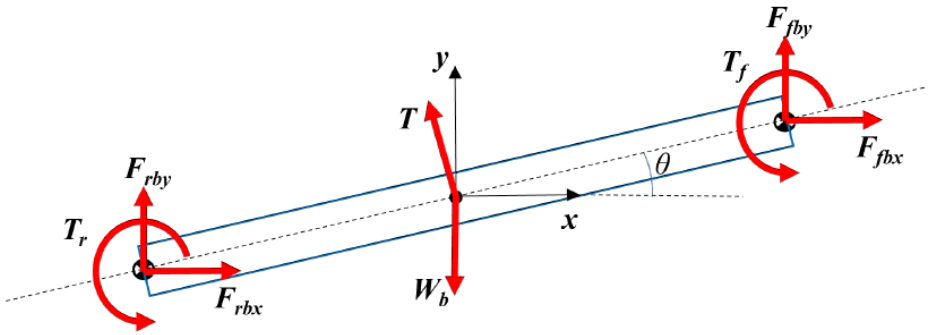

Figure 2.11. Free body diagram of 4 legged RHex [1]

Thanks to Gültekin's thesis, which offers many new propositions about the flight phase and control during the flight phase, the first foundations of the RHex robot with a short flight phase were laid. In short, the thrust vector that will be formed with a thrust system at the robot's center of gravity is put into the mathematical model, and pitch angle control is provided with the torque and forces resulting from the rotation of the legs. Based on a mathematical model, simulations have demonstrated that the RHex robot with four legs is capable of entering and controlling the flight phase. Therefore, this thesis aims to develop a hybrid model for the RHex robot inspired by Gültekin's work and to subsequently test this model..

2.4. Ducted Fans

Nowadays, there are many studies and research on propulsion systems. Many investments are being made, especially in electric propulsion systems, to reduce fossil fuel use and be more environmentally friendly. Unfortunately, especially for large vehicles, electric propulsion systems cannot yet produce as much thrust as fossil fuel-powered ones. However, small-sized electrical systems produce the required thrust and are more efficient in energy consumption. For this reason, electric ducted fans have begun to be used in systems such as UAVs and drones..

Drew Darrah and his colleagues worked on the design and testing of electric ducted fans for UAVs [11]. This study showed that electric ducted fans take up much less space than the open propeller system and perform similarly. This is one of the reasons why electric ducted fans are used in small vehicles. Andy Ko et al. have developed a vehicle with VTOL capability, including a ducted fan, for situations where fixed-wing UAVs are

insufficient and inefficient [12]. The immense morale of these developments is that ducted fans are much more efficient regarding both sound and safety. Although electric ducted fans are not used, it is seen that ducted fans are used in new technologies. Yacoubi Moaad and his friends developed a drone called Dulbema that works with an electric ducted fan [13]. The reason for using an electric ducted fan for this drone is that it is resistant to wind gusts due to its closed structure. The greater thrust it provides in vertical mode. Finally, due to its closed structure, the fins are not hit by objects in the environment.

2.5. Conclusion

In the present section, a comprehensive literature review has been conducted to explore the state-of-the-art advancements in robotics, with a particular focus on the RHex robot and hybrid ground- and aerial-based vehicles. First, detailed information about the RHex robot was obtained, and the studies on the RHex robot were examined. Secondly, studies on hybrid robots were analyzed. In particular, ground vehicles with short-flight capabilities were reviewed. Finally, this thesis sheds light on the latest propulsion systems technologies required for developing such vehicles and focuses on ducted fans as a promising solution.

3. MODEL

3.1. Introduction

This section aims to explicate the mathematical models that will be employed for the RHex robot. Primarily, the ground model will be elucidated, encompassing an in-depth explanation of the algorithm utilized, along with the presentation of the simulation performance of the ground model in isolation. Secondly, the flight model will be explained and simulation models taken with different propulsion systems will be shown. In addition, the battery that will be used for the energy required for the flight phase of the RHex robot will be selected. Finally, the entire system selection will be completed and a hybrid model will be created.

3.2. Ground Model

The ground model of the hybrid Rhex robot is based on SLIP dynamics. This thesis basic SLIP model will be used. Especially, only longitudinal dynamics will be calculated in this thesis.

3.2.1. Introduction

In this chapter, the ground model of the hybrid Rhex robot model will be introduced. The Rhex robot ground model based on SLIP (Spring-Loaded Inverted Pendulum) dynamics [14]. Basically, in SLIP, robot leg assume like a spring and this spring compression and decompression moves to robot body in x and y axis. SLIP model is created by using Newton's Method. For this thesis, SLIP model mathematically modelling just for longitudinal (x) axis.

The reader will understand the SLIP model and longitudinal ground dynamics of the hybrid Rhex robot with this chapter.

3.2.2. Kinematics of the Ground Model

3.2.2.1. SLIP Model

The Spring-Loaded Inverted Pendulum (SLIP) model has using for different types of animals running broadly distinct size and length. Also, this model has using to in hopping robot designs. This SLIP model gives a better solution to running or hopping robot dynamic. Because these type of robot dynamics has normally nonintegrable dynamics, but this SLIP model gets a good approximation this problem.

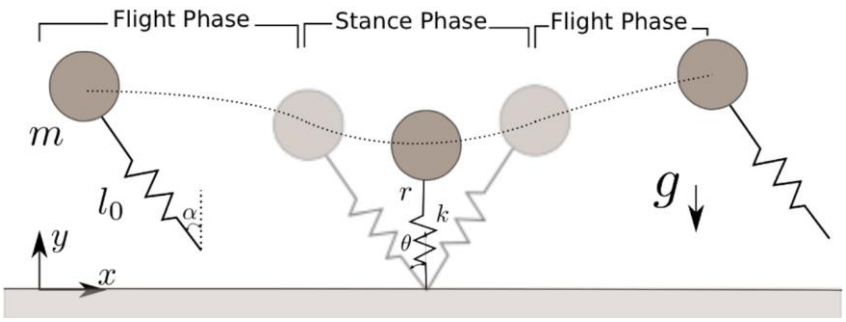

Figure 3.1. SLIP Model Schmatic [15]

In SLIP model, there are 2 main phases. These are listed below.

1) Flight Phase
2) Stance Phase

Flight Phase means the leg or spring does not touch the ground hereby the leg or spring can not create any force to body. Just gravitational force acting to body.

$$\ddot{x}_b = 0 \tag{1}$$

$$\ddot{y}_b = -g \tag{2}$$

When the robot is in Stance Phase, leg, or spring touches the ground and create a force that acts to body.

$$\ddot{x}_b = \frac{F_{x,leg}}{m_b} \tag{3}$$

$$\ddot{y}_b = \frac{F_{y,leg}}{m_b} \tag{4}$$

This Stance Phase occurs an angle "θ" between touchdown and liftoff moment. This angle changes with leg dimension and shape.

Two different phases of the SLIP model explained. These two events repetitive at running time. In this thesis, these events modelling together.

3.2.2.2. Leg Model

Simple leg model is created in this thesis. The actuator on the leg creates a torque and rotate the leg 360 degree.

$$\dot{\omega} = \frac{\tau_a}{I_{leg}} \tag{5}$$

However, when the phase changed, the kinematic of the leg change too. In Flight phase, leg does not touch on the ground, so no torque needed. But moment the leg touches the ground, leg need a torque for rotating. At last time of Stance Phase, the last torque that applied from actuator has enough force to rotating for leg.

3.2.3. Ground Dynamics

The ground dynamics of the hybrid Rhex robot is created by using SLIP model and Leg model together. Phase transitions of the models were added in the ground dynamic using resets. Also, vertical (y) axis not modelling in this section because assuming the vertical movement as "0" all legs are perfectly balanced and working properly. Additionally, this vertical (y) axis modelling in Flight Model that is described another section.

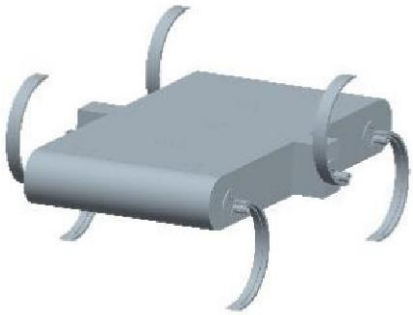

Figure 3.2. Rhex Robot CAD Drawing [16]

The legs are assumed solid and incompressible. In this thesis, the legs just create force to body when its touch the ground.

A resistance to motion is arbitrarly modelled in order to limit the longitudinal velocity of the Rhex robot. This force ise assumed to be of a drag force composed of a polynomial component to determine a resistance to motion coefficient, the same way the concept is

used in vehicle dynamcis [17], and the velocity of the robot. The formulation for the resistance force is gives in Eq. 6.

$$F_R = R(\dot{x}) \tag{6}$$

$$R = sign(\dot{x})0.15\dot{x}^2 + 0.15\dot{x} \tag{7}$$

Thus, equation of motion becomes,

$$F_{x,leg} - F_R = F_{body} \tag{8}$$

In Eq. 8, $F_{x,leg}$ is the total tractive force developed on the contact points.

After found equation of motion, the ground model tested in SIMULINK with the parameters of the hybrid Rhex robot. The parameters for grond model listed below in Table 3.1.

Table 3.1. Ground Model Parameters of Hybrid Rhex Robot

Parameter Name	**Value**	**Unit**
Actuator Torque	0.005	$\frac{kgm^2}{s^2}$
Leg Inertia	6.24845e-5	kgm^2
Body Mass	3.15	kg
Leg Force (in x-dir.)	1.5	N
Sweep Angle	18	deg

Leg mass did not add the total mass because of leg mass is too small compared to body mass. Also, the ground is flat and smooth. Ground model tested with these parameters with 30 seconds simulation.

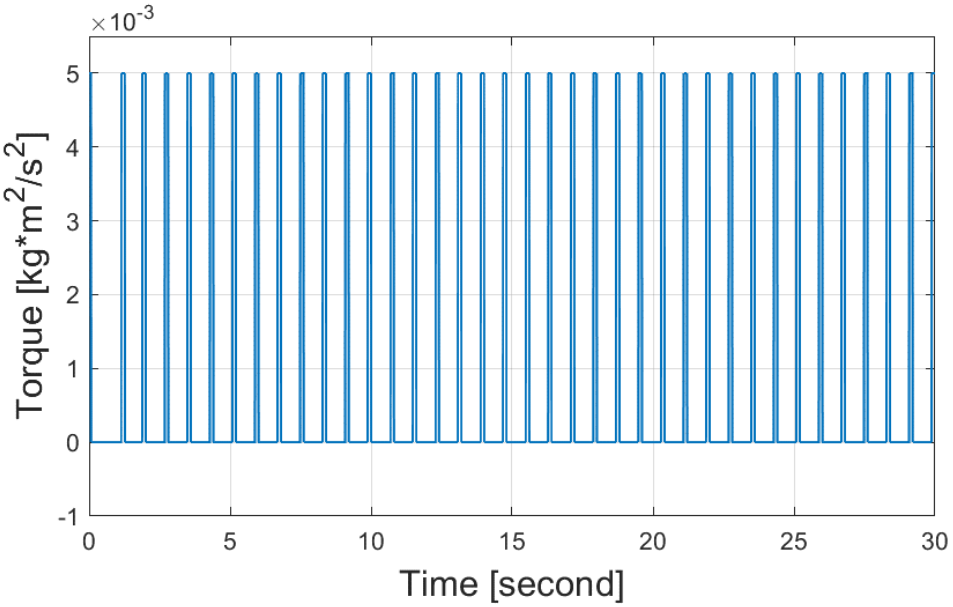

Figure 3.3. Torque Input to Leg

Some moments torque is zero that can be seen in figure 3.3 because of Flight Phase. In Flight Phase, no torque needed to leg for rotating. The Flight Phase calculation is based on sweep angle of leg. If the leg angle is between 9° and 351°, the actuator understand model is in Flight Phase.

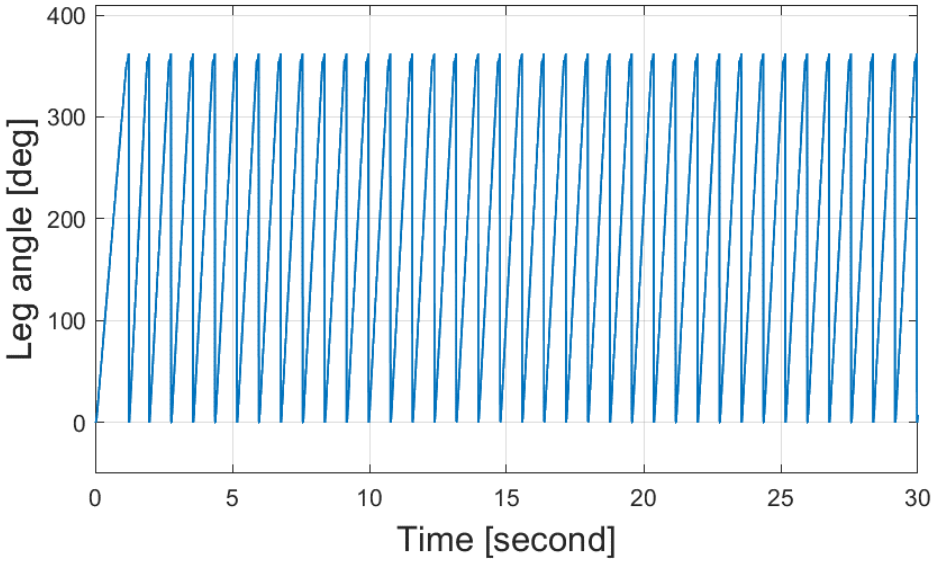

Figure 3.4. Leg Angle During Simulation

Approximately every one second the leg complete one lap. If the torque decreases, completing duration is longer. Chose torque as 0.001 different than Table 3.1. The result of the leg angle,

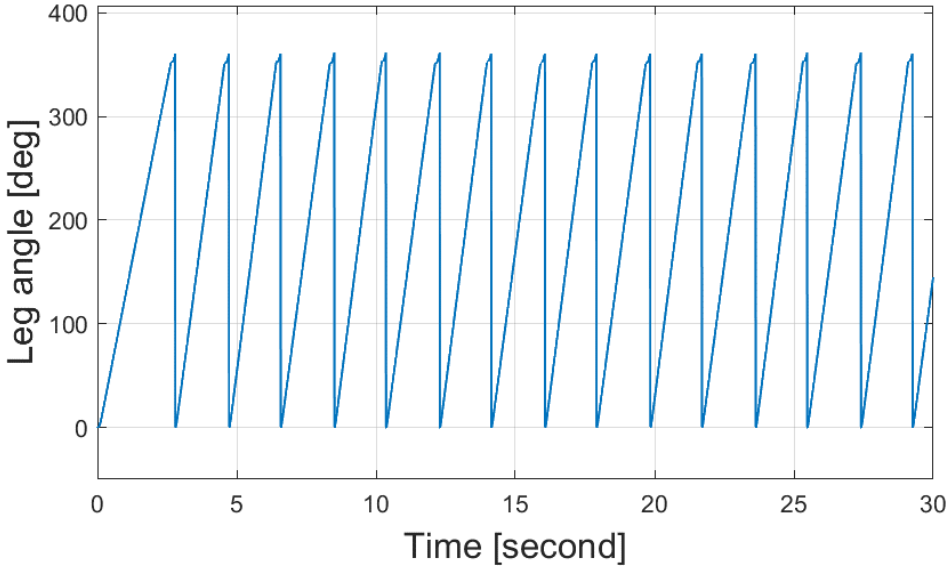

Figure 3.5. Leg Angle with Less Torque

In figure 3.5, completing one lap is about 2 seconds. It shows that ground model is appropriate with physical and mathematical law.

The force coming leg calculation is based on stance phase. If the leg touches the ground, the force occurs seen in figure 3.6. The stance phase is found with sweep angle. When the sweep angle is less than 9° and greater than 351°, the leg creating a force because it touches the ground.

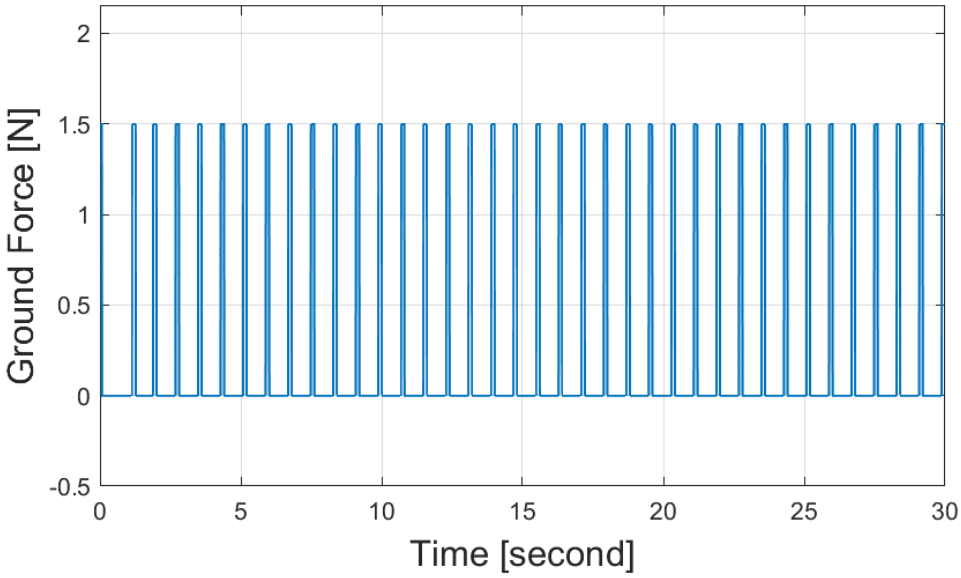

Figure 3.6. Ground Force During Simulation

For the limiting velocity of the body, arbitrary value used and create a reaction force that can be seen in Eq. 8. The reaction force can be seen below figure 3.7.

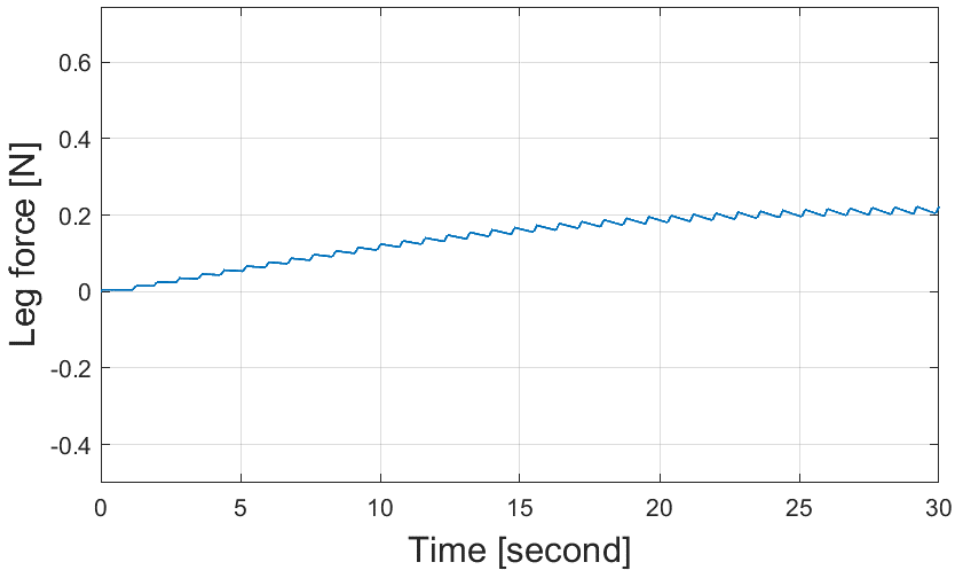

Figure 3.7. Leg Force During Simulation

After getting a force that acts to body, obtained the longitudinal velocity that can be seen in figure 3.8 and displacement that can be seen in figure 3.9 with using Eq. 3.

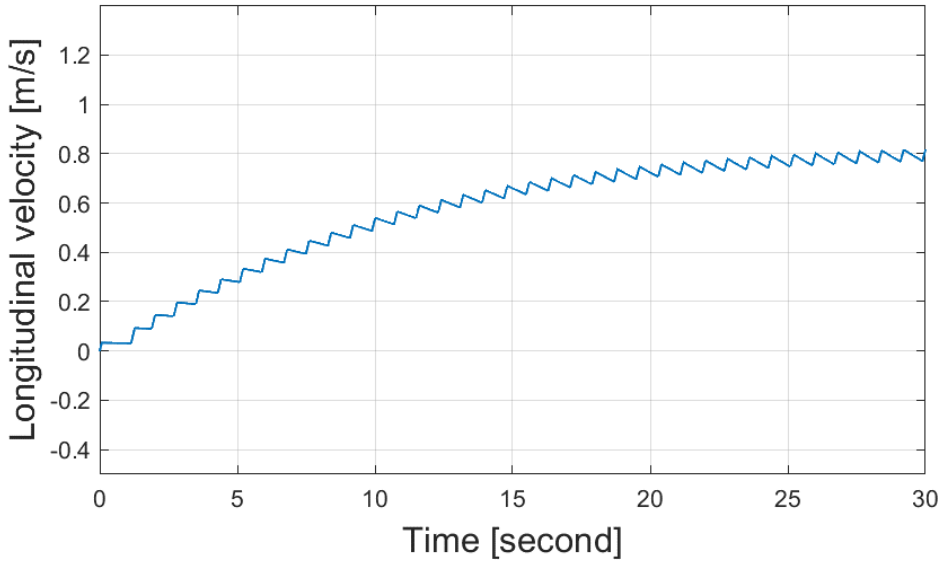

Figure 3.8. Longitudinal Velocity During Simulation

Chose arbitrary value limit the velocity almost 0.8 m/s. Figure 3.8 shows that the reaction force calculation fixes the longitudinal velocity well. And the last result is longitudinal displacement in the figure 3.9, displacement is almost linear after constant velocity.

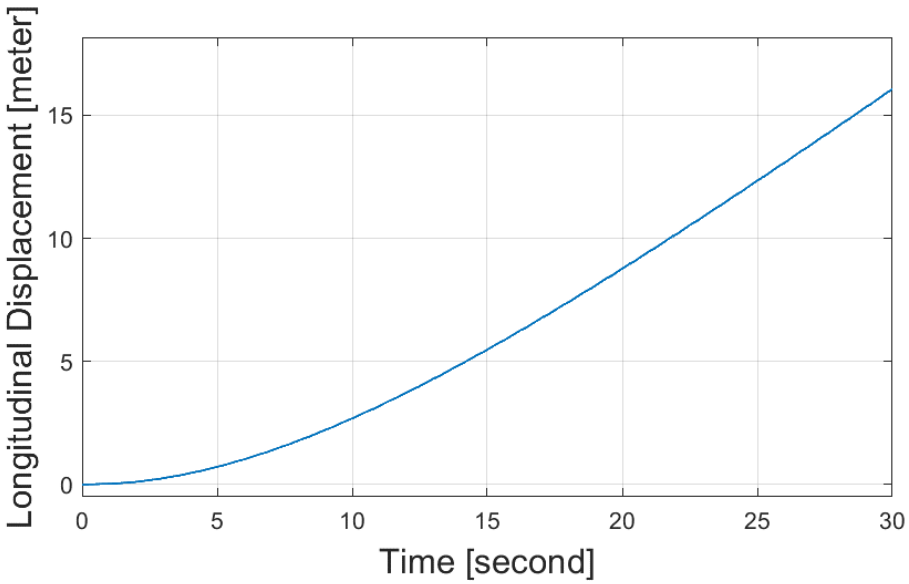

Figure 3.9. Longitudinal Displacement During Simulation

3.3. Flight Model

3.3.1. Introduction

In this chapter, the flight model of the hybrid Rhex robot will be discussed. The hybrid Rhex robot flight model based on UAV and drone dynamics. Briefly, a thruster or propeller provide a thrust in vertical (y) axis. In this thesis, flight model is covered only longitudinal (x) and vertical (y) axis. 2D flight model is developed by using newton's method.

In developing flight model, some approaches are tried to different configuration. Every diverse configuration will be explained detailly after. The reader will understand the flight model developing with Newton's method and different configurations of the hybrid Rhex robot with this chapter.

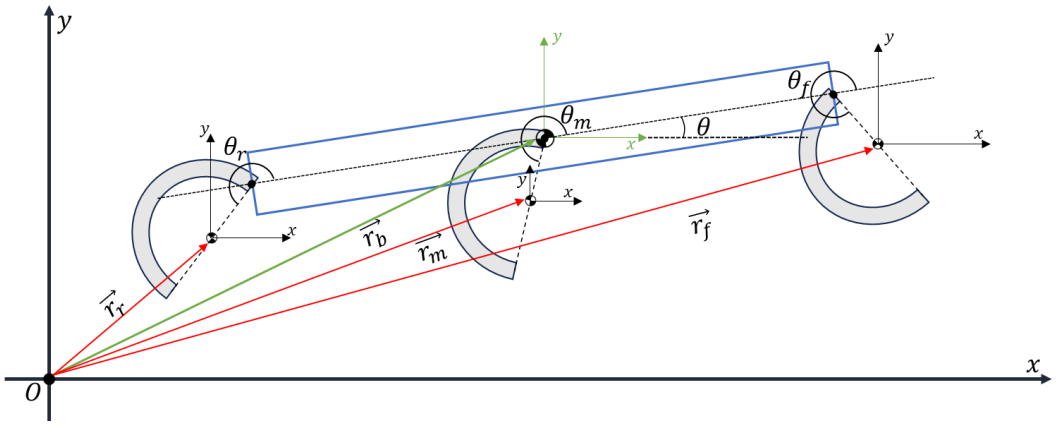

Figure 3.10. 2D hybrid Rhex robot

In figure 3.10, there is one body part and three legs in 2D space. These are main part of the hybrid Rhex robot. Each part has a vector from origin to part's center of mass.

$$\vec{r}_b = xi + yj \tag{9}$$

$$\vec{r_f} = xi + yj + L_f\cos(\theta)i + L_f\sin(\theta)j + R_f\cos(\theta+\theta_f)i + R_f\sin(\theta+\theta_f)j \tag{10}$$

$$\vec{r_m} = xi + yj + R_m\cos(\theta_f)i + R_m\sin(\theta_f)j \tag{11}$$

$$\vec{r_r} = xi + yj + L_r\cos(\theta+\pi)i + L_r\sin(\theta+\pi)j + R_r\cos(\theta+\theta_r)i + R_r\sin(\theta+\theta_r)j \tag{12}$$

Each part's velocity and acceleration are calculated by taking time derivatives of each part's position vector that can be seen in Equation 9, 10, 11 and 12.

$$\vec{v}_b = \frac{d\vec{r}_b}{dt}, \quad \vec{v}_f = \frac{d\vec{r}_f}{dt}, \quad \vec{v}_m = \frac{d\vec{r}_m}{dt}, \quad \vec{v}_r = \frac{d\vec{r}_r}{dt} \tag{13}$$

$$\vec{a}_b = \frac{d\vec{v}_b}{dt}, \quad \vec{a}_f = \frac{d\vec{v}_f}{dt}, \quad \vec{a}_m = \frac{d\vec{v}_m}{dt}, \quad \vec{a}_r = \frac{d\vec{v}_r}{dt} \tag{14}$$

After getting linear position, velocity and acceleration, angular velocities and accelerations were defined for each part.

$$\vec{\omega}_{b/e} = \dot{\theta}\hat{k} \tag{15}$$

$$\vec{w}_{f/e} = \vec{w}_{b/e} + \vec{\omega}_{f/b} = \dot{\theta}\hat{k} + \dot{\theta}_f\hat{k} \tag{16}$$

$$\vec{w}_{m/e} = \vec{w}_{b/e} + \vec{\omega}_{m/b} = \dot{\theta}\hat{k} + \dot{\theta}_m\hat{k} \tag{17}$$

$$\vec{w}_{r/e} = \vec{w}_{b/e} + \vec{\omega}_{r/b} = \dot{\theta}\hat{k} + \dot{\theta}_r\hat{k} \tag{18}$$

$$\vec{a}_{b/e} = \ddot{\theta}\hat{k} \tag{19}$$

$$\vec{a}_{f/e} = \vec{a}_{b/e} + \vec{a}_{f/b} = \ddot{\theta}\hat{k} + \ddot{\theta}_f\hat{k} \tag{20}$$

$$\vec{a}_{m/e} = \vec{a}_{b/e} + \vec{a}_{m/b} = \ddot{\theta}\hat{k} + \ddot{\theta}_m\hat{k} \tag{21}$$

$$\vec{a}_{r/e} = \vec{a}_{b/e} + \vec{a}_{r/b} = \ddot{\theta}\hat{k} + \ddot{\theta}_r\hat{k} \tag{22}$$

The subscript "e" represents origin(earth) frame. Finally, getting both linear and angular equations of each part, equation of motion of the hybrid Rhex robot can be derivate with Newton's Method.

3.3.2. Drag Force Calculation

In this thesis, friction force was added to the flight model. Friction force is also called fluid resistance resulting from the interaction of an object with a fluid. When the Rhex robot is in flight phase, the robot body and the air interact with each other. This force will be calculated only in the y direction. The equation providing the friction force is below.

$$F_{d\text{rag}} = \frac{1}{2}\rho v_{b,y}^2 C_D A \tag{23}$$

Where,

$$\rho: air\ density \tag{24}$$

$$v_{b,y}^2: vertical\ velocity\ of\ the\ robot\ body \tag{25}$$

$$C_d: drag\ coefficient\ of\ the\ object \tag{26}$$

$$A: cross-sectional\ area \tag{27}$$

ρ, $v_{b,y}^2$ and A values are known. However, the C_d value is not directly known. Therefore, the experimentally found C_d value of a rectangular shaped object found in the literature was accepted. As a reference from Munson B.R et al. "Fundamentals of Fluild Mechanics" book [18], the C_d value for the rectangle appears to be "2.17". The above equation 23 will be used to obtain the friction force in the flight model.

3.3.3. Equation of Motion of Flight Model

For obtaining equation of motion, firstly defined external forces. The hybrid Rhex robot has four external forces that one of is due to thruster and the other ones due to legs. Also, gravitational force affects the hybrid Rhex robot. Additionally, each leg creates a torque

to body. Free-Body diagram that is contained the all forces of hybrid Rhex robot can be seen in figure 3.11.

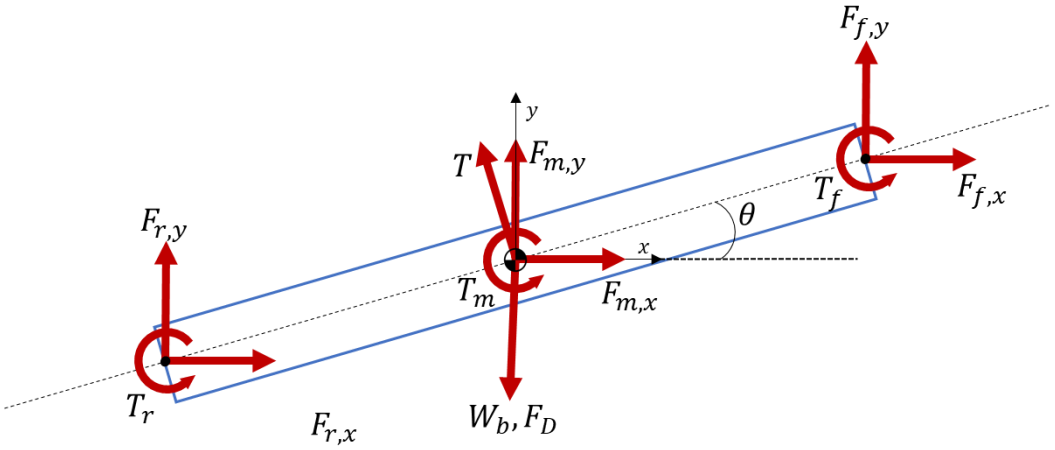

Figure 3.11. Free Body Diagram of Body

Linear and angular acceleration of the body can be obtained in 2D with using Newton's Method.

$$\sum F_x = m_b a_{b,x} \tag{28}$$

$$F_{r,x} + F_{m,x} + F_{f,x} + \sum T \cos\left(\frac{\pi}{2} + \theta\right) = m_b a_{b,x} \tag{29}$$

$$\sum F_y = m_b a_{b,y} \tag{30}$$

$$F_{r,y} + F_{m,y} + F_{f,y} + T \cos\left(\frac{\pi}{2} + \theta\right) - F_{drag} = m_b a_{b,y} \tag{31}$$

$$\sum M_z = I_{b,z} \ddot{\theta}_b \tag{32}$$

$$T_f + T_m + T_r - L_f sin(\theta) F_{f,x} + L_f cos(\theta) F_{f,y} - L_m sin(\theta) F_{m,x} + L_m cos(\theta) F_{m,y} + L_r sin(\theta) F_{r,x} - L_r cos(\theta) F_{r,y} = I_b \alpha_b \tag{33}$$

$$\sum M_y = I_{b,y} \ddot{\varphi}_b \tag{34}$$

$$\tau = I_{b,y} \ddot{\varphi}_b \tag{35}$$

Also, each leg has own equation of motion. The leg is affected by gravitational force and, torque that is creating by actuator. Lastly, force is created by the joint. Each leg has own free body diagram.

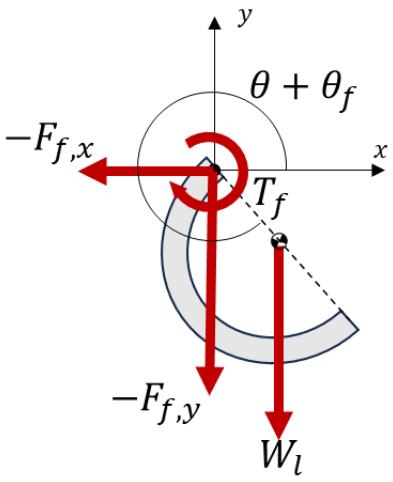

Figure 3.12. Free Body Diagram of Front Leg

Equation of motion of front leg can be obtained figure 3.12.

$$-F_{f,x} = m_l a_{f,x} \tag{36}$$

$$-F_{f,y} - w_l = m_l a_{f,y} \tag{37}$$

$$-T_f + Rsin(2\pi - \theta - \theta_f)F_{f,x} + Rcos(2\pi - \theta - \theta_f)F_{f,y} = I_l \ddot{\theta}_f \tag{38}$$

The same way, the middle and rear leg equation of motion is determined.

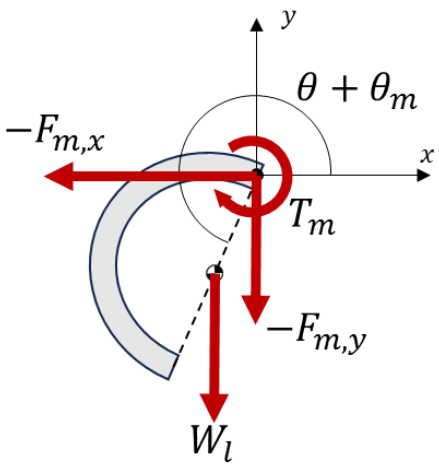

Figure 3.13. Free Body Diagram of the Middle Leg

$$-F_{m,x} = m_l a_{m,x} \tag{39}$$

$$-F_{m,y} - w_l = m_l a_{m,y} \tag{40}$$

$$-T_m + Rsin(\theta_m)F_{m,x} + Rcos(\theta_m)F_{m,y} = I_l \ddot{\theta}_m \tag{41}$$

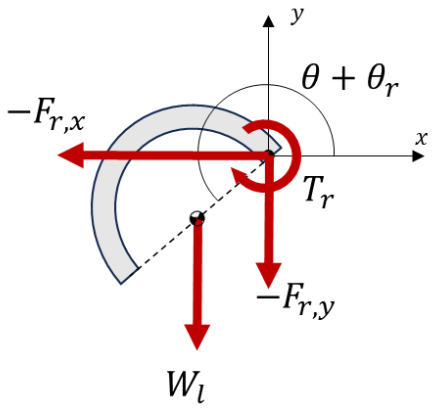

Figure 3.14. Free Body Diagram of the Rear Leg

$$-F_{r,x} = m_l a_{r,x} \tag{42}$$

$$-F_{r,y} - w_l = m_l a_{r,y} \tag{43}$$

$$-T_r - Rsin(\theta + \theta_r)F_{r,x} + Rcos(\theta + \theta_r)F_{r,y} = I_l \ddot{\theta}_r \tag{44}$$

Considered that $a_{f,x}$, $a_{m,x}$ and $a_{r,x}$ are identify as the same notation used for body. The constraint forces can be seen in equations 36, 37, 39, 40, 42 and 43. For elimination these constraint forces substitute into the equations 29, 31, 33, 38, 41 and 44. The equation of motion of the systems are given in the Appendix A.

In this thesis, the known variables are position and velocity parameters. Also input variables are known.

$$Position\ variables = \begin{Bmatrix} x \\ y \\ \theta \\ \varphi \\ \theta_f \\ \theta_m \\ \theta_r \end{Bmatrix} \tag{45}$$

$$Velocity\ variables = \begin{Bmatrix} \dot{x} \\ \dot{y} \\ \dot{\theta} \\ \dot{\varphi} \\ \dot{\theta}_f \\ \dot{\theta}_m \\ \dot{\theta}_r \end{Bmatrix} \tag{46}$$

$$Input\ variables = \begin{Bmatrix} T \\ \tau \\ T_f \\ T_m \\ T_r \end{Bmatrix} \tag{47}$$

Acceleration variables are not known in the 7 EOMs. If it is rearranged these 7 equations as a known and unknown variable. The new readjust equations of motion form shown in below.

$$[M(t)]_{7x7} \times \begin{Bmatrix} \ddot{x} \\ \ddot{y} \\ \ddot{\theta} \\ \ddot{\varphi} \\ \ddot{\theta}_f \\ \ddot{\theta}_m \\ \ddot{\theta}_r \end{Bmatrix} = \{n(t)\}_{7x1} \tag{48}$$

Solution of the equation 48 is leaving alone the acceleration variables the left side of the equation. This is possible by crossing n with the inverse of M.

$$\begin{Bmatrix} \ddot{x} \\ \ddot{y} \\ \ddot{\theta} \\ \ddot{\varphi} \\ \ddot{\theta}_f \\ \ddot{\theta}_m \\ \ddot{\theta}_r \end{Bmatrix} = [M(t)]^{-1}{}_{7x7} \times \{n(t)\}_{7x1} \tag{49}$$

3.3.4. Flight Dynamics

The flight dynamics of the hybrid Rhex robot is contained the EOM that derived Newton's Method in last chapter. The flight dynamics modelled as 2D (x and y axis). The flight model has some options or configurations for creating thrust. The different approaches to flight model are tried in this chapter. And the best option selected for hybrid model.

In the flight modeling, the propulsion system attached to the middle of the robot will be modeled so that it stays in the air during the flight. The propulsion system will essentially provide us with the ability to move in the y-axis (positive up). Movements such as nose up or down will be tried with different approaches and the results will be evaluated. The

yaw angle shift that may occur due to the installed propulsion system will be minimized with different approaches.

Model parameters of the flight model can be seen below table 1.

Table 3.2. Hybrid Rhex Robot Specifications

Parameter Name	**Value**	**Unit**
Body Length	25	cm
Body Width	12	cm
Body Height	7	cm
Body Mass	3.15	kg
Leg Mass	0.05184	kg
Body Inertia in y axis	0.0176925	kgm^2
Body Inertia in z axis	0.020507	kgm^2
Leg Inertia	6.24e-5	kgm^2
Dist. Front Leg Joint to Body CoM	0.125	meter
Dist. Middle Leg Joint to Body CoM	0	meter
Dist. Rear Leg Joint to Body CoM	0.125	meter
Dist. Leg CoM to Leg Joint	0.06	meter

Flight model needed a thruster for take-off. So next chapter there are choosing appropriate thruster for hybrid Rhex Robot. Thruster will choose as parameters given in table 3.2. Different type of thruster and thruster config will simulate next chapters.

3.3.5. Propeller

For the hybrid Rhex robot to make short flights, equipment to provide thrust in the y direction is required. As one of these equipment, the "propeller (rotor)", which is like the helicopter logic, was chosen. The first issue that this propeller selection should provide is that it produces more thrust than the hybrid Rhex robot weight. In addition, the different positioning or configutation of the selected propellers was also discussed.

3.3.5.1. One Propeller

Table 3.2 gives the design parameters of the hybrid rhex robot. According to these parameters, appropriate propeller and engine selections were made in table 3.3.

Table 3.3. One Propeller Option 1 Parameters [19]

Parameters	Value	Unit
Motor Name	Turnigy 2836 Brushless 1000kv	n/a
Propeller Name	HY 1047 Plastic Blade	n/a
Propeller Diameter	25.4	Cm
Thrust	1.643	kgf
Torque	0.2843	Nm
Rotation Speed	10992	rpm

The flight model simulation result of the first configuration can be seen below. In one propeller system there is no creating the pitch angle for hybrid Rhex robot. Because of that, the robot can move only in y directions. In figure 3.15, distance in x axis is always zero during the simulation for option 1. Naturally, both body velocity and body acceleration are always zero, as can be seen in figure 3.16 and figure 3.17.

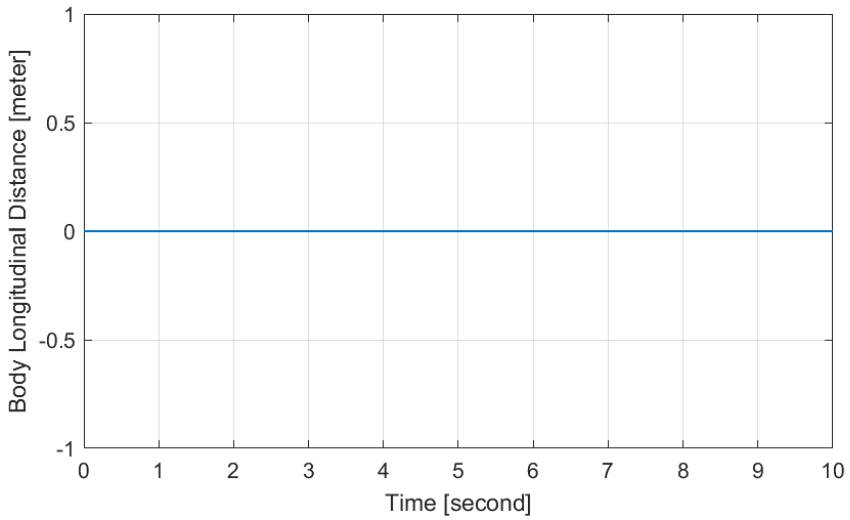

Figure 3.15. Body distance in x-axis for Option-1

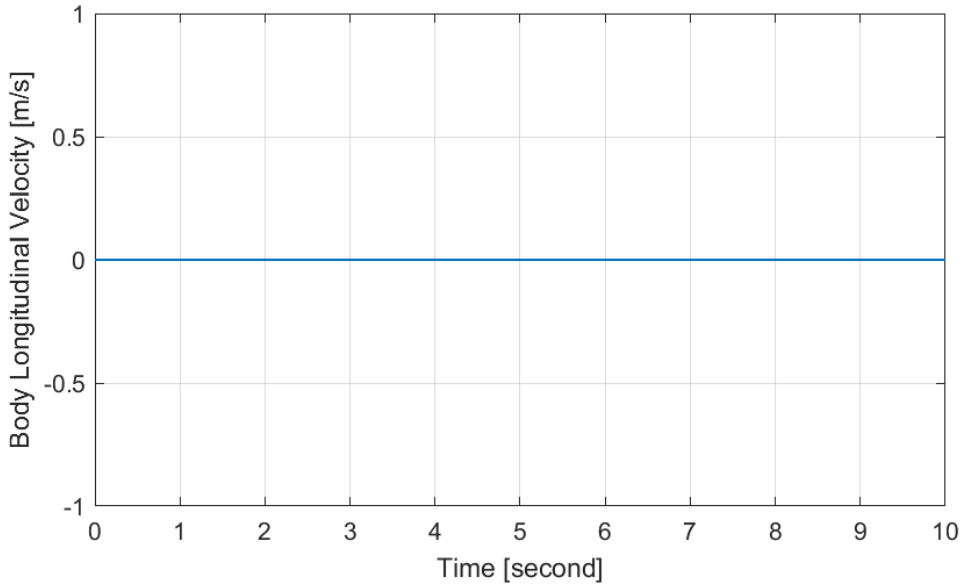

Figure 3.16. Body velocity in x-axis for Option-1

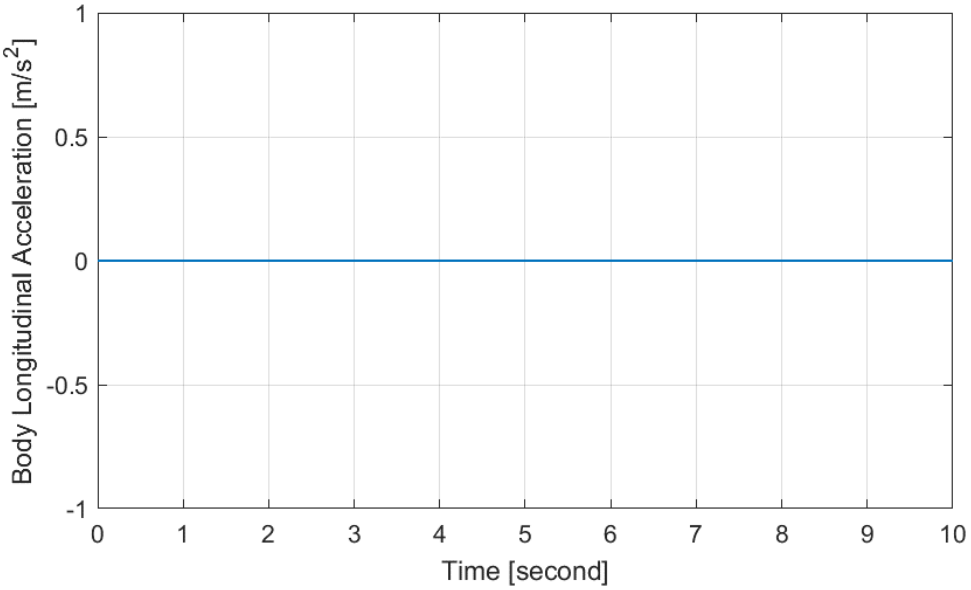

Figure 3.17. Body acceleration in x-axis for Option-1

As can be seen in figure 3.18, the thrust produced by the propeller selected in option 1 on the y-axis is insufficient to lift the robot into the air.

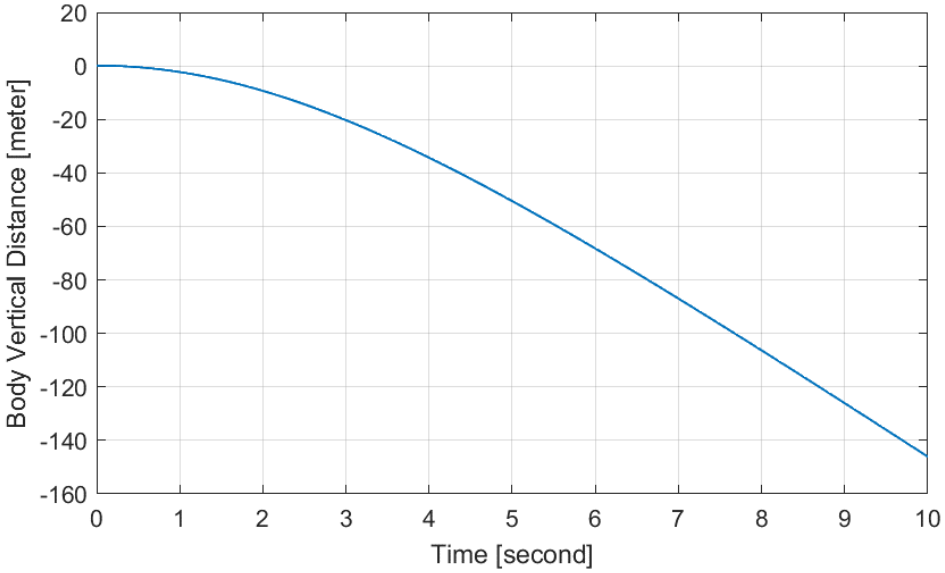

Figure 3.18. Body Distance in y-axis for Option-1

Since the weight of the robot is more than the thrust produced by the propeller and motor selected in option-1, both body velocity and body acceleration are negative. Velocity and acceleration graphs with negative values are seen in figures 3.19 and 3.20.

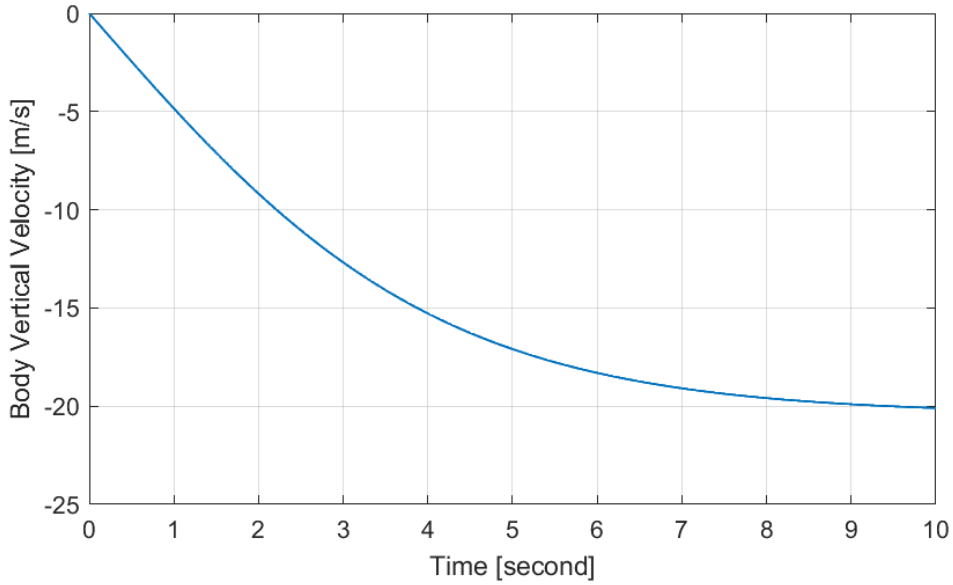

Figure 3.19. Body Velocity in y-axis for Option-1

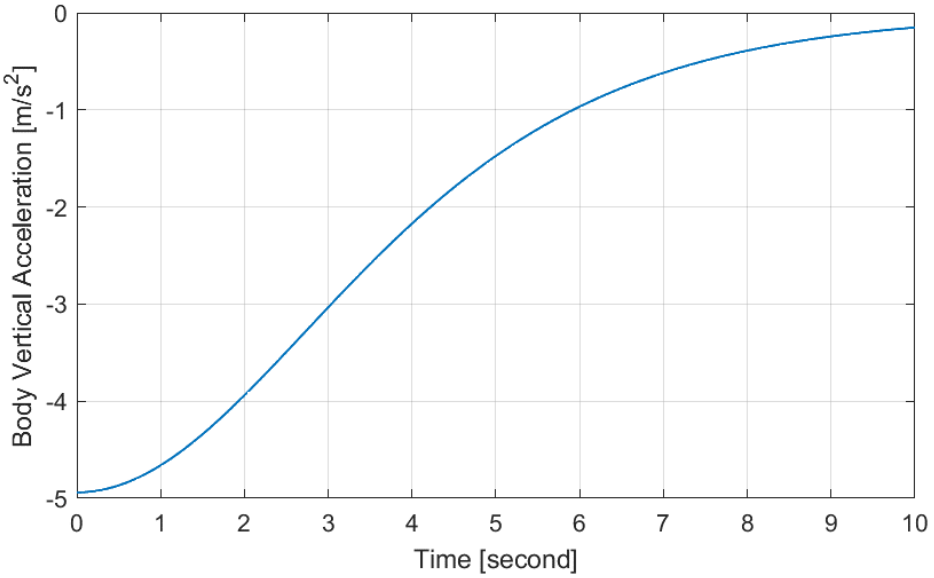

Figure 3.20. Body acceleration in y-axis for Option-1

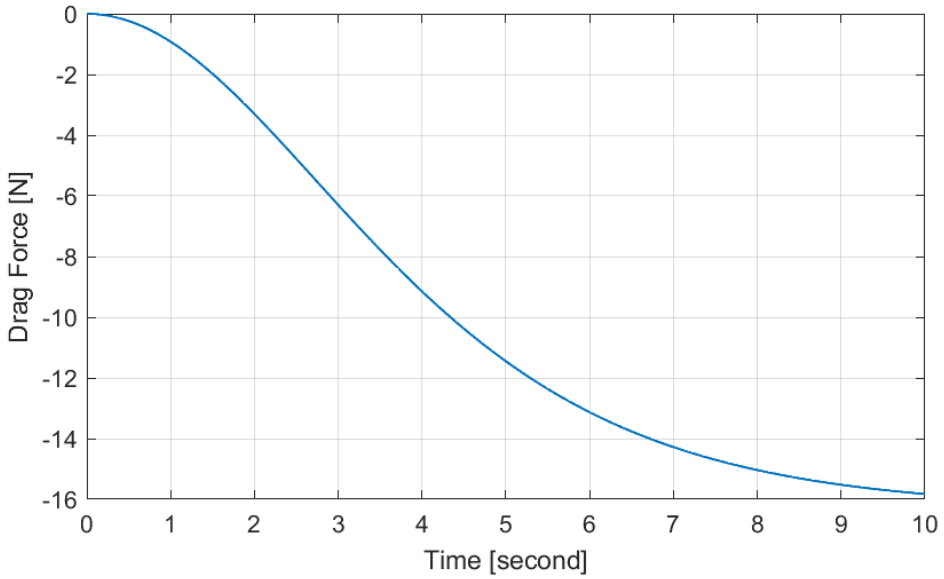

Figure 3.21. Drag Force in y-axis for Option-1

Since a single propeller is used, the yaw angle does not remain constant due to the torque created by the propeller. The yaw angle formed throughout the simulation can be seen in figure 3.22.

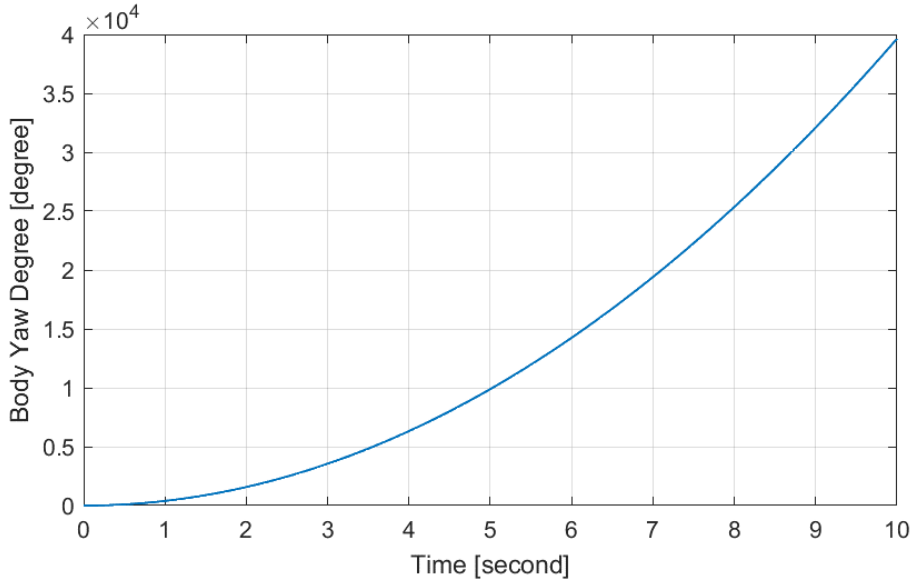

Figure 3.22. Yaw Angle of body for Option-1

In option 1, the robot reached the 45 degrees in yaw angle at almost 0.5 second. Also total rotation of the body during simulation is 110.

The propeller was operated at full performance throughout the simulation. Therefore, the torque value produced by the selected propeller for option-1 affects the robot throughout the simulation. Due to this effect, the acceleration of the yaw angle remained constant, as seen in Figure 3.23. Due to constant acceleration, yaw angle velocity also increases linearly throughout the simulation. This yaw angle velocity is seen in figure 3.24.

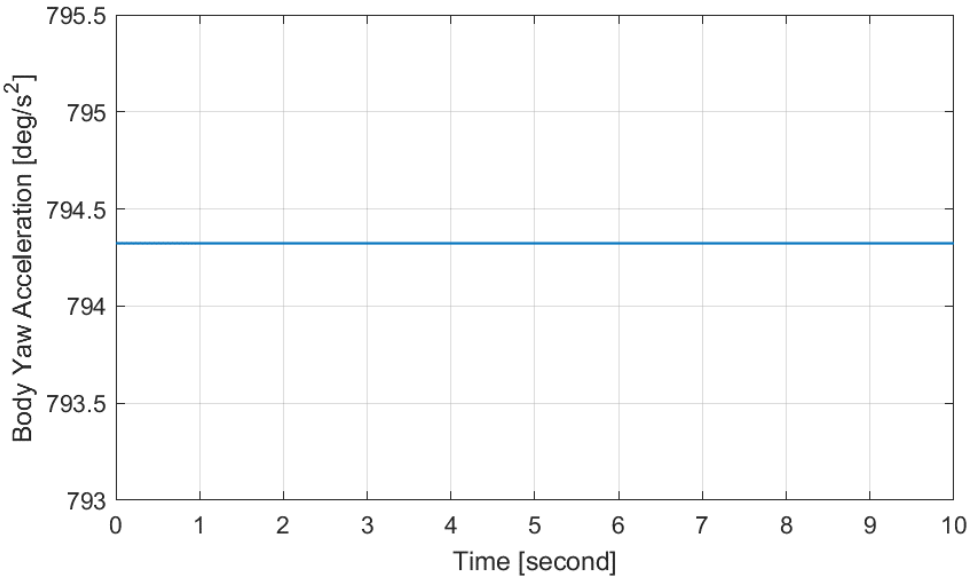

Figure 3.23. Yaw Angle Acceleration of body for Option-1

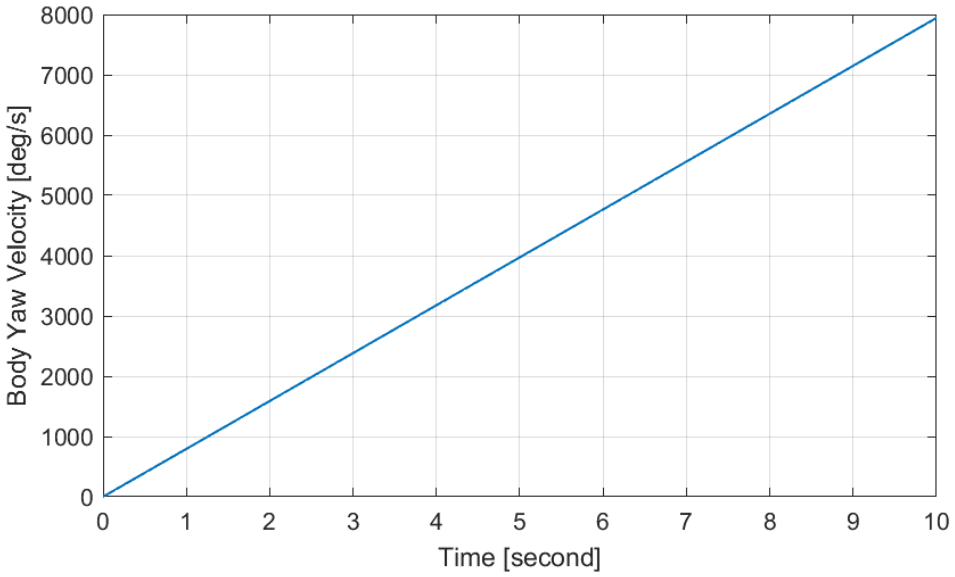

Figure 3.24. Yaw Angle Velocity of body for Option-1

The motor and propeller characteristics selected for the second analysis in a one propeller option are given in table 3.4 below.

Table 3.4. One Propeller Option 2 Parameters [20]

Parameters	**Value**	**Unit**
Motor Name	T-Motor U3 700KV	n/a
Propeller Name	T-Motor 12x4 Carbon	n/a
Propeller Diameter	30.48	cm
Thrust	1.663	kgf
Torque	0.2635	Nm
Rotation Speed	8575	rpm

In option 2, there will be no change in the x axis, just like in option 1. The graph showing the displacement in the x axis is given in figure 3.25.

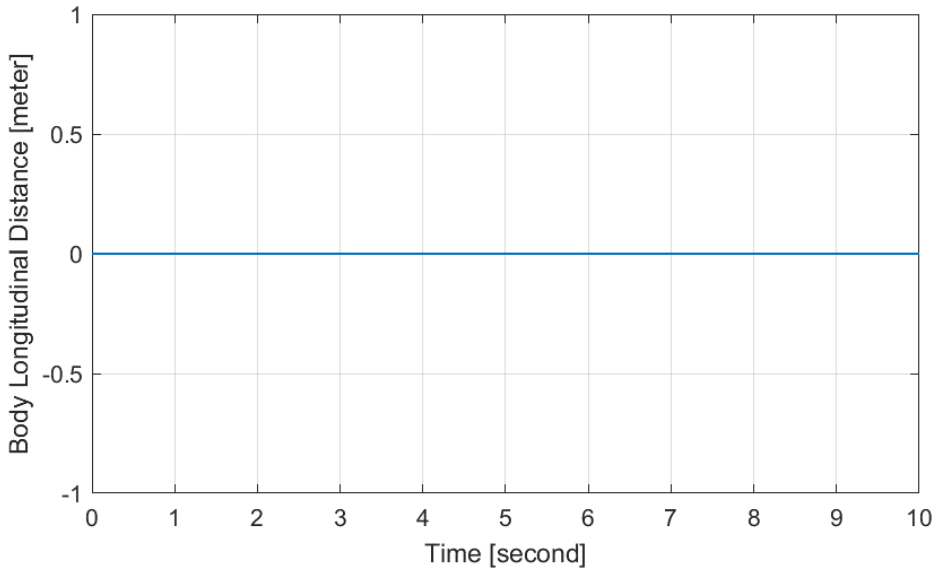

Figure 3.25. Body distance in x-axis for Option-2

Accordingly, there is no change in both body velocity and body acceleration. These two parameters take the value of zero throughout the simulation. These body acceleration and velocity in x axis graphs can be seen in figures 3.26 and 3.27.

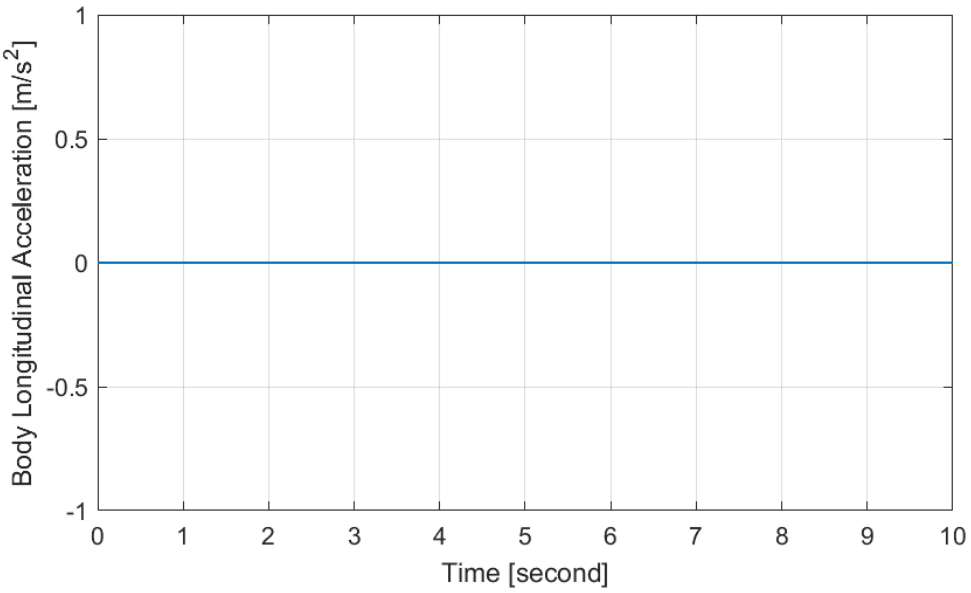

Figure 3.26. Body acceleration in x-axis for Option-2

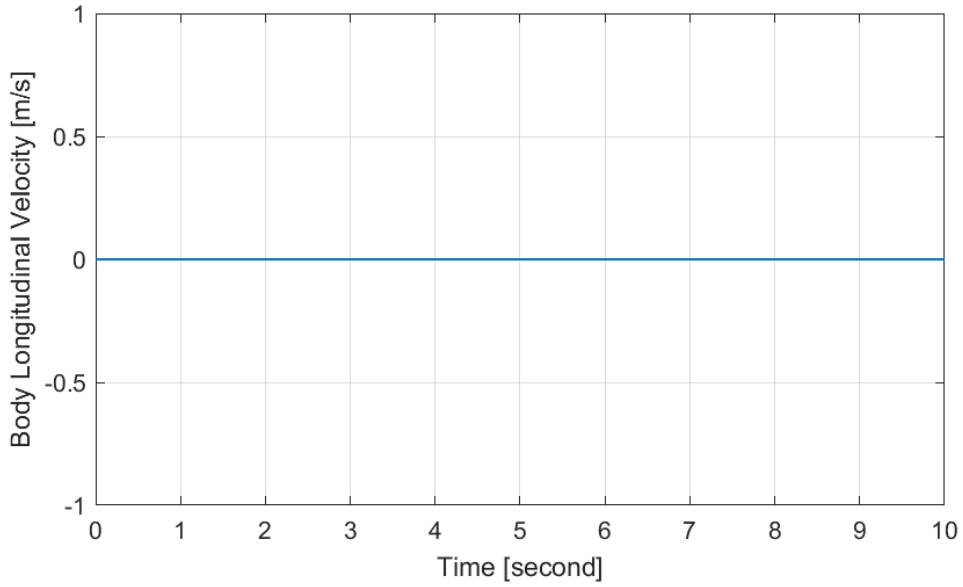

Figure 3.27. Body velocity in x-axis for Option-2

In option 2, the thrust produced by the propeller is insufficient to lift the weight of the robot. The displacement made by the robot in the y axis is shown in figure 3.28.

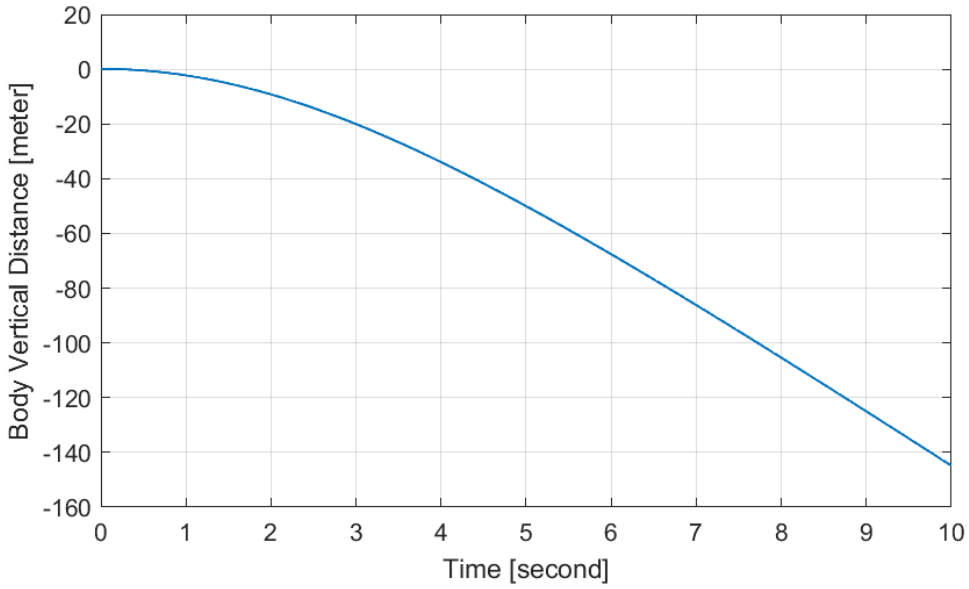

Figure 3.28. Body Distance in y-axis for Option-2

As seen in figure 3.28, it can be seen that the robot has negative displacement on the y-axis. The body velocity and acceleration in y axis graphs that cause this decrease are given

in figures 3.29 and 3.30 below. The friction force that slows down the fall throughout the simulation is given in figure 3.31.

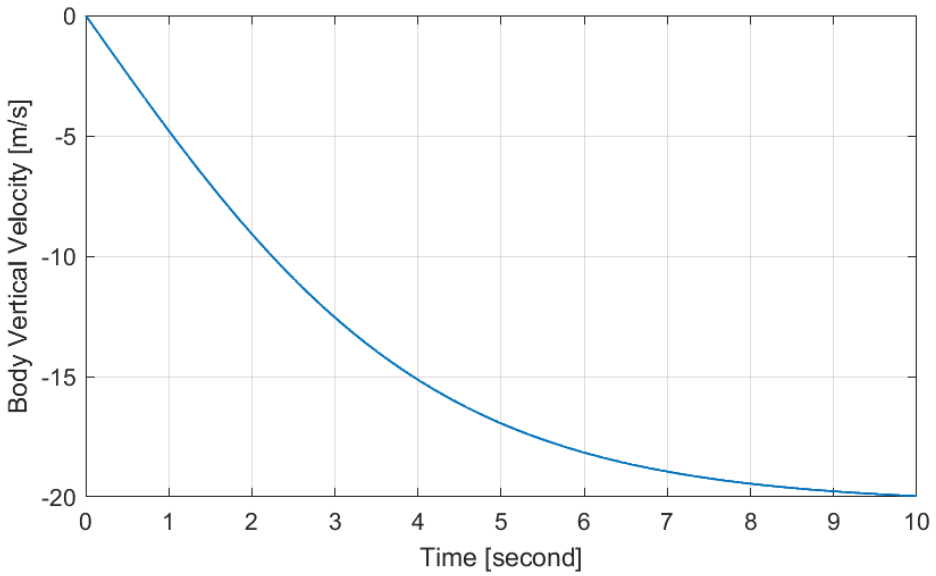

Figure 3.29. Body velocity in y-axis for Option-2

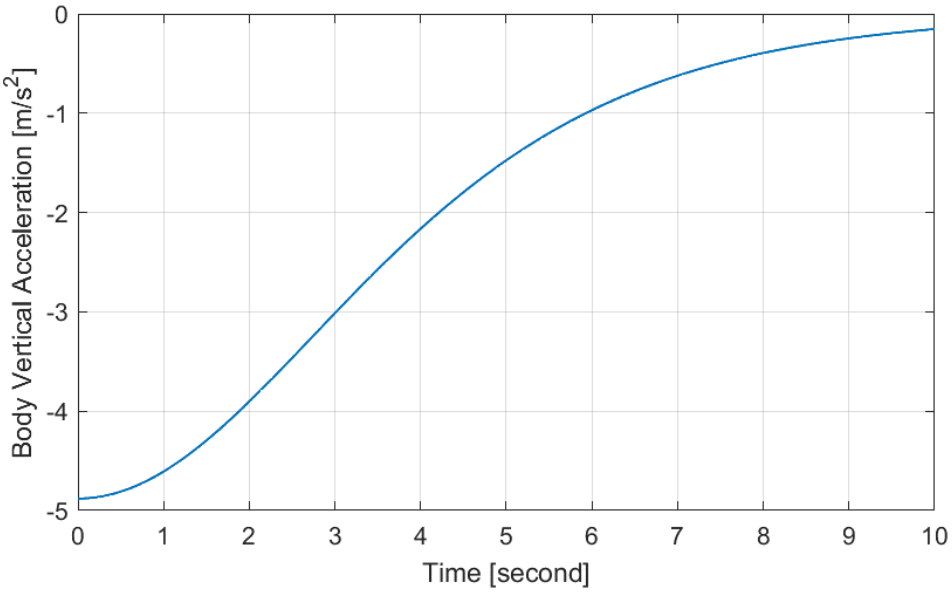

Figure 3.30. Body acceleration in y-axis for Option-2

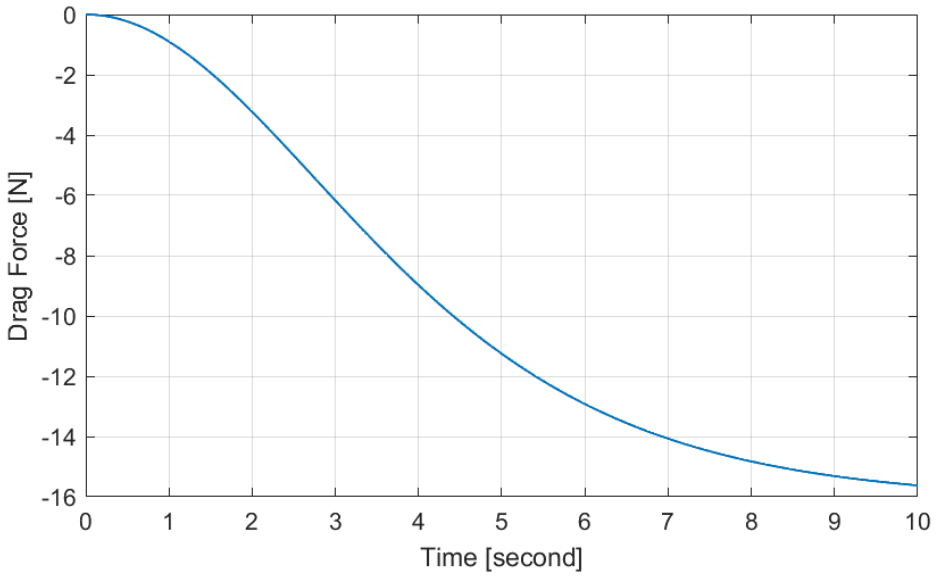

Figure 3.31. Drag Force in y-axis for Option-2

In option-2, the yaw angle formed throughout the simulation is the same as in option 1. Because the torques produced by the propeller used in both options are very similar. The yaw angle formed in option 2 is given in figure 3.32.

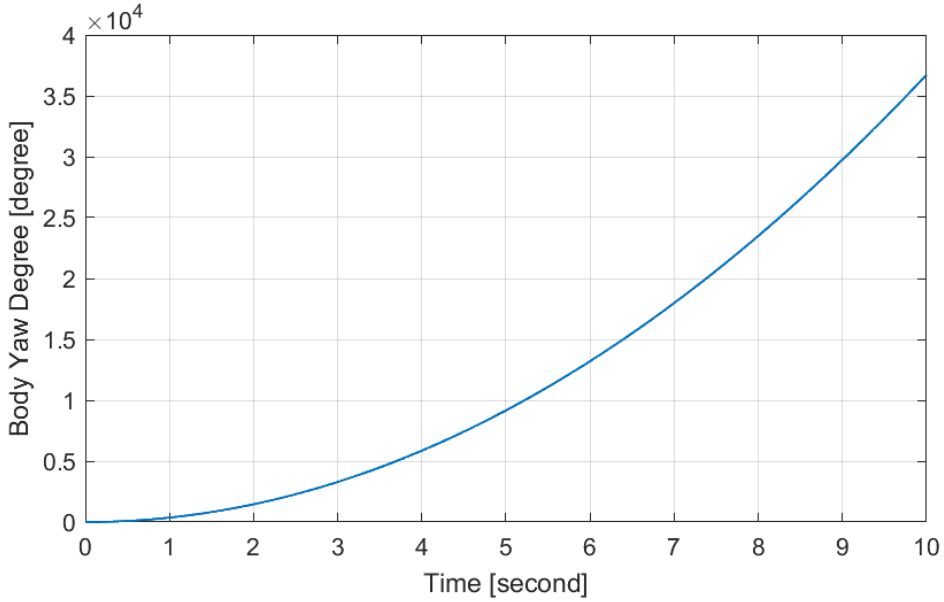

Figure 3.32. Yaw Angle of body for Option-2

In option 2, the robot reached the 45 degrees in yaw angle at almost 0.5 second. Also total rotation of the body during simulation is 102. The body velocity and body acceleration graphs that create this rotation can be seen in figures 3.33 and 3.34.

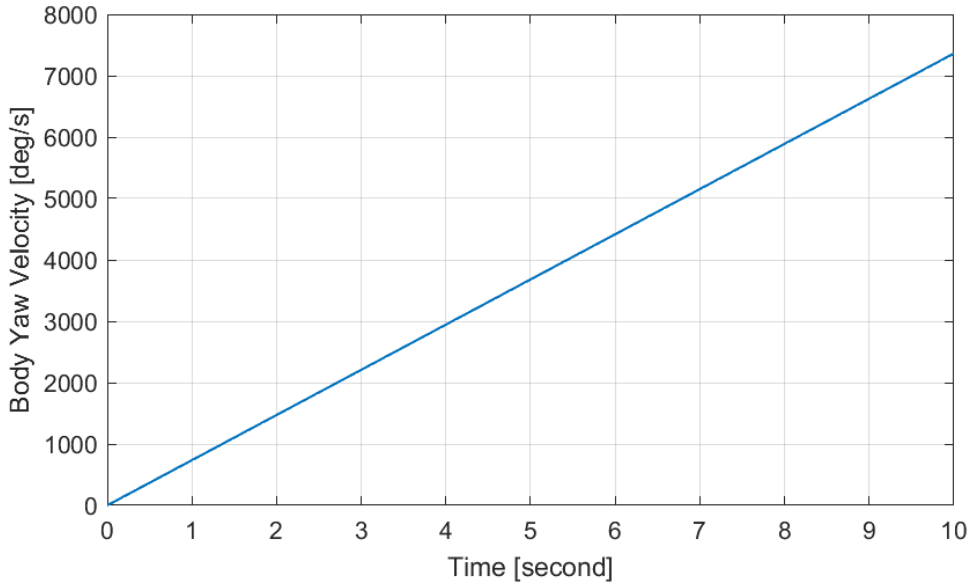

Figure 3.33. Yaw Velocity of body for Option-2

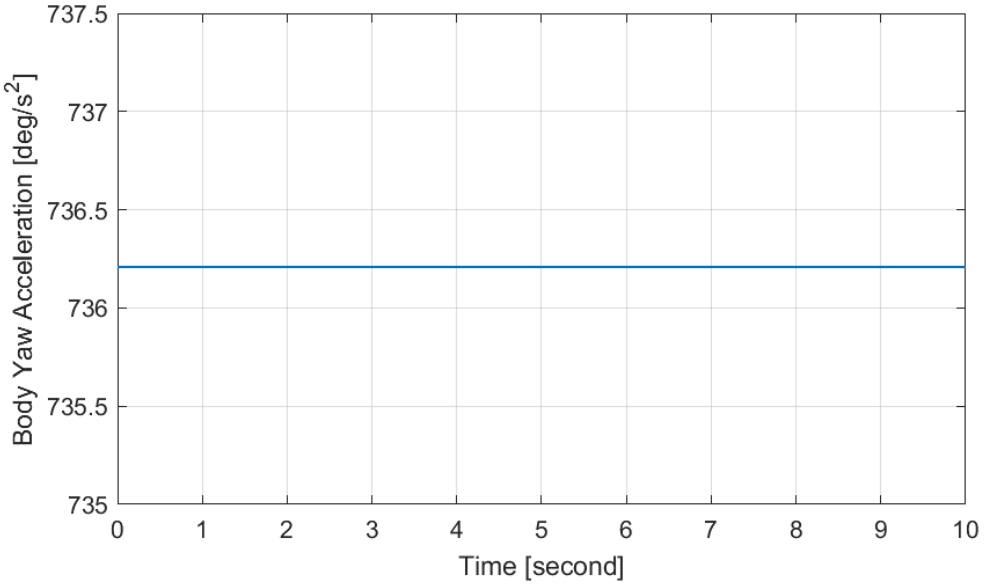

Figure 3.34. Yaw Acceleration of body for Option-2

As can be seen in the graphs, the robot did not show a positive value in the y direction in both options in the 10-second simulations. According to the first study, a propeller that

fits the dimensions of the hybrid Rhex robot cannot provide sufficient thrust force. Although a single propeller is the best option in terms of usage and battery, unfortunately it remains unusable as it causes deviation in "yaw angle". It takes less than 0.5 second for the yaw angle to reach 45 degrees. It rotates 1000 degrees (about 3 full rotations) in 1 second. Therefore the single propeller can no longer be used.

3.3.5.2. Tandem Propellers

When wanting to put propellers back-to-back in the 12 cm section, there is the possibility of fitting one longer and the other shorter in the fuselage to meet the dimensions With this approach, the total thrust value will be increased. However, propellers operated with different performance to change the pitch angle will change the yaw angle this time. Because obtaining different thrust values will cause different torque values. In this thesis, torque and thrust will vary in a linear ratio. Schematic of the tandem propellers can be seen in figure 3.35.

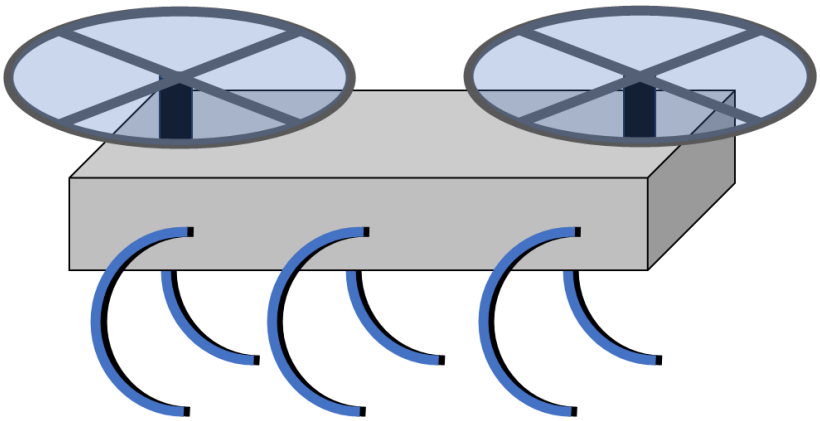

Figure 3.35. Rhex Robot Tandem Schematic

The engine and propeller specifications determined for the tandem propeller analysis are shown in table 1.

Table 3.5. Tandem Propeller Option 3 Parameters [21]

Parameters	**Value**	**Unit**
Motor Name	T-Motor U5 KV400	n/a
Propeller Name	T-Motor P15x5	n/a
Propeller Diameter	38.1	cm
Thrust	2.369	kgf
Torque	0.4323	Nm
Rotation Speed	8122	rpm

When 2 pieces of the propeller and motor selected above are installed, the total thrust will be $2.37 \times 2 = 4.74$ kgf, so the rhex robot, which weighs 3.2 kg, can easily be lifted into the air. The displacement graph on the y-axis is given in figure 3.39.

In option 3, full performance was run on both motor and propeller for the first analysis. Additionally, in this analysis, the total torque value was reset by rotating the propellers in the opposite direction. Also, same thrust generated from propellers so there is no change in the pitch angle first analysis for option-3. This means that, the body no movement in x-axis. The displacement of body in x-axis can be seen in figure 3.36.

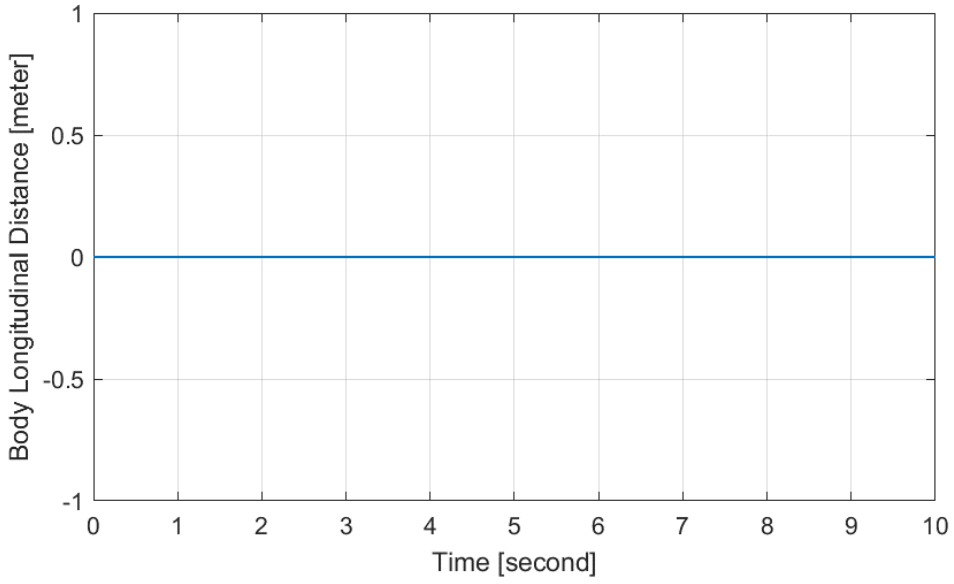

Figure 3.36. Body displacement in x-axis for Option-3 First Analysis

The body velocity and body acceleration graphs on the x-axis of the first analysis are given in figures 3.37 and 3.38 below. Naturally, these two graphs will not differ from zero throughout the simulation.

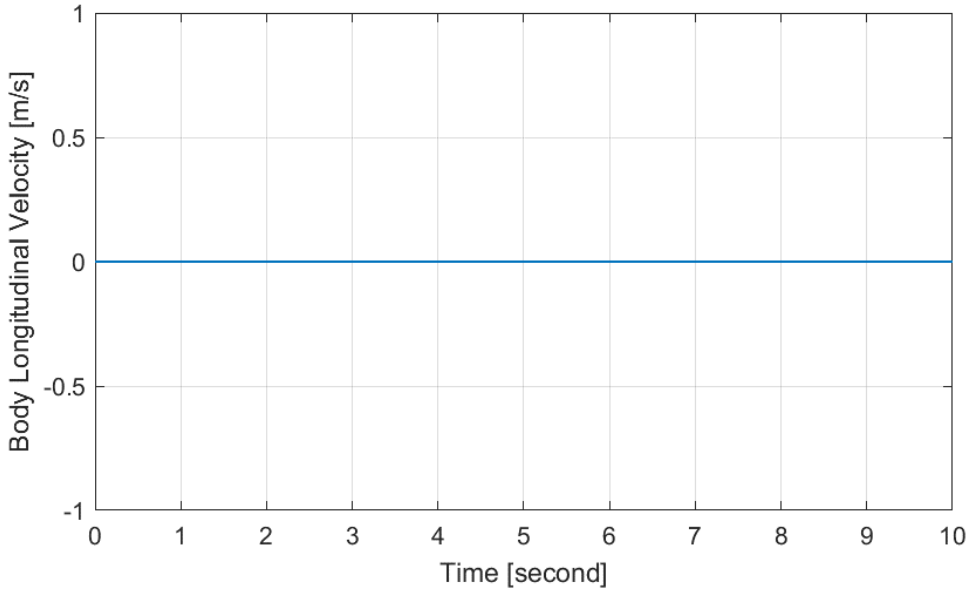

Figure 3.37. Body velocity in x-axis for Option-3 First Analysis

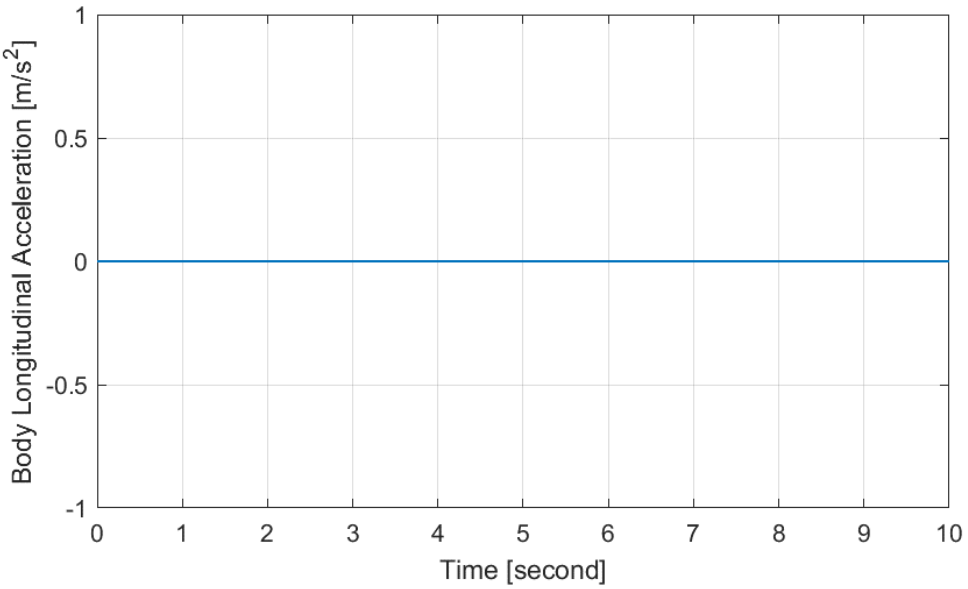

Figure 3.38. Body acceleration in x-axis for Option-3 First Analysis

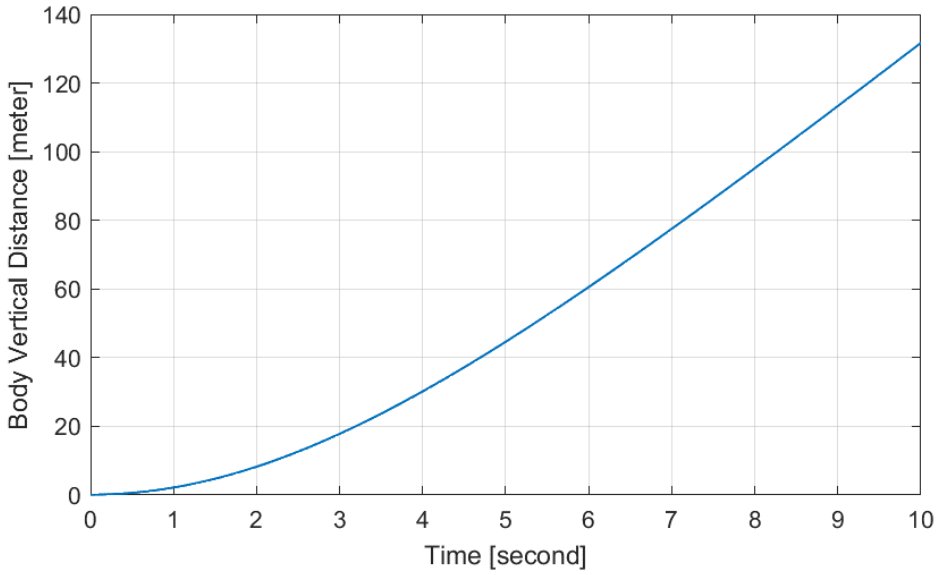

Figure 3.39. Body displacement in y-axis for Option-3 First Analysis

Body Velocity and body acceleration on the y-axis graphs that allow you to see a positive value in displacement on the y-axis are shown in figures 3.40 and 3.41. The friction force the robot is exposed to while moving in the air is shown in figure 3.42.

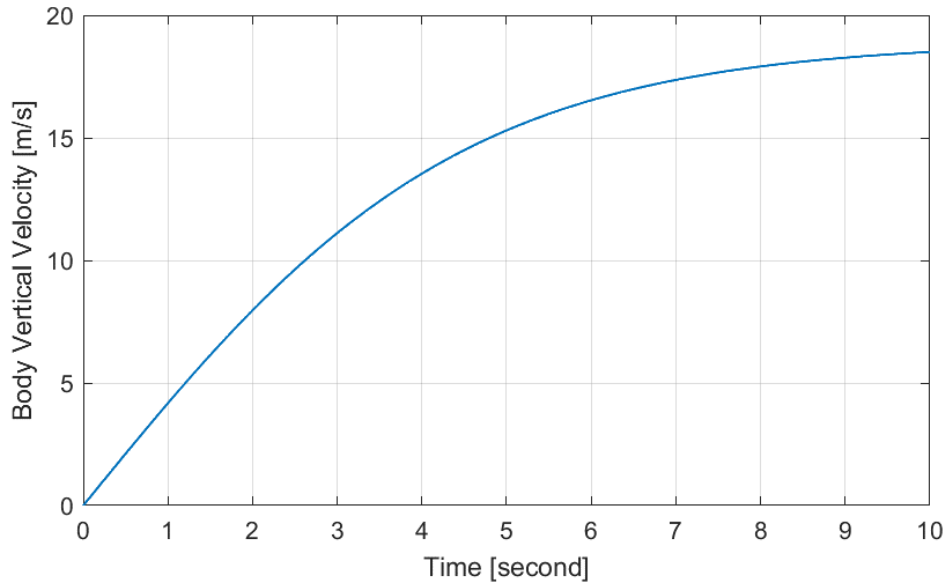

Figure 3.40. Body velocity in y-axis for Option-3 First Analysis

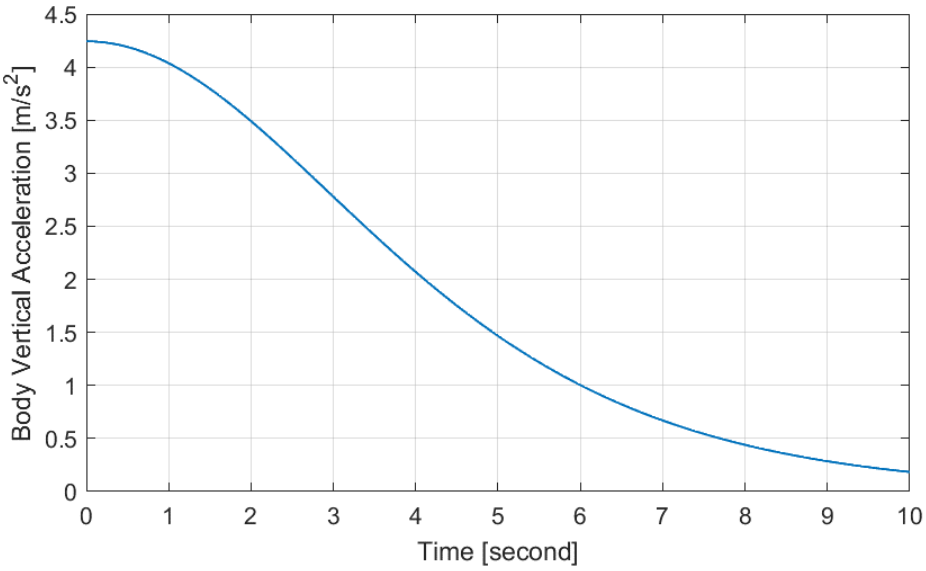

Figure 3.41. Body acceleration in y-axis for Option-3 First Analysis

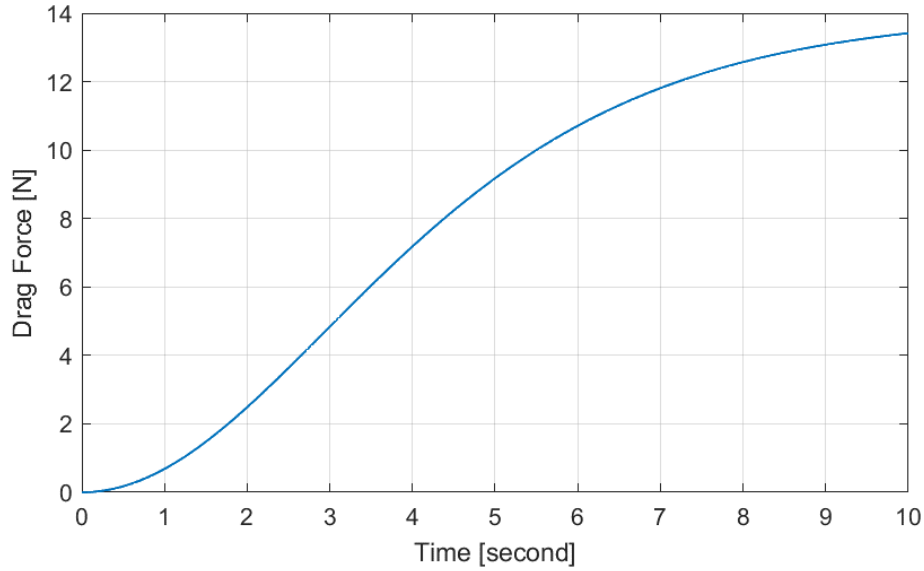

Figure 3.42. Drag Force in y-axis for Option-3 First Analysis

In the first analysis, since both motor and propellers are operated at full performance, they produce the same value of torque. Additionally, since the propellers are rotated in the opposite direction, the total torque value will be zero. Therefore, there will be no change in the yaw angle throughout the simulation. The yaw angle graph is seen in figure 3.43.

Naturally, both yaw velocity and yaw acceleration values will be zero throughout the simulation. Yaw velocity and yaw acceleration graphs are shown in figures 3.44 and 3.45, respectively.

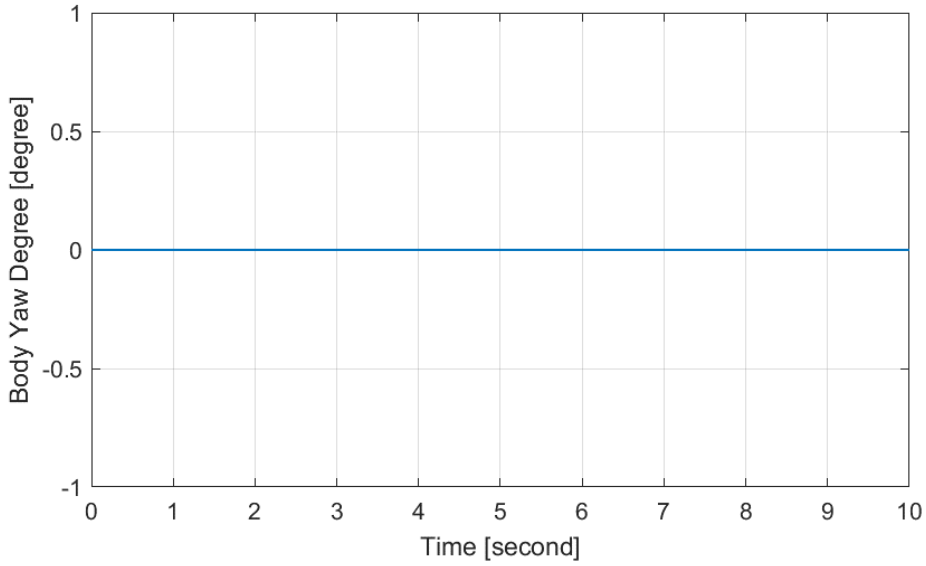

Figure 3.43. Yaw angle of body for Option-3 First Analysis

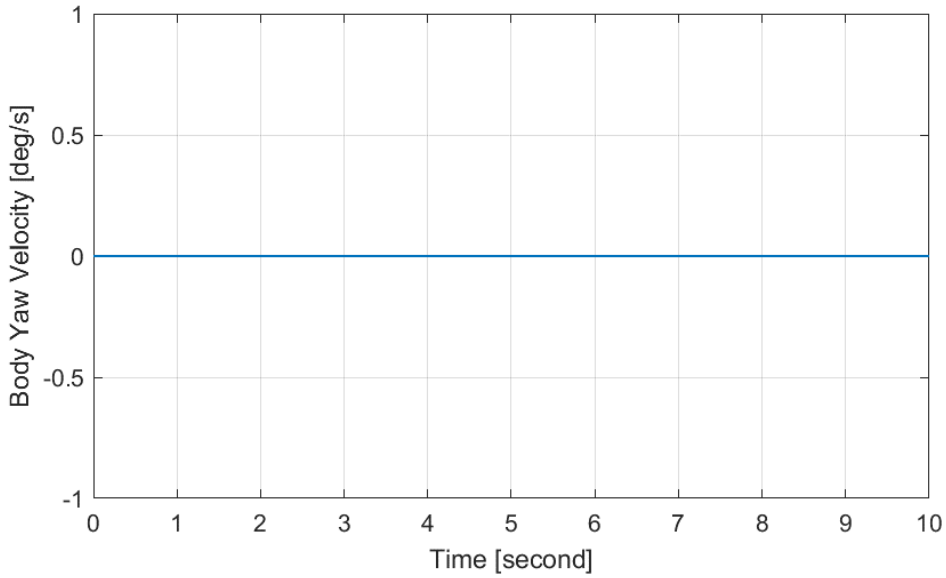

Figure 3.44. Yaw velocity of the body for Option-3 First Analysis

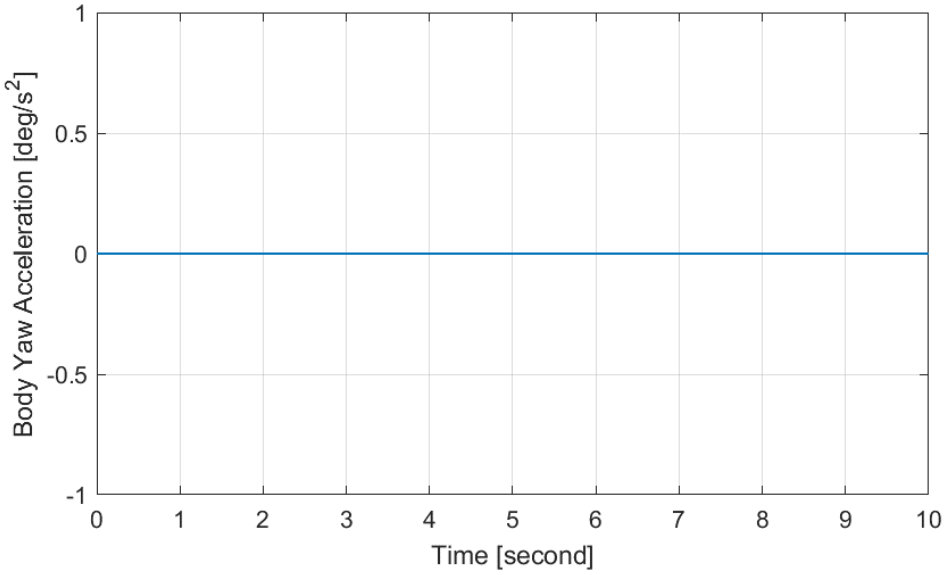

Figure 3.45. Yaw acceleration of the body for Option-3 First Analysis

In the second analysis, one of the propellers will not be operated at full performance. Rear motor was running at 0.995 power. Thus, there will be a thrust difference between the propellers. Due to this thrust difference, a change in pitch angle will be observed. Body pitch angle can be seen in figure 3.46 for second analysis.

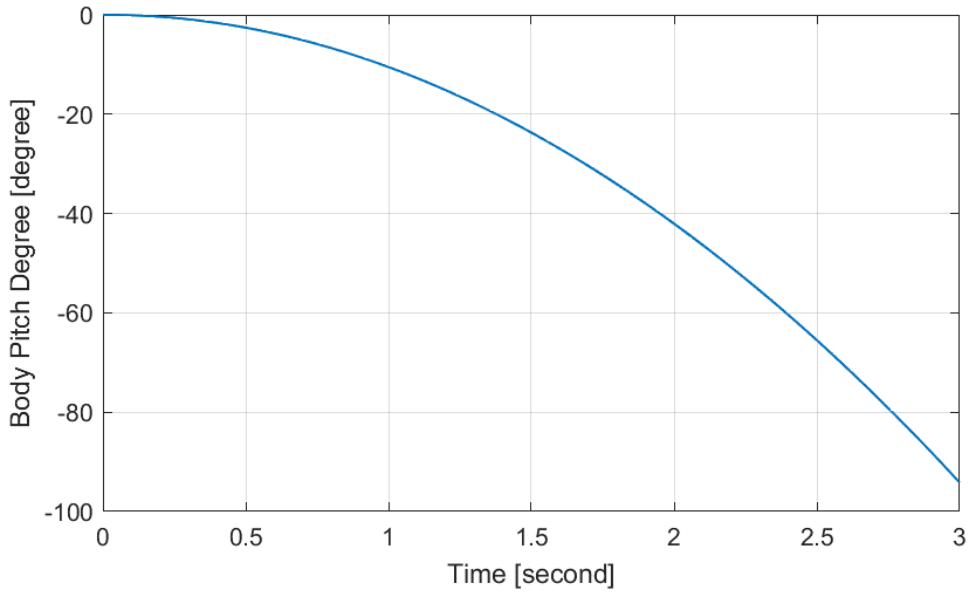

Figure 3.46. Pitch Angle of the body for Option-3 Second Analysis

Due to the constant thrust difference, the robot reaches a 90 degree pitch angle in a very short time (3 seconds). The pitch velocity and pitch acceleration graphs that cause this rotation are given in figures 3.47 and 3.48, respectively.

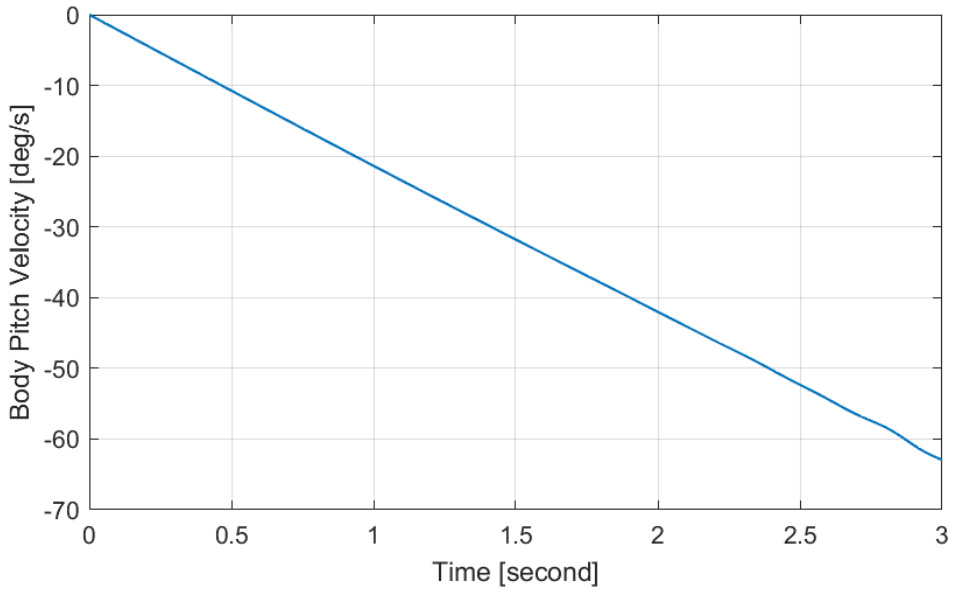

Figure 3.47. Pitch velocity of the body for Option-3 Second Analysis

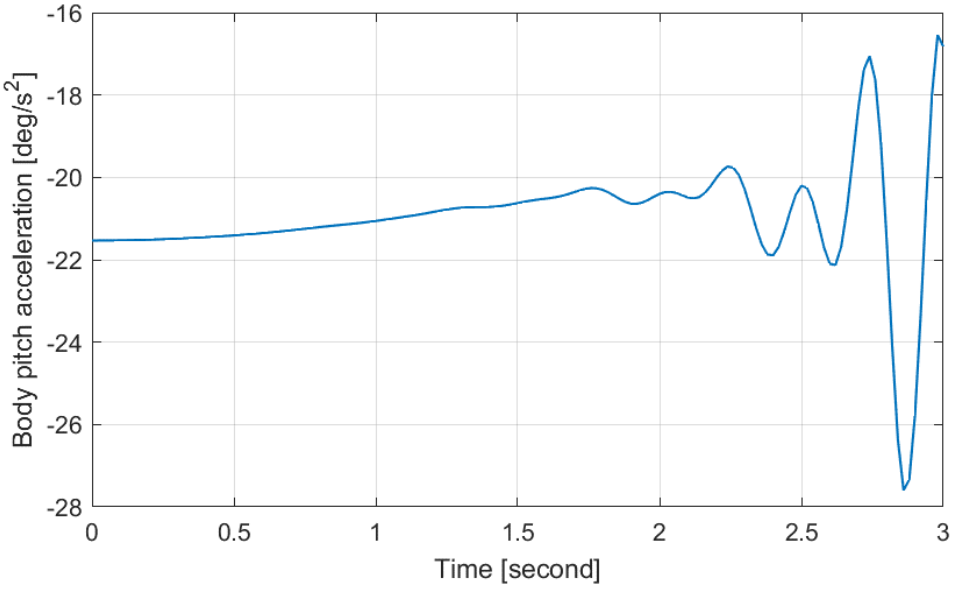

Figure 3.48. Pitch acceleration of the body for Option-3 Second Analysis

As seen in figure 3.48, pitch acceleration becomes unstable towards the end of the simulation.

This change in pitch angle allows the robot to move in the x-axis. Body displacement in x-axis can be seen figure 3.49 for sencond analysis.

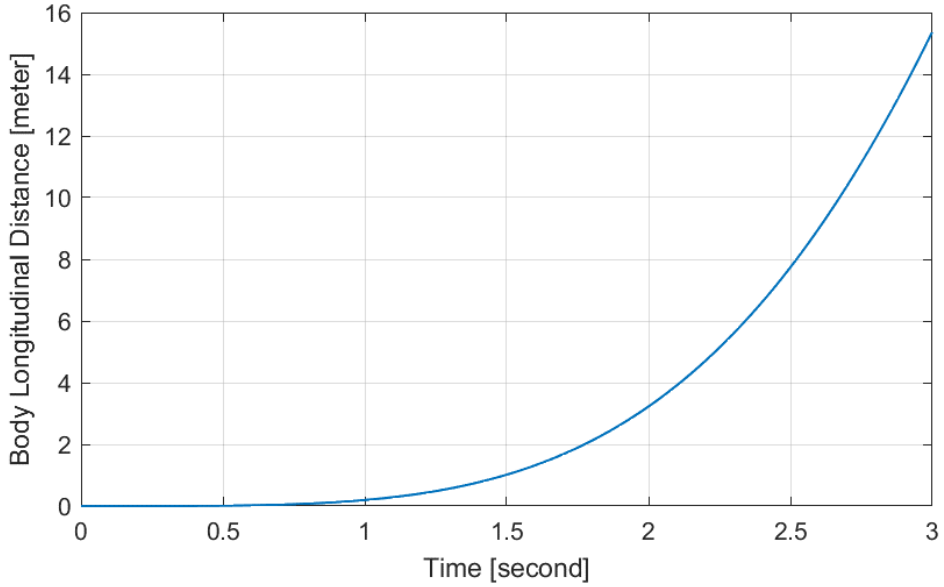

Figure 3.49. Body distance in x-axis for Option-3 Second Analysis

The body velocity and body acceleration graphs that cause us to displacement on the x-axis are given below in figures 3.50 and 3.51, respectively.

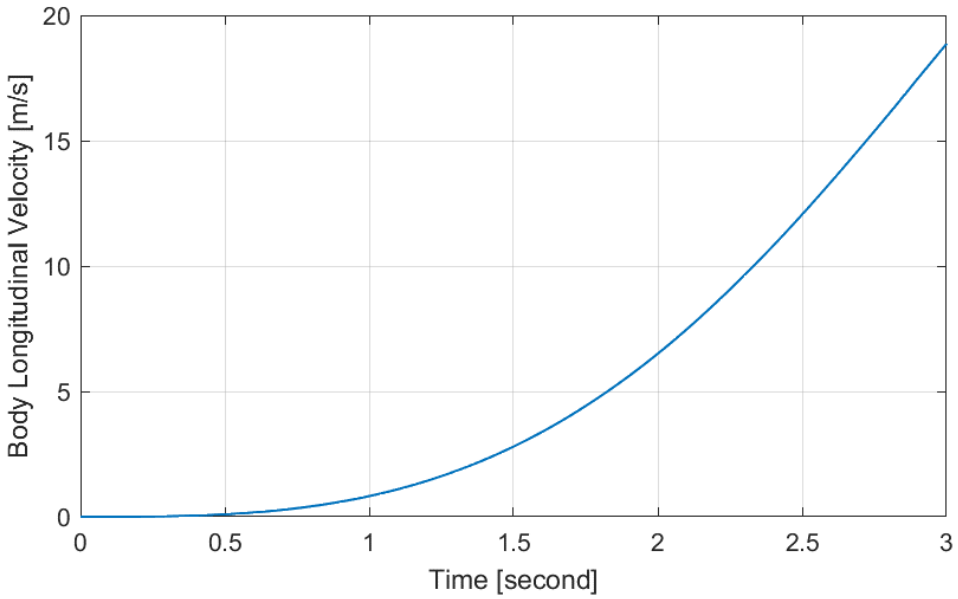

Figure 3.50. Body velocity in x-axis for Option-3 Second Analysis

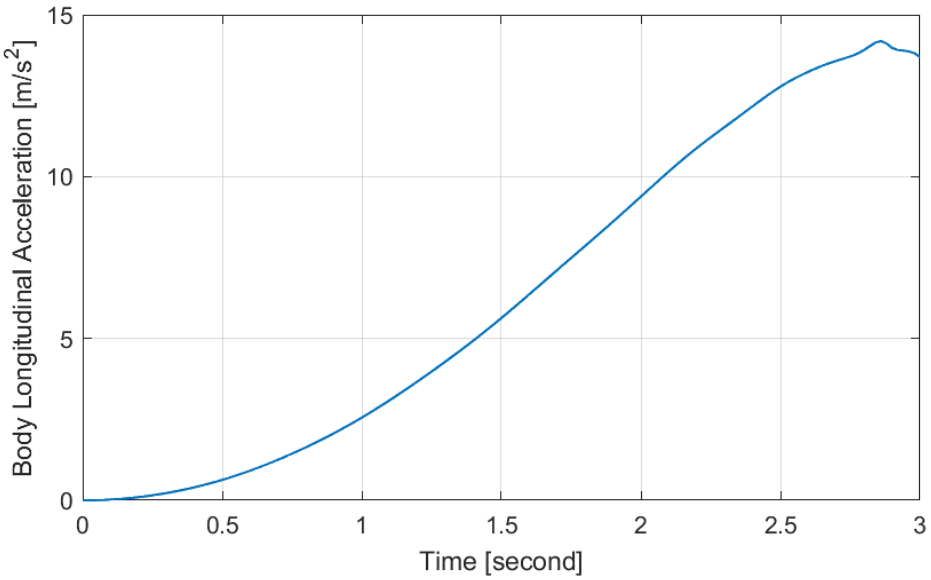

Figure 3.51. Body acceleration in x-axis for Option-3 Second Analysis

It was seen with the second analysis that it has the ability to move the robot in the x axis, thanks to the motors operated at different performances. While this is moving in the x-axis, the robot is also moving in the y-axis because the total thrust is more than the robot weight. In the second analysis, the displacement taken by the robot in the y-axis is given in figure 3.52.

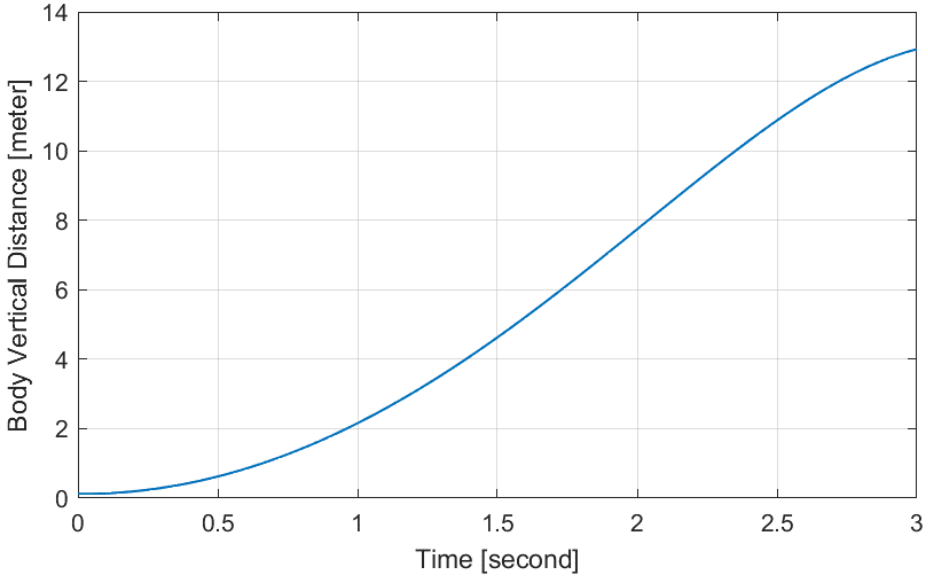

Figure 3.52. Body distance in y-axis for Option-3 Second Analysis

For the second analysis, the robot body velocity and body acceleration in y-axis graphs are given in figures 3.53 and 3.54.

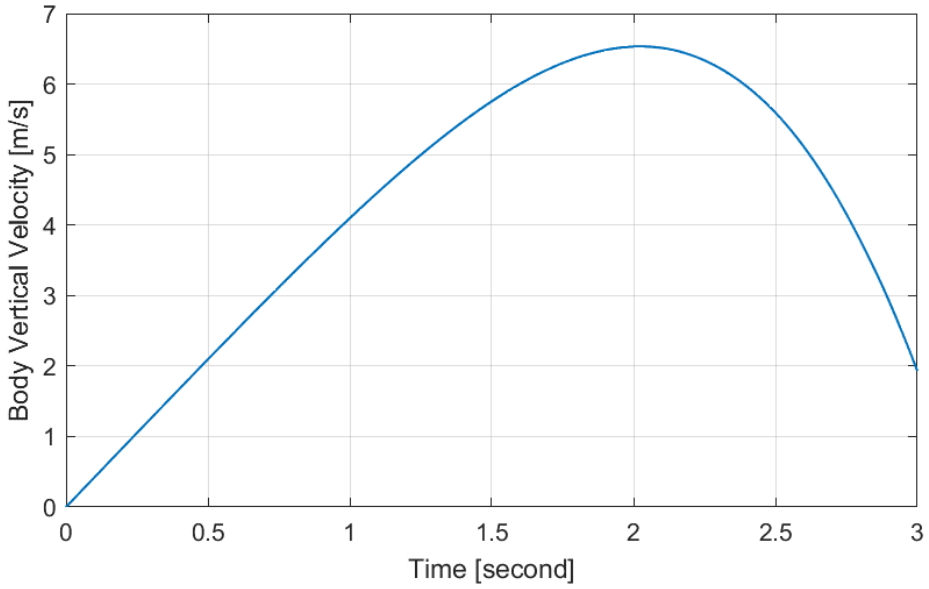

Figure 3.53. Body velocity in y-axis for Option-3 Second Analysis

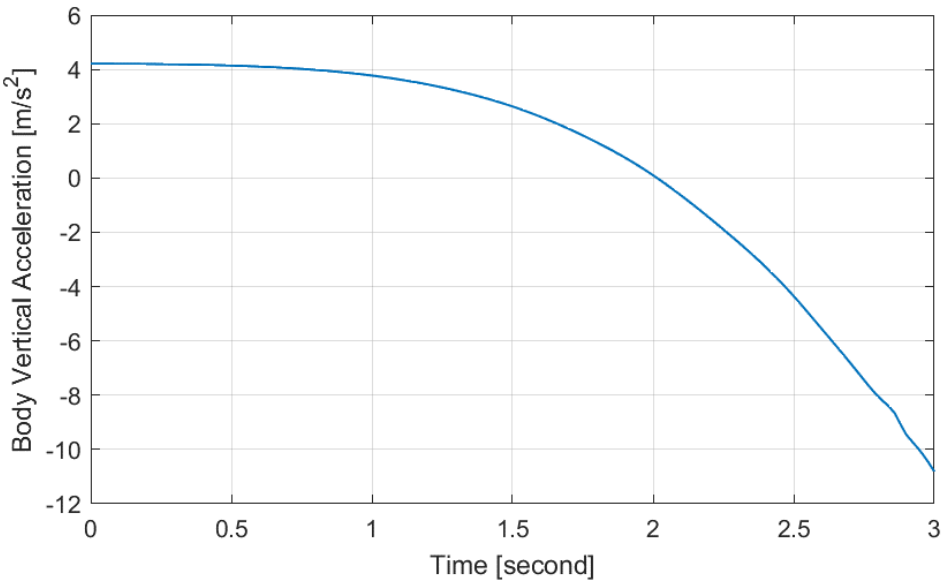

Figure 3.54. Body acceleration in y-axis for Option-3 Second Analysis

The drag force in the y axis due to the pitch angle is given in figure 3.55.

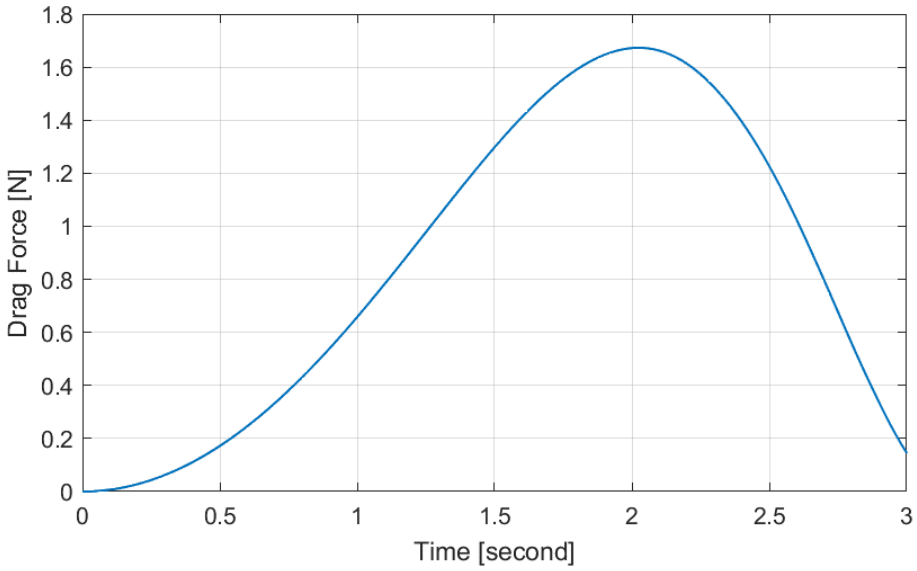

Figure 3.55. Drag Force in y-axis for Option-3 Second Analysis

Although engines operating at different performances allow the pitch angle to be controlled, they create yaw angle problems due to different torque values. The yaw angle obtained for the second analysis is shown in figure 3.56.

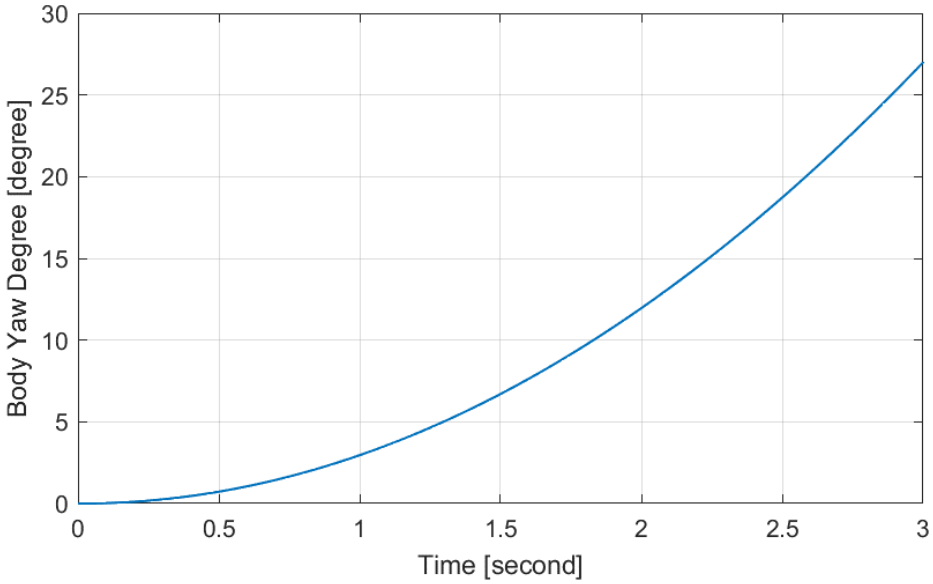

Figure 3.56. Yaw angle of the body for Option-3 Second Analysis

In option 3 second analysis, the robot can not reached the 45 degrees in yaw angle. Also total rotation of the body during simulation is zero. The body velocity and body acceleration graphs that create this rotation can be seen in figures 3.57 and 3.58.

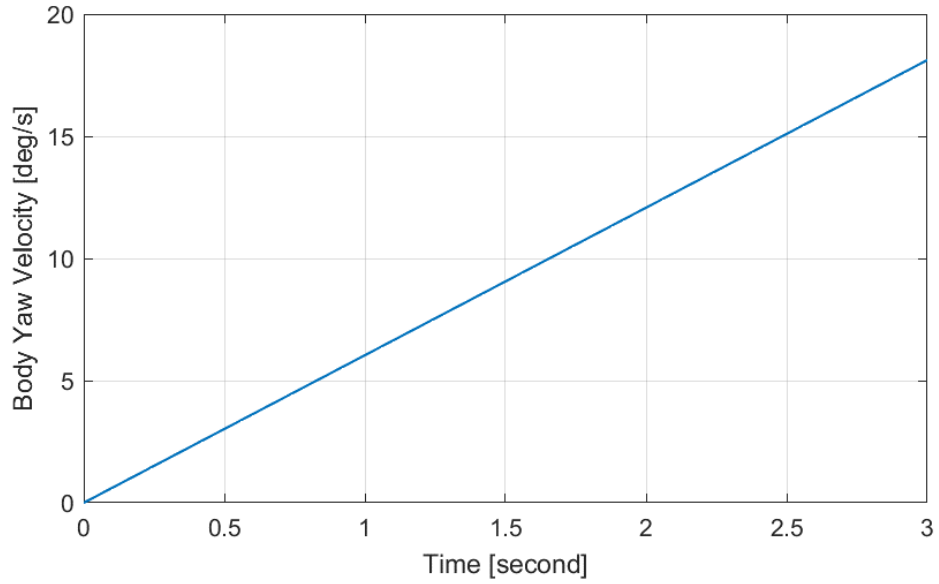

Figure 3.57. Yaw velocity of the body for Option-3 Second Analysis

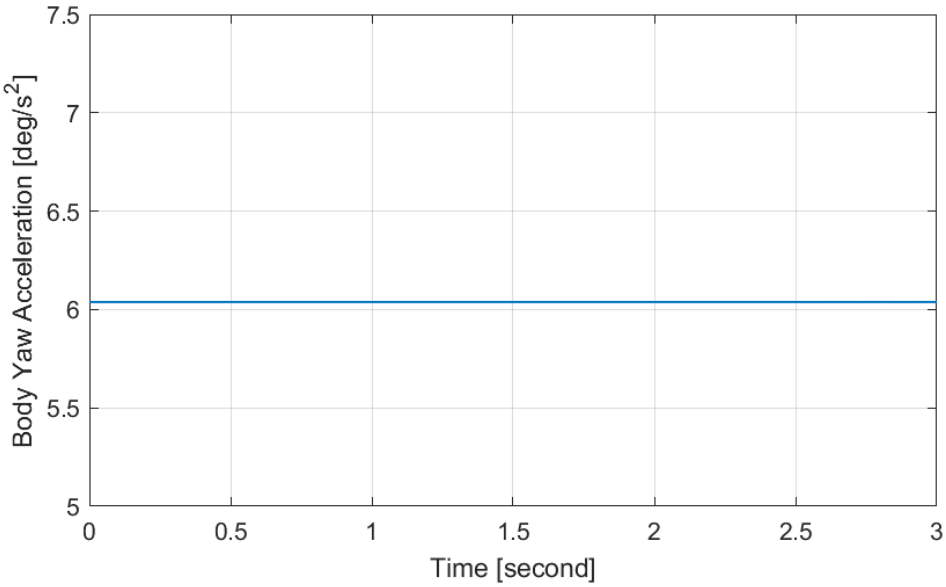

Figure 3.58. Yaw acceleration of the body for Option-3 Second Analysis

The tandem propeller option provides both sufficient thrust and control of the pitch angle. However, controlling the pitch angle causes the yaw angle to deteriorate. Additionally, the tandem propeller option has been abandoned due to its difficulty in size and placement.

3.3.5.3. Coaxial Contra-Rotating Propellers

The third design option is co-axial positioned propellers. Installing propellers in this way saves a lot of space. At the same time, the yaw angle problem can be avoided by contra-rotating the propellers installed in this way. The motor and propeller specifications to be used for coxial contra-rotating are given in Table 3.5.

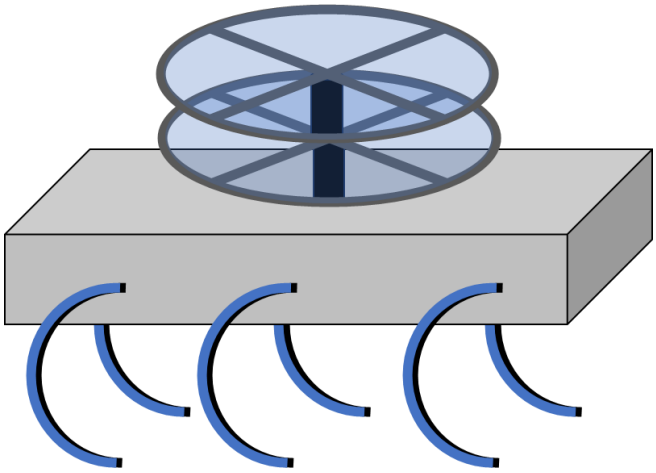

Figure 3.59. Rhex Robot Coaxial Contra Rotating Schematic

In research for design, which is one of the options for both saving space and increasing thrust. The statement "This is achieved with the upper rotor producing more thrust ($CT_u/CT_l = 1.25$)" was found [22]. When two propellers with the same torque value are installed in this way, the following propeller will have to operate at 0.8 efficiency. Coaxial contra rotating schmatic for RHex robot can be seen in figure 3.59.

Table 3.6. Coaxial Contra-Rotating Propeller Option 4 Parameters [21]

Parameters	**Value**	**Unit**
Motor Name	T-Motor U5 KV400	n/a
Propeller Name	T-Motor P15x5	n/a
Propeller Dimension	38.1	cm
Thrust	2.369	kgf
Torque	0.4323	Nm
Rotation Speed	8122	rpm

When the engine and propeller given in the table 3.6 above are used, the total power is $2.37 + 2.37 \times (0.8) = 4.266\ kgf$. This provides a thrust to keep the rhex robot in the air and at the same time it will not create a yaw angle problem.

Since the coaxial contra rotating propellers would not change the pitch angle, the robot did not move at all in the x-axis. The pitch angle formed in the simulation for option 4 is shown in figure 3.60. The resulting body displacement in the x axis is shown in figure 3.61.

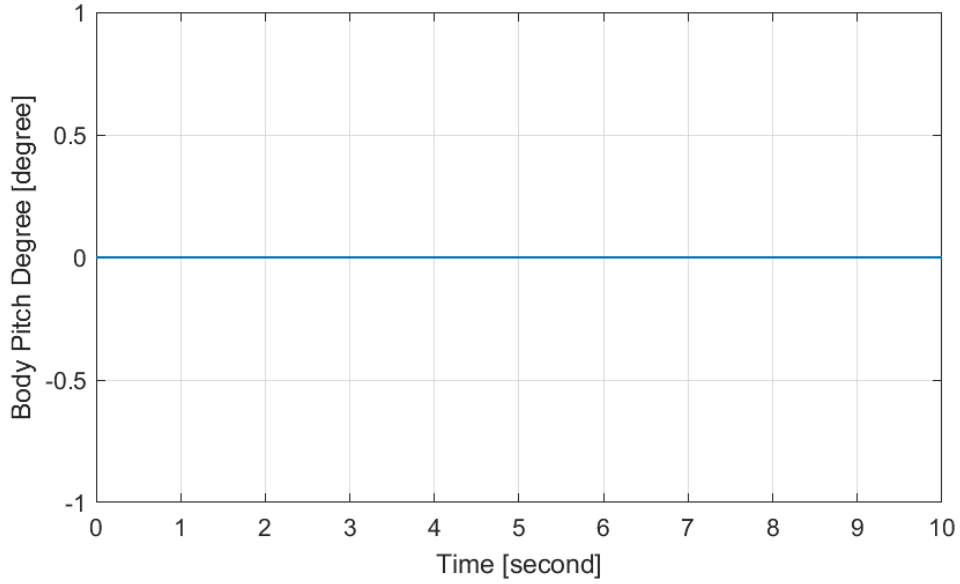

Figure 3.60. Pitch angle of the body for Option-4

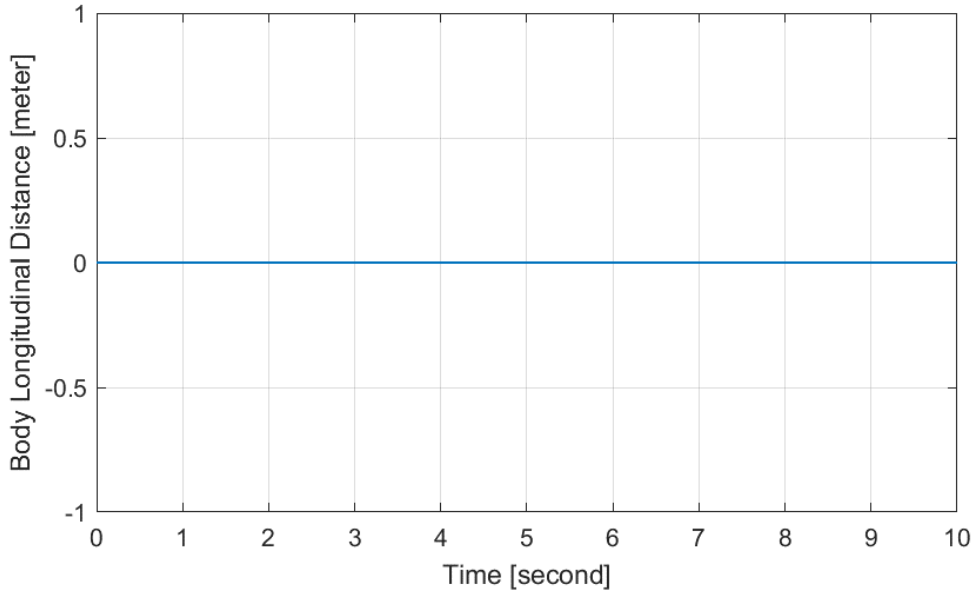

Figure 3.61. Body displacement in x axis for Option-4

Since two propellers are used, it has a high total thrust production capacity. The body displacement in the y axis resulting from this thrust is shown in figure 3.62. The body velocity and body acceleration in y-axis graphs created by this thrust are given in figures 3.63 and 3.64, respectively.

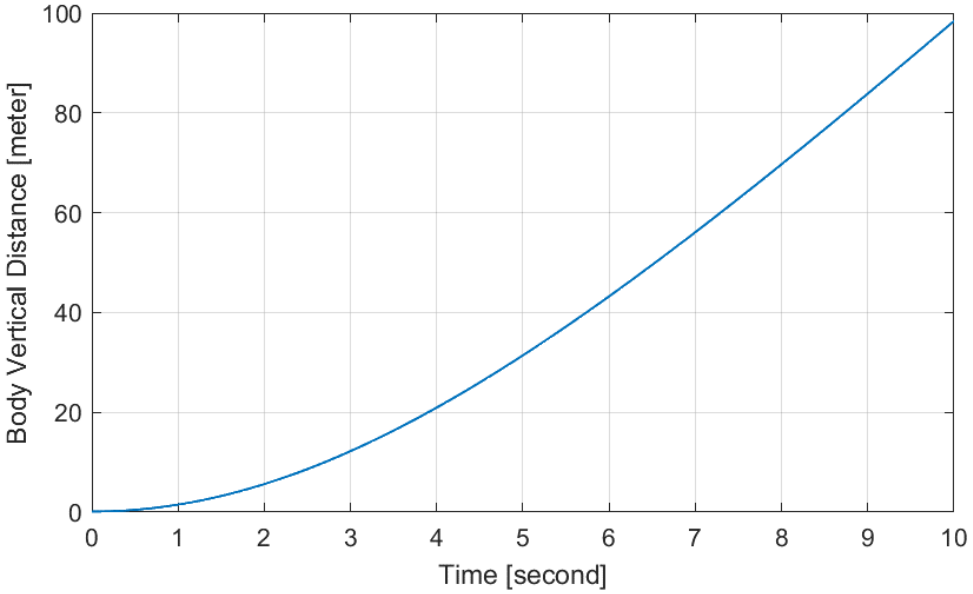

Figure 3.62. Body distance in y-axis for Option-4

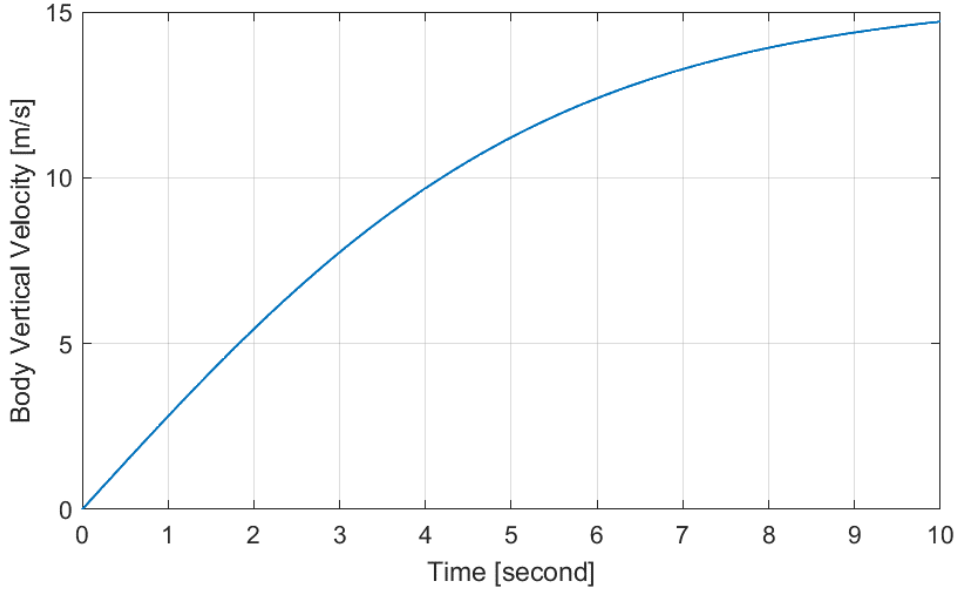

Figure 3.63. Body velocity in y-axis for Option-4

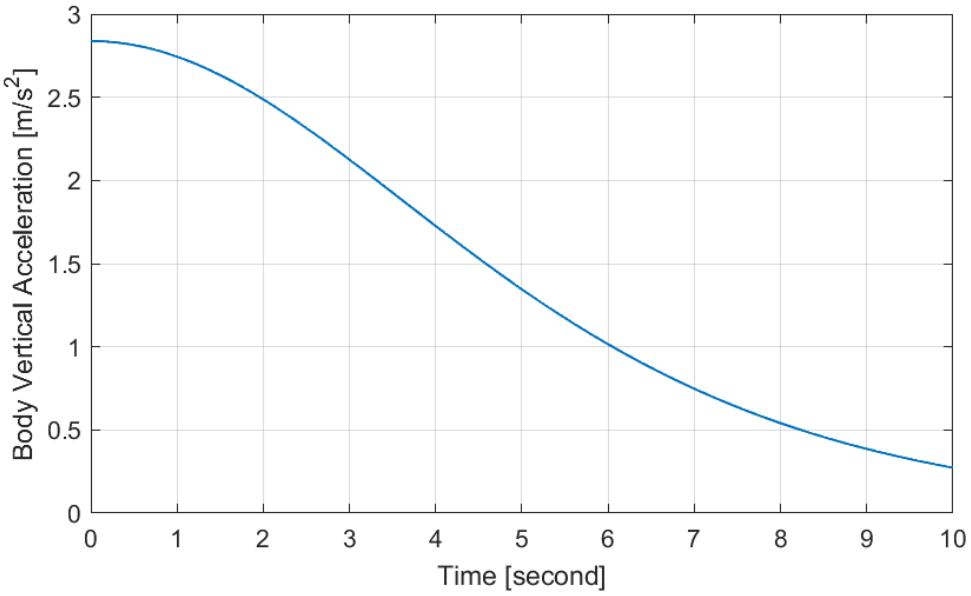

Figure 3.64. Body acceleration in y-axis for Option-4

In the simulation for option 4, the drag force acting on the robot in the y axis is given in figure 3.65.

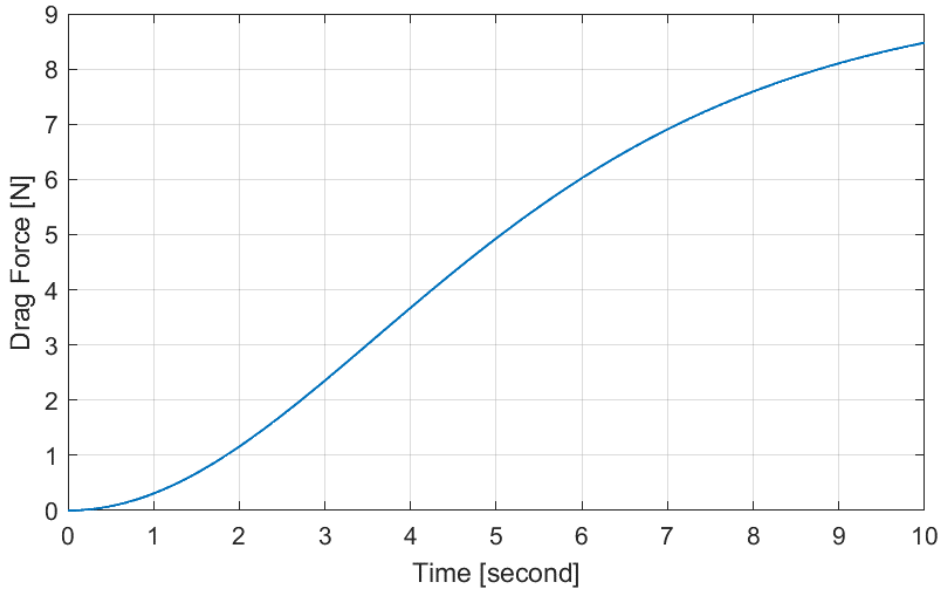

Figure 3.65. Drag Force in y-axis for Option-4

Since the propellers rotate in the opposite direction, the total torque created by the propellers is zero. Therefore, the yaw angle takes the value as zeo throughout the entire simulation. The yaw angle graph is seen in figure 3.66.

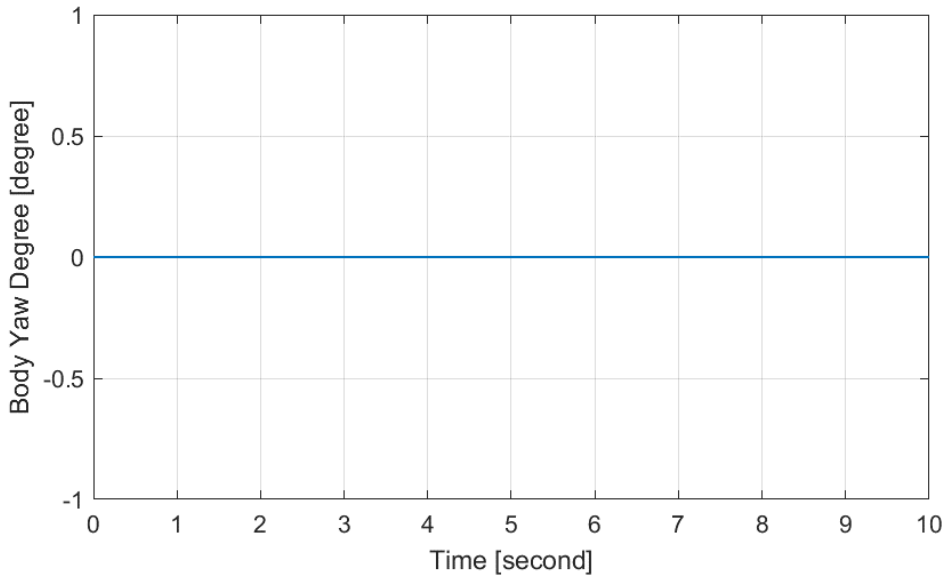

Figure 3.66. Yaw angle of the body for Option-4

Although option 4(coaxial contra-rotating) provides high thrust compared to other options and does not create yaw angle problems, it is not a realistic approach in terms of dimensions. Therefore, it is more appropriate not to use option 4(coaxial contra-rotating) in mission simulations.

3.3.5.4. Simulation Results of Propeller

In the simulations made using propellers, it was seen that although the single-propeller approach is very good in energy efficiency, unfortunately, it cannot produce enough thrust and creates problems in the yaw angle. It is envisaged to eliminate the yaw angle problem by using two-propeller approaches. Although propellers installed in tandem are an excellent option for controlling the pitch angle, it was revealed in the simulations that propellers operated at different powers, which created a yaw angle problem. Coaxial-mounted propellers will be much larger in size than the hybrid robot and will be challenging to install. Therefore, the propeller option will not be used in mission simulations based on the simulation results for the hybrid rhex robot.

In the next section, different electric ducted fan options will be tested in simulations instead of the propeller option to test whether they suit most mission simulations.

3.3.6. Electric Ducted Fan

A ducted fan that fits very comfortably in a hybrid Rhex robot body has been shown to have the capacity to produce almost twice as much thrust in some types. Again, to solve the "yaw angle" problem from a single motor, similar solutions will have to be used as in the propeller part. It was seen in the previous section that the front and back option is not as good in terms of both yaw angle and pitch angle as the propeller. Since the side-by-side option is dimensionally impossible, it was deemed appropriate to test the contra rotating option directly on the hybrid Rhex robot.

As seen in the article titled “Experimental study of a ducted contra-rotating lift fan for vertical/short takeoff and landing unmanned aerial vehicle application”, the thrust value of the double blade contra-rotating ducted fan is higher than the single blade ducted fan [23]. In high RPM, the thrust is much more higher in coaxial contra-rotating setup. The rate of increase of thrust is seen in this article as 40%. Therefore, simulations will be made to be 40% more than the thrust value given by the engine manufacturer for a single propeller. Moreover, it is foreseen that by putting a coaxial contra rotating ducted fan, it will both solve the "yaw angle" problem and make a more thrust hybrid Rhex robot.

The first selected motor and fan specifications for Electric Ducted fan analysis are given in table 3.7 below.

Table 3.7. Electric Ducted Fan Option 5 Parameters [24]

Parameters	**Value**	**Unit**
Motor Name	HET 800-68-685	n/a
Fan Name	EDF Schubeler DS-68-AXI 110mm	n/a
Fan Diameter	11	cm
Weight	759	gr
Thrust	5.23	kgf
Torque	1.01	Nm
Watt	3063	W
Total Cost	490	€

There will be no change in the simulation pitch angle due to the use of coaxial propeller. The pitch angle obtained for option 5 is given in figure 3.67 below.

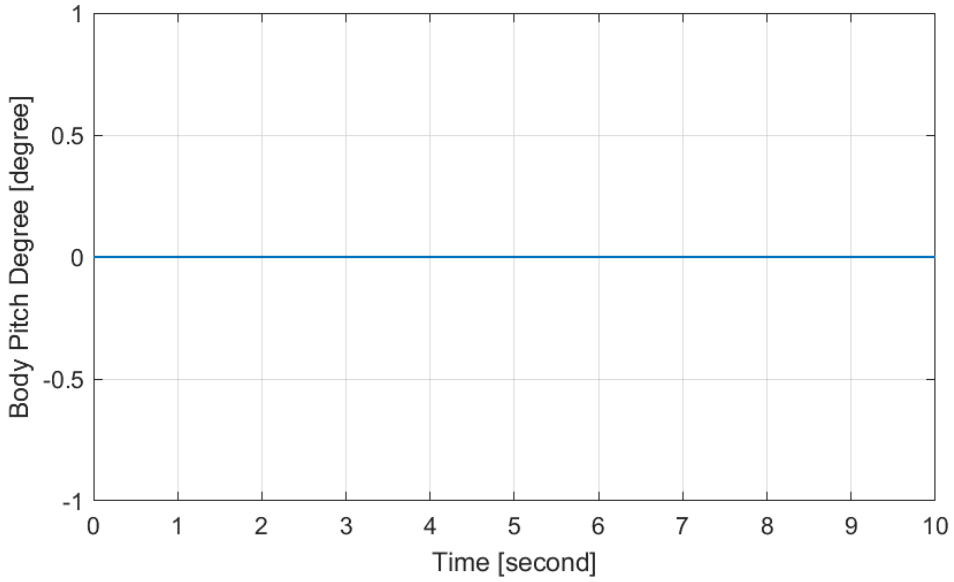

Figure 3.67. Pitch angle of the body for Option-5

Since the pitch angle does not change throughout the simulation, the robot will not have any force on the x-axis and will not make any displacement in the x-axis throughout the simulation. This displacement can be seen in figure 3.68.

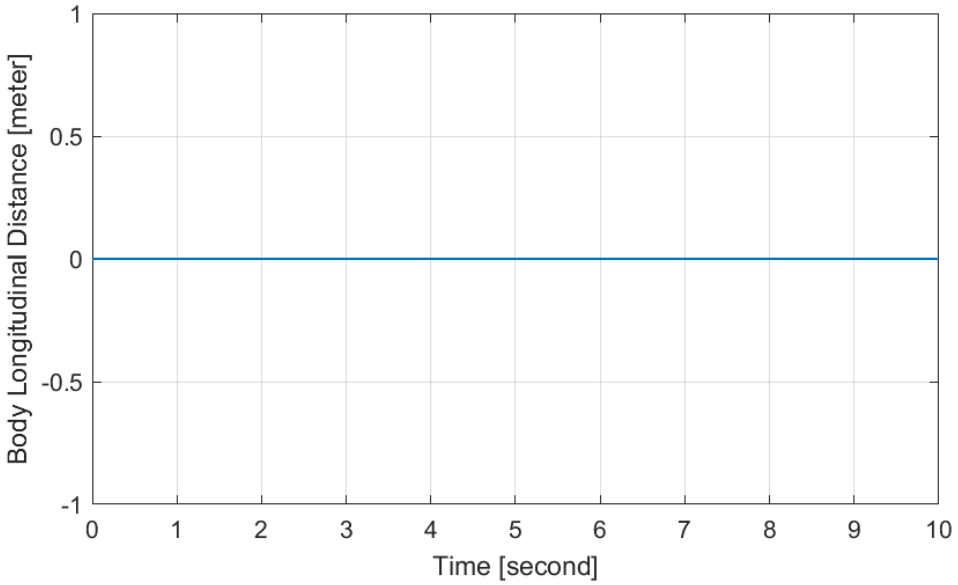

Figure 3.68. Body displacement in x axis for Option-5

Subsequently the thrust force produced by the electric ducted fan was only on the y-axis throughout the simulation, the robot moved only on the y-axis. The body acceleration and

body velocity graphs that provide this movement are given in figures 3.69 and 3.70, respectively.

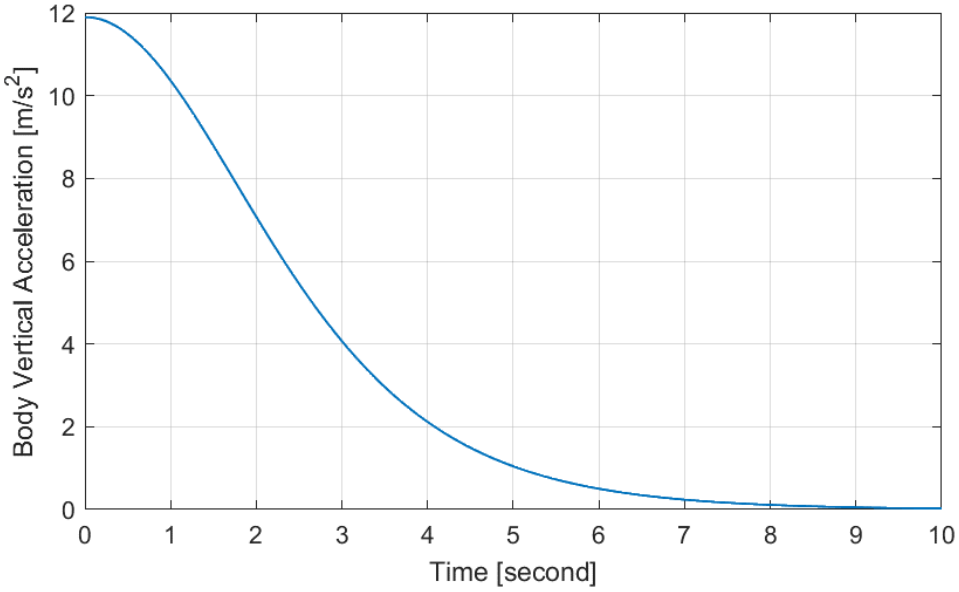

Figure 3.69. Body acceleration in y axis for Option-5

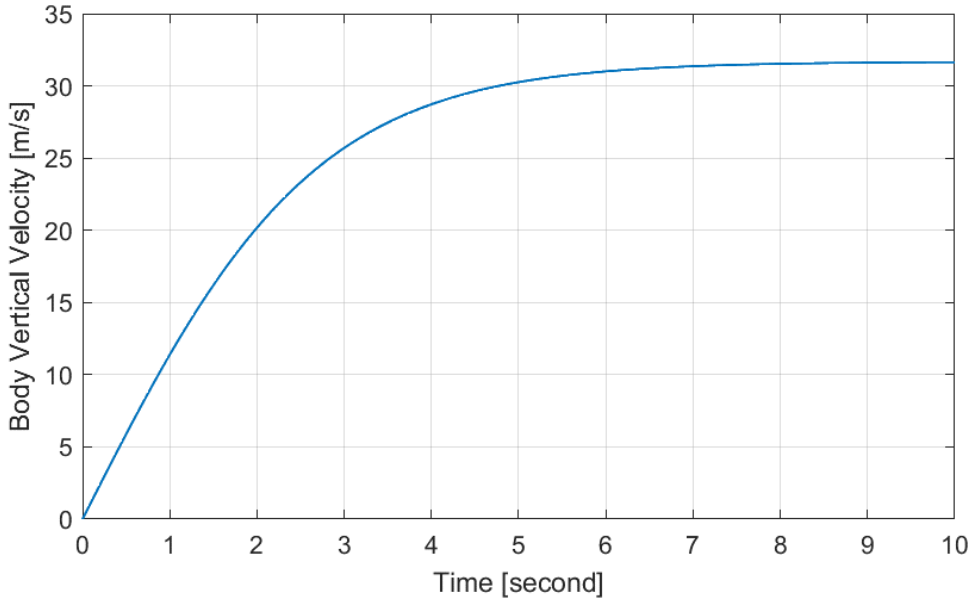

Figure 3.70. Body velocity in y axis for Option-5

The taken displacement by the robot on the y-axis according to the body acceleration and body velocity values taken for option 5 is given in figure 3.71.

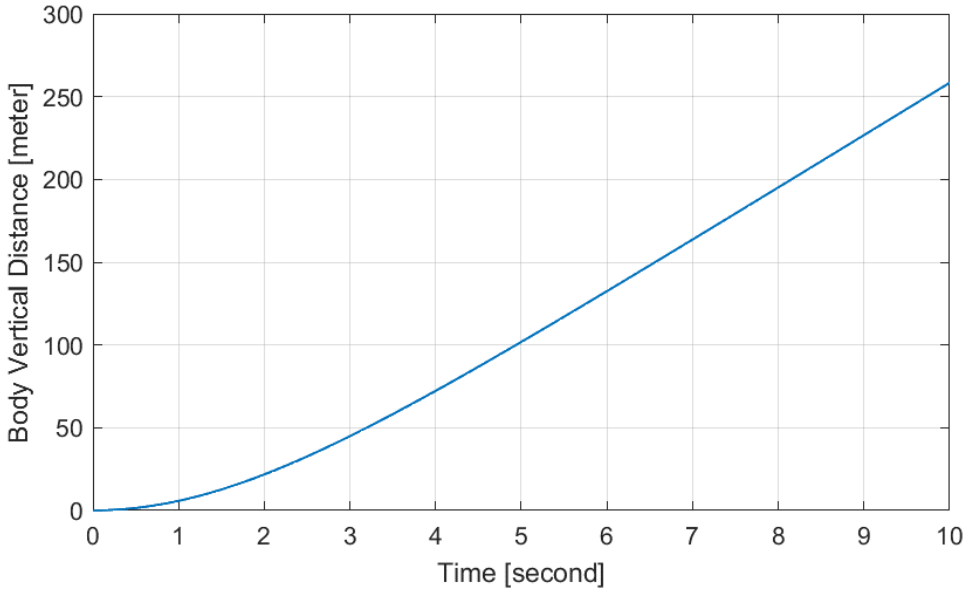

Figure 3.71. Body displacement in y axis for Option 5

The drag force that resets the acceleration and affects the robot towards the end of the simulation for option 5 is given in figure 3.72.

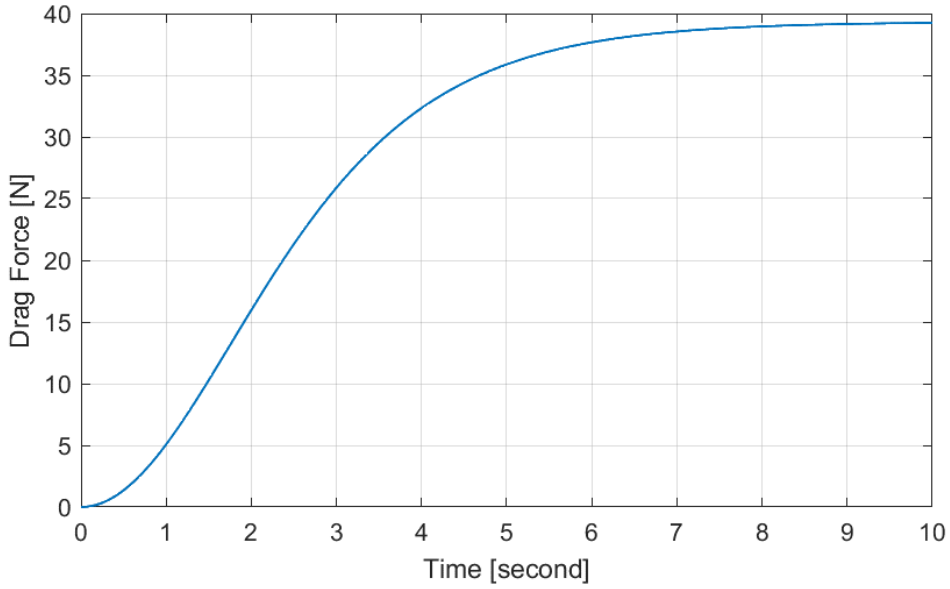

Figure 3.72. Drag Force in y-axis for Option-5

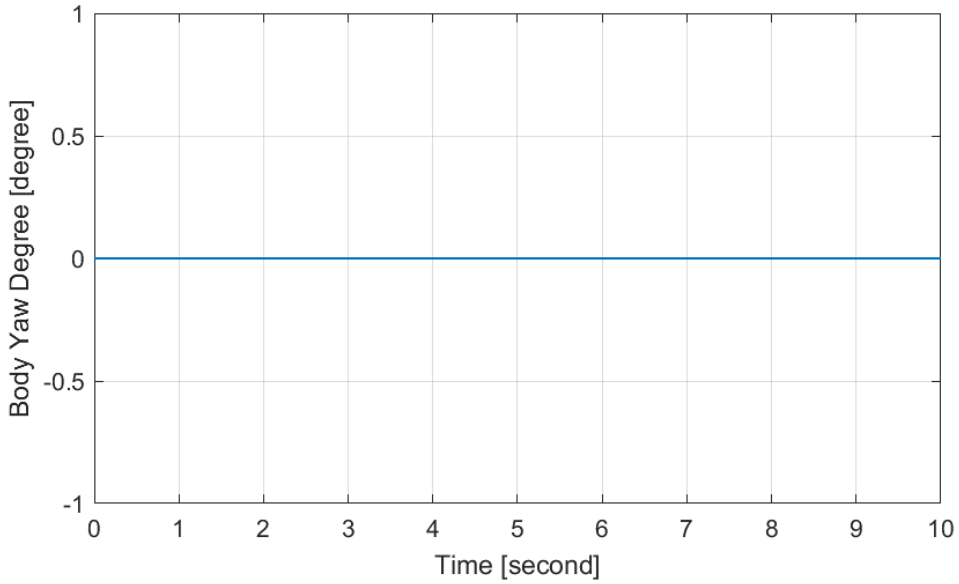

Figure 3.73. Yaw angle in y axis for Option-5

Since contra-rotating propellers were used, there was no change in the yaw angle throughout the simulation. The graph showing the yaw angle is given in figure 3.73.

In the electric ducted fan analysis, a system that produces high thrust was selected for option 5, and a system that produces less thrust but smallest size and lightest will be used for option 6. The system selected for option 6 is given in table 3.8.

Table 3.8. Electric Ducted Fan Option 6 Parameters [25]

Parameters	**Value**	**Unit**
Motor Name	HET 700-68-1200Kv	n/a
Fan Name	EDF Schubeler DS-51-AXI 90mm	n/a
Fan Diameter	9	cm
Weight	407	gr
Thrust	4.2	kgf
Torque	0.69	Nm
Watt	2890	W
Total Cost	340	€

Since the blades in the system are installed coaxial in option 6, as in option 5, there will be no change in both the pitch and the body displacement it takes in the x-axis throughout the simulation. The graphs of the pitch and the body displacement it takes on the x-axis are given below in figures 3.74 and 3.75, respectively.

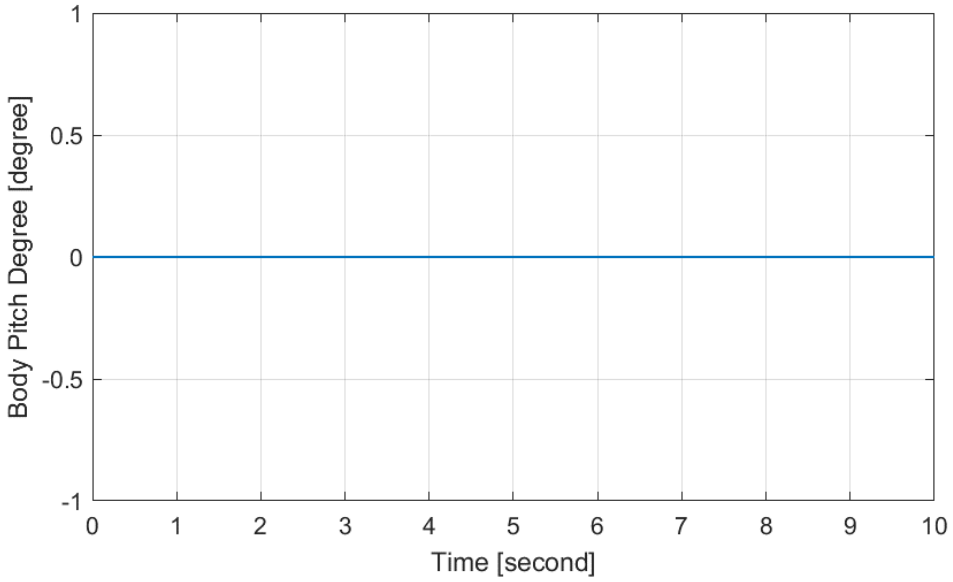

Figure 3.74. Pitch angle of the body for Option-6

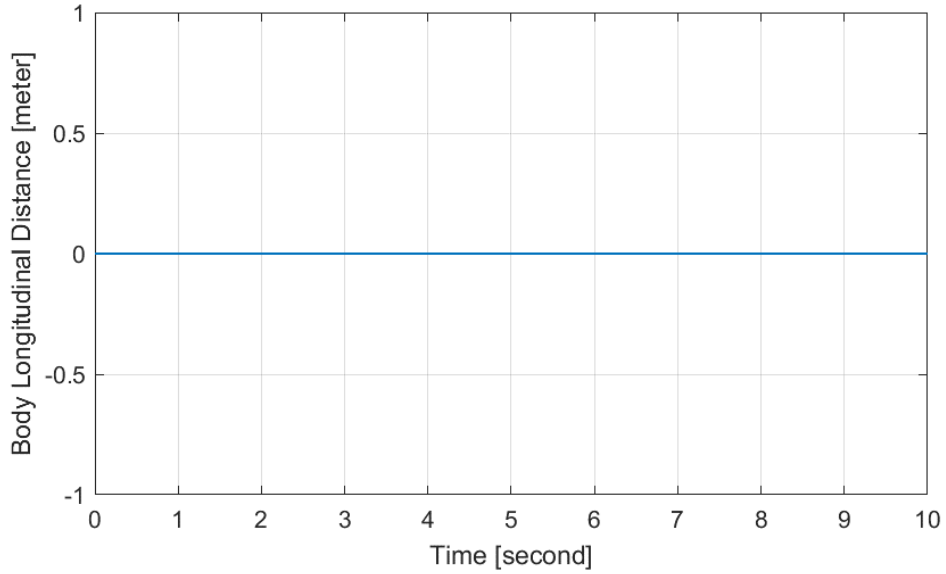

Figure 3.75. Body displacement in x axis for Option 6

The body acceleration, body velocity and body displacement graphs created by the robot on the y-axis of the thrust produced by the system used in option 6 are given below in figures 3.76, 3.77 and 3.78, respectively.

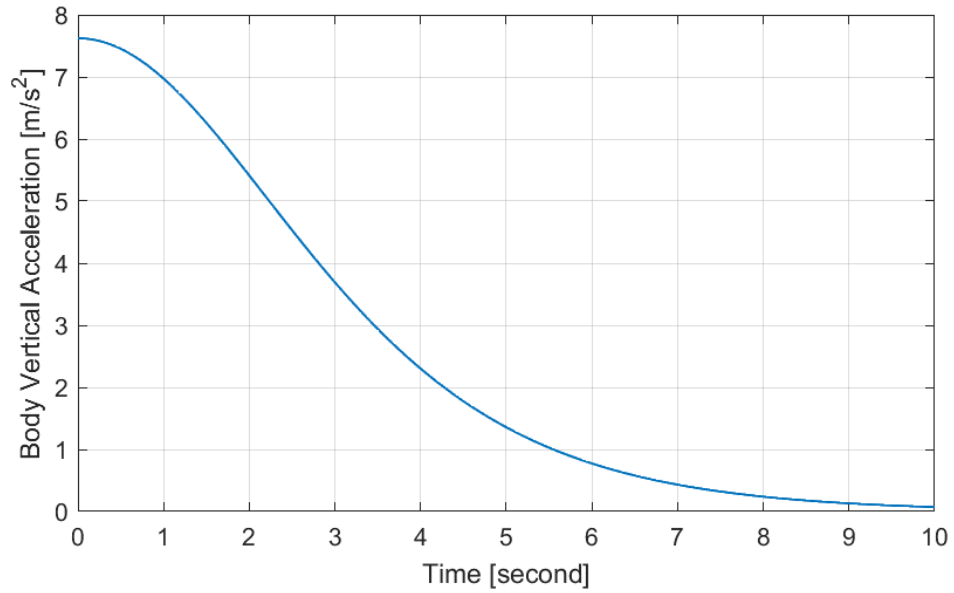

Figure 3.76. Body acceleration in y axis for Option 6

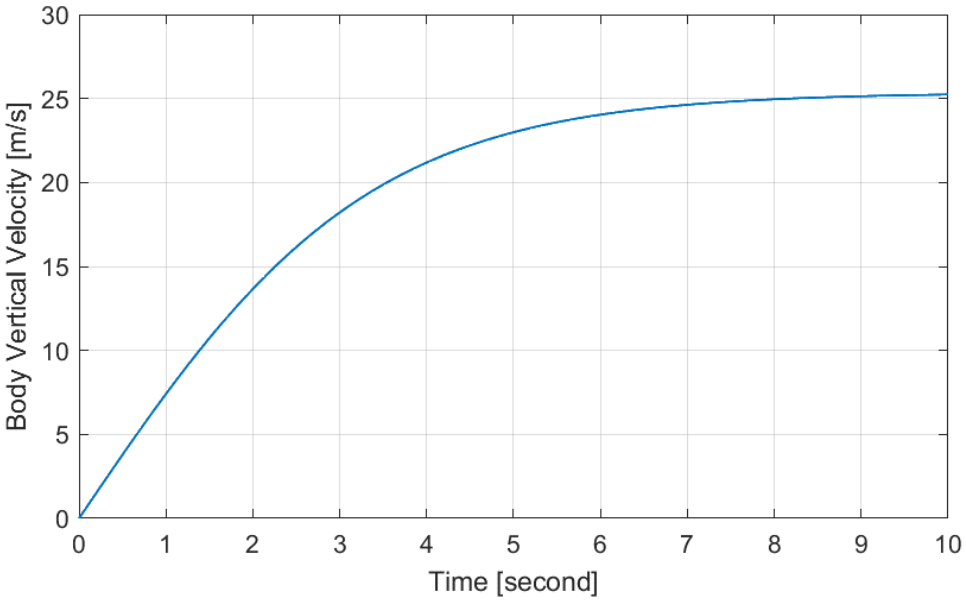

Figure 3.77. Body velocity in y axis for Option-6

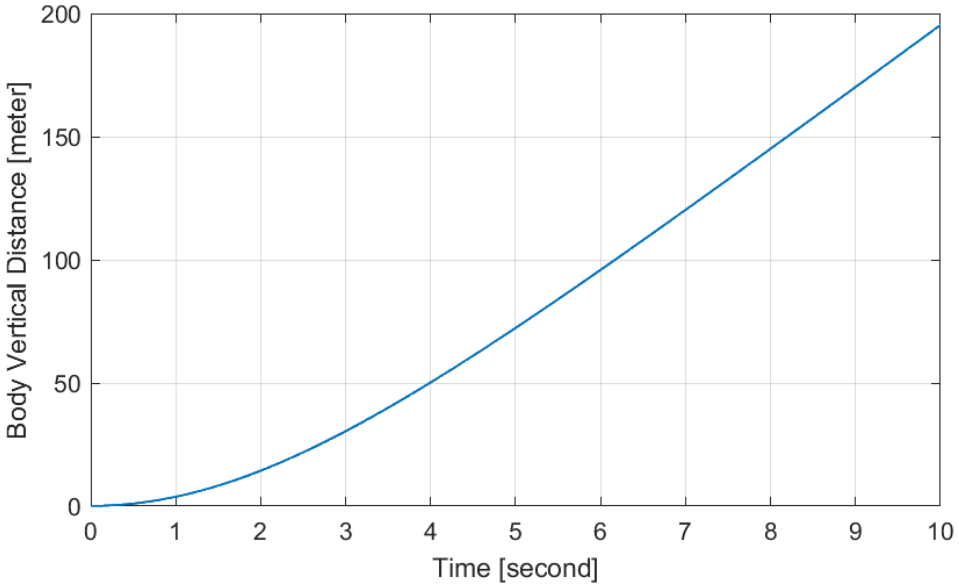

Figure 3.78. Body displacement in y axis for Option-6

The drag force acting on the robot in the simulation for option 6 is shown in figure 3.79.

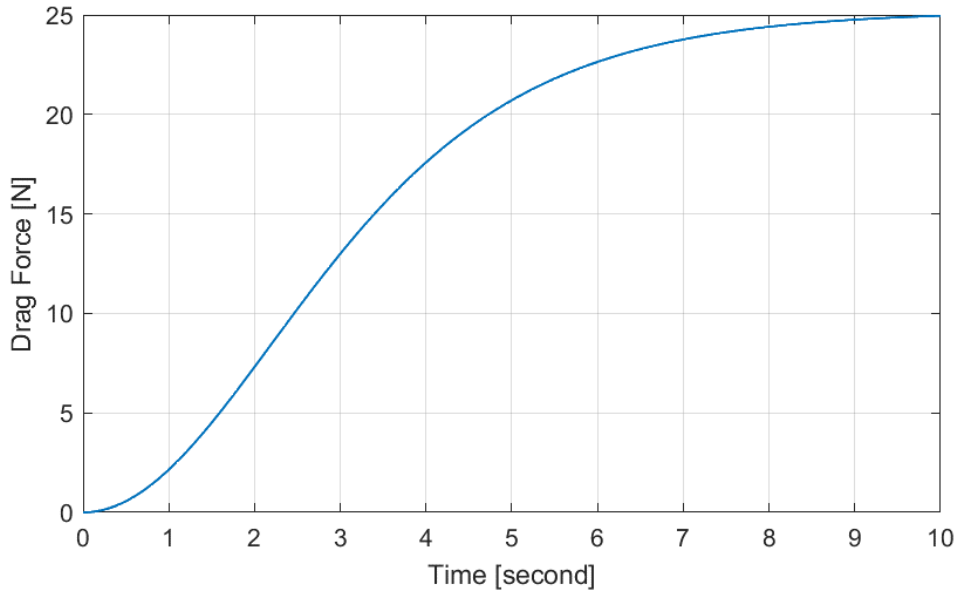

Figure 3.79. Drag Force in y axis for Option-6

Since contra-rotating propellers were used again for option-6, there was no change in the yaw angle throughout the simulation. The graph showing the yaw angle is given in figure 3.80.

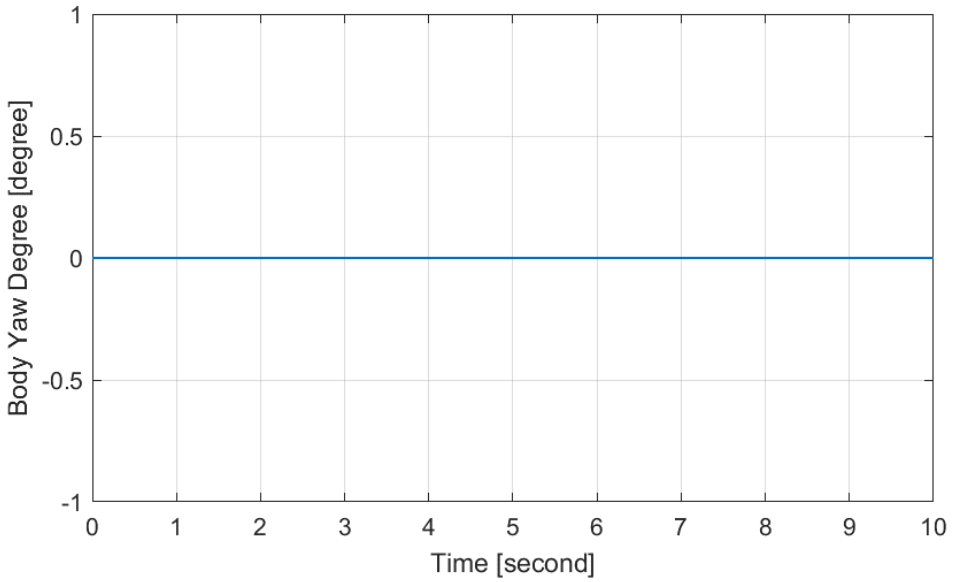

Figure 3.80. Yaw angle in y axis for Option-6

In option 7, which is the last option for the electric ducted fan, unlike the first two systems, the cheapest system was chosen. The specifications of the selected system are given in table 1.

Table 3.9. Electric Ducted Fan Option 7 Parameters [26]

Parameters	**Value**	**Unit**
Motor Name	Hacker E50L 1,5Y 1070Kv	n/a
Fan Name	EDF Hacker Stream-Fan 100	n/a
Fan Diameter	10	cm
Weight	560	gr
Thrust	5.1	kgf
Torque	0.85	Nm
Watt	3256	W
Total Cost	262	€

In option 7, both pitch angle body displacement in x axis and yaw angle take zero values throughout the simulation due to the coaxial mounted and counter-rotating propellers. Graphs showing pitch angle, body displacement in x axis and yaw angle are shown below in figures 3.81, 3.82 and 3.83 respectively.

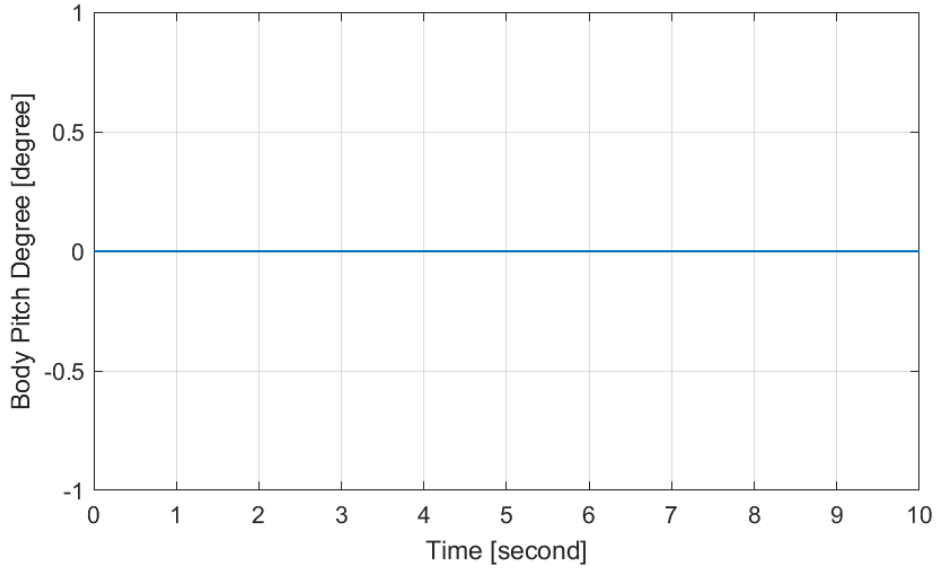

Figure 3.81. Pitch angle of the body for Option-7

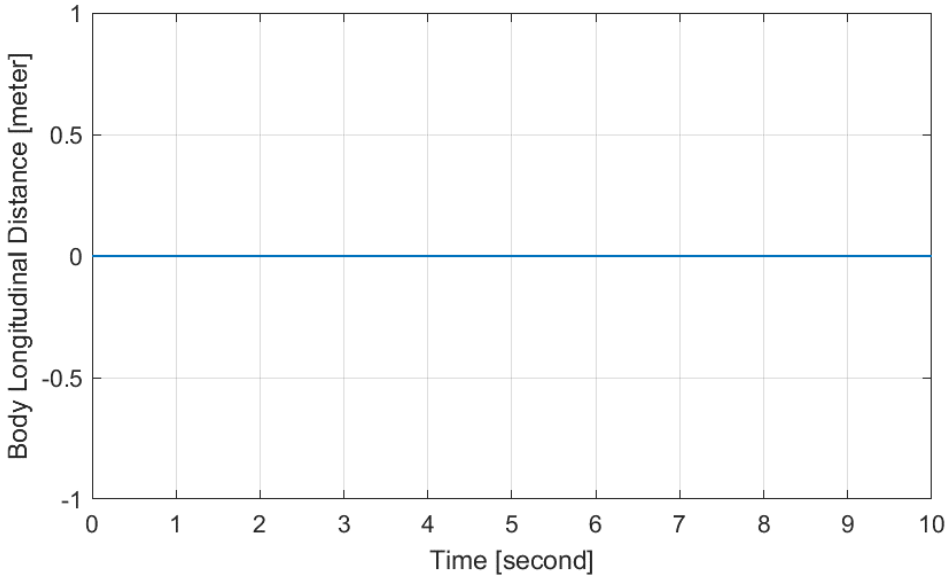

Figure 3.82. Body diplacement in x axis for Option-7

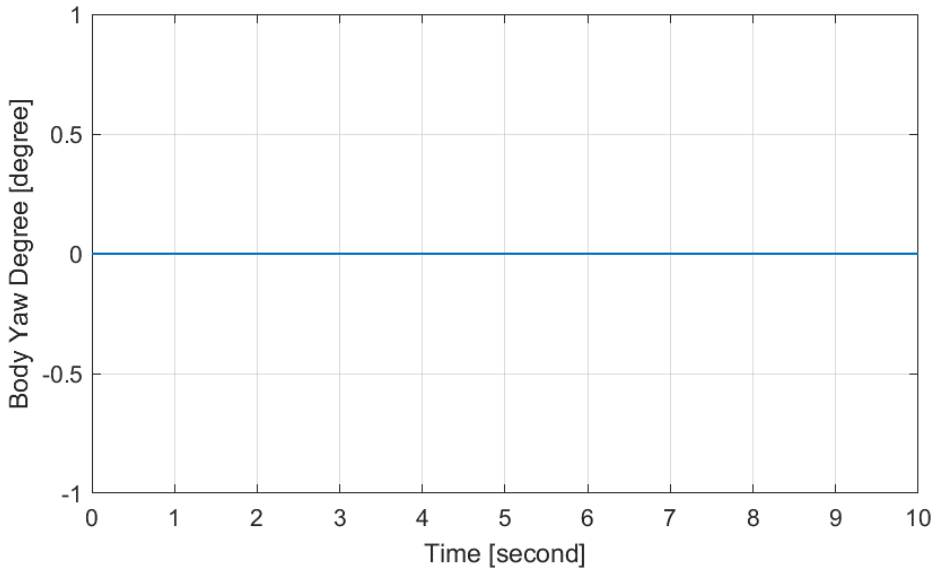

Figure 3.83. Yaw angle of the body for Option-7

Although less thrust was produced in option 7 than the thrusts obtained in option 6 and option 5, this thrust was greater than the weight of the robot, so the robot lift to the air. Acceleration, velocity and displacement graphs for the y-axis in the simulation are given in figures 3.84, 3.85 and 3.86, respectively.

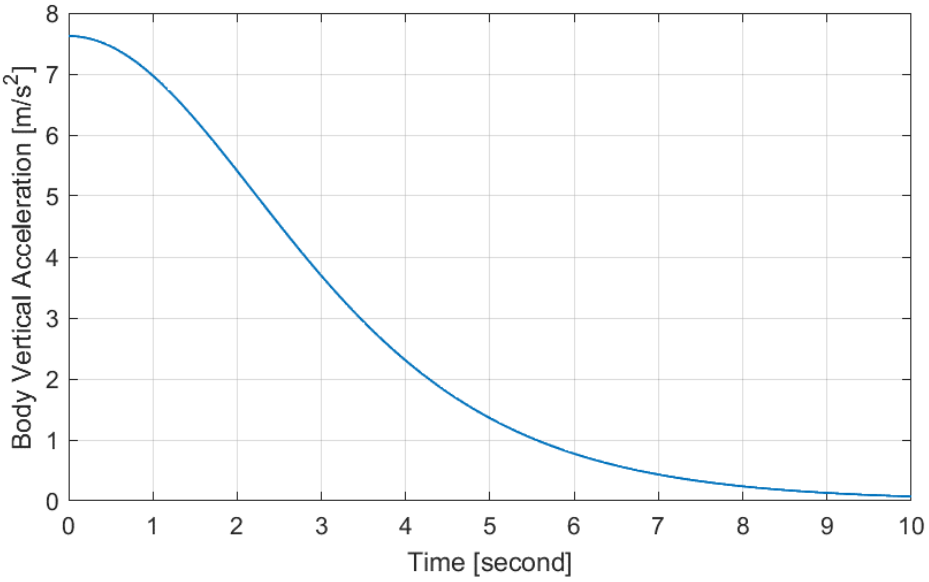

Figure 3.84. Body acceleration in y axis for Option-7

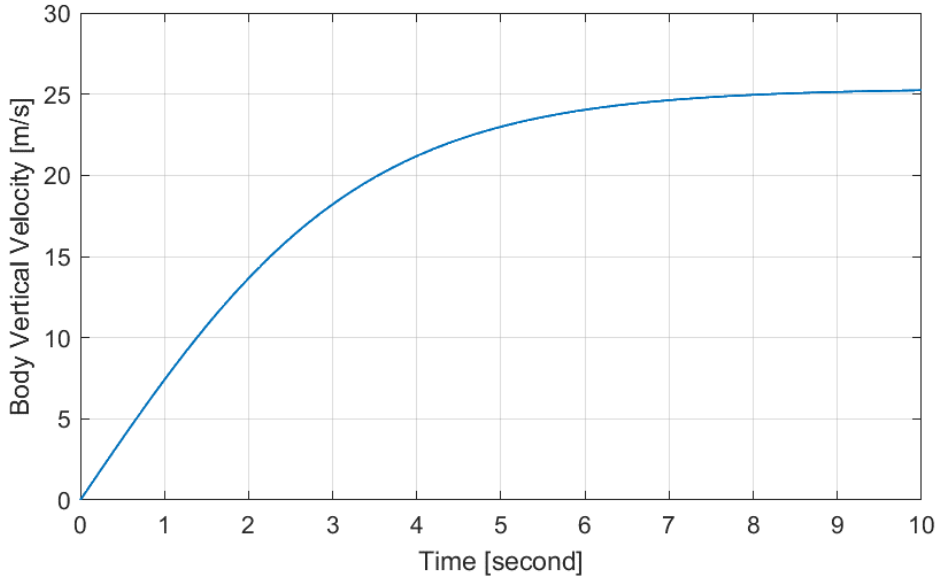

Figure 3.85. Body velocity in y axis for Option-7

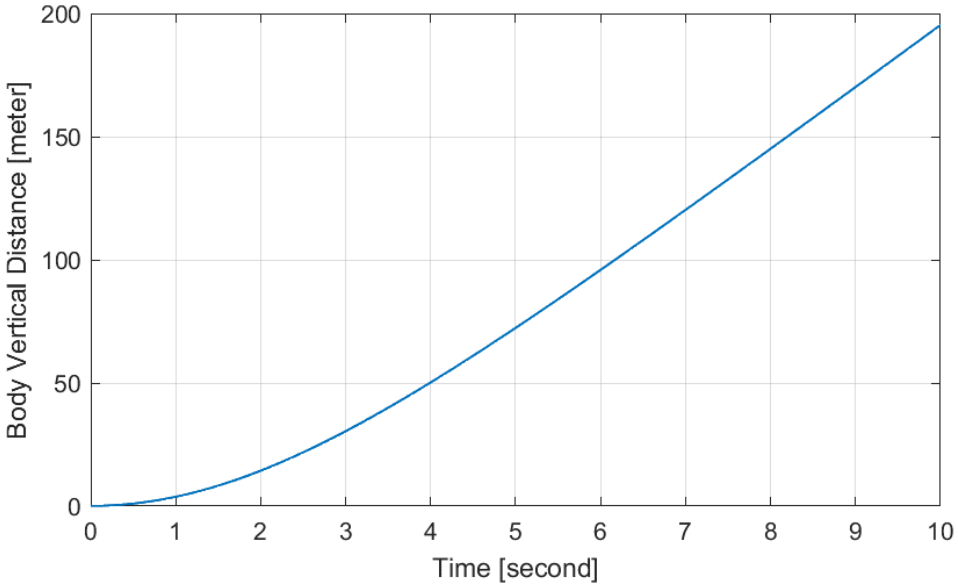

Figure 3.86. Body displacement in y axis for Option-7

Since less thrust is produced in option 7 compared to other ducted fans, the drag force acting on the robot will be less compared to other simulations. The drag force acting on the robot in the simulation for option 7 is shown in figure 3.87.

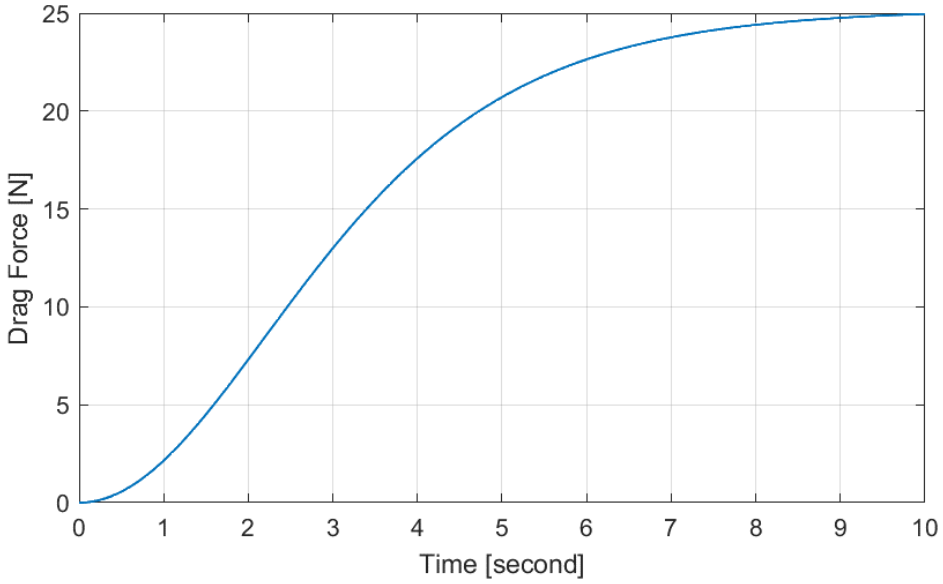

Figure 3.87. Drag Force in y axis for Option-7

3.3.6.1. Simulation Results of Electric Ducted Fan

The electric ducted fan produces much more thrust than the propeller approach. It is also dimensionally more suitable for the rhex robot. Ducted fan, which does not create any yaw angle problems due to the internal propellers installed in a contra-rotating manner, is a much more suitable choice than propellers due to these features.

Since mission simulations within the scope of this thesis will not be long-term operations, although the electric ducted fan is less efficient than the propeller in terms of consuming energy and battery life, it will still have the capacity to complete the task.

3.4. Battery Performance

In this thesis, appropriate battery selection will be made to determine the task duration in mission simulations for the hybrid rhex robot. The method to be used to calculate battery performance is explained in section 3.4.1

3.4.1. Battery Duration Calculation

To calculate battery life, you must first find the current the motor will draw. To find this current, the "Kv" value given by the motor manufacturer is required. This "Kv" value is

also called "RPM Constant". The Kv value indicates the RPM that will occur at full throttle when the input voltage is applied to the motor at no load.

“Kt” value is needed to find the current drawn. "Kt" means It is how much current the motor will draw instantly depending on the torque. The "Kt" value is found from the "Kv" value received from the engine manufacturer. The relationship between Kt and Kv is given in equation 50 below.

$$Kt = \frac{1}{Kv} \tag{50}$$

After finding the “Kt” value, the torque value coming from the motor and the current drawn by the motor at full throttle are calculated from the equation 51 below.

$$Current = \frac{Torque}{Kt} \tag{51}$$

Using these two equations, it can be determined how much current the motor to be used will draw. After finding the current, battery life can be found along with the battery capacity. Battery life calculation equation 52 is given below.

$$Battery\ Life = \frac{Battery\ Capacity}{Consumpiton} \times (1 - Discharge\ Safety) \tag{52}$$

Discarge safety value given from battery manufacturer. Generally, discharge safety is 20% and higher for Lipo type batteries. The battery life of the batteries to be selected in the next section will be calculated according to the calculations explained in this section.

The electric ducted fans to be used in mission simulations were selected with batteries with recommended specifications determined by the manufacturer, and their dimensions were determined to fit into the hybrid rhex robot. In research, electric ducted fans used in option 5-6-7 are generally recommended together with batteries with 5s-18.5v and 6s-22.2v lipo and average discharge rate. Based on this suggestion, three batteries with different capacities, weights and costs were determined.

The purpose of this section is to determine an average duty time by researching suitable batteries. The weights of the batteries will be added to the model in the mission simulations. Also, inertia of the batteries will be calculated for each battery seperetely.

3.4.2. Batteries

The first battery was specified to have low weight and cheaper. Thus, it can work with a motor and ducted fan that will consume less energy. First battery selection is shown in table 3.10.

Table 3.10. Battery Number 1 Specifications [27]

Parameters	Value	Unit
Battery Name	Overlander 18.5V 5S 35C LiPo	n/a
Weight	320	gr
Battery Capacity	2900	mAh
Battery Dimension	103x33x42	mm
Cost	57	€

In the second battery selection, the weight and capacity of the battery were chosen to be greater. At the same time, dimensionally limit values were not exceed . Table 3.11 showing the characteristics of the second battery is given below.

Table 3.11. Battery Number 2 Specifications [28]

Parameters	Value	Unit
Battery Name	Gens ace 2800mAh 6S 22.2V	n/a
Weight	410	gr
Battery Capacity	2800	mAh
Battery Dimension	117x35x49	mm
Cost	80	€

In the last battery selection, the battery capacity was determined to be maximum. However, high battery capacity creates dimensional problems. Extra space is required to fit this battery into the hybrid robot. The characteristics of the battery selected as the third option are given in table 3.12.

Table 3.12. Battery Number 3 Specifications [29]

Parameters	**Value**	**Unit**
Battery Name	6s 5000 mAh Black Lithium	n/a
Weight	507	gr
Battery Capacity	5000	mAh
Battery Dimension	136x45x41	mm
Cost	124	€

The calculated inertia table of the above mentioned batteries is given below table 3.13. Since the values found are approximately 200 times lower than the inertia of the robot that is given in table 3.2, these inertia values will not be added to the hybrid model.

Table 3.13. Batteries Inertia Values

	Battery Number 1	**Battery Number 2**	**Battery Number 3**
Body Inertia in y axis (kgm^2)	0.0000329946	0.000054974167	0.000085247825
Body Inertia in z axis (kgm^2)	0.0000311946	0.000050956167	0.000086701225

3.5. Selection Setup

In this section, the most appropriate setup for mission simulations will be selected. In previous analyses, it was seen that electric ducted fan was more suitable to provide the necessary thrust. The use of electric ducted fan will be coaxial contra rotating, as stated in previous simulations. However, the duration of mission simulations will be determined by the battery to be installed. The maximum duty time of the engine operated at full power

will be calculated using the calculation method described in Section 3.4.1. The results of this calculation are seen in table 3.14.

Table 3.14. Batteries Endurances with Different EDFs in seconds

	Option 5 EDF	**Option 6 EDF**	**Option 7 EDF**
Battery Number 1	not suitable	67	60
Battery Number 2	77	not suitable	not suitable
Battery Number 3	138	not suitable	not suitable

As seen in Table 3.14, it is calculated that the robot has a short flight capability of at least 1 minute in mission simulations. When cost analysis is made, option-6 and battery number 1 appear as the cheapest options. Also, option-6 and battery number 1, are also dimensionally suitable and also the lightest option. The selection setup specifications can be seen in table 3.15 that is given below.

Table 3.15. Selection Setup Properties

Parameters	**Value**	**Unit**
Motor Name	HET 700-98-670Kv	two piece
Fan Name	EDF Schubeler DS-51-AXI 90mm	two piece
Battery Name	Overlander 18.5V 5S 35C LiPo	two piece
Total Weight	4.52	kg
Thrust Capacity	5.88	kgf
Mission Time	67	seconds
Total Cost	454	€

3.6. Hybrid Model

The hybrid model was created by running the ground model that is describe in section 3.2 and the flight model that is explained section 3.3 together. The main task of the hybrid model will be to perform the 2 tasks selected in this thesis. The first task is to cross a pond with a width of more than 5 meters. The second task will be to climb over a 7-meter-tall vertical obstacle that is impossible to climb with only using legs To fully perform these tasks, a pitch angle controller has been added to the hybrid model. By installing a PD controller, the pitch angle can be controlled in the flight phase. PD controller details can be seen APPENDIX C. The hybrid model created in SIMULINK can be seen in figure 3.88

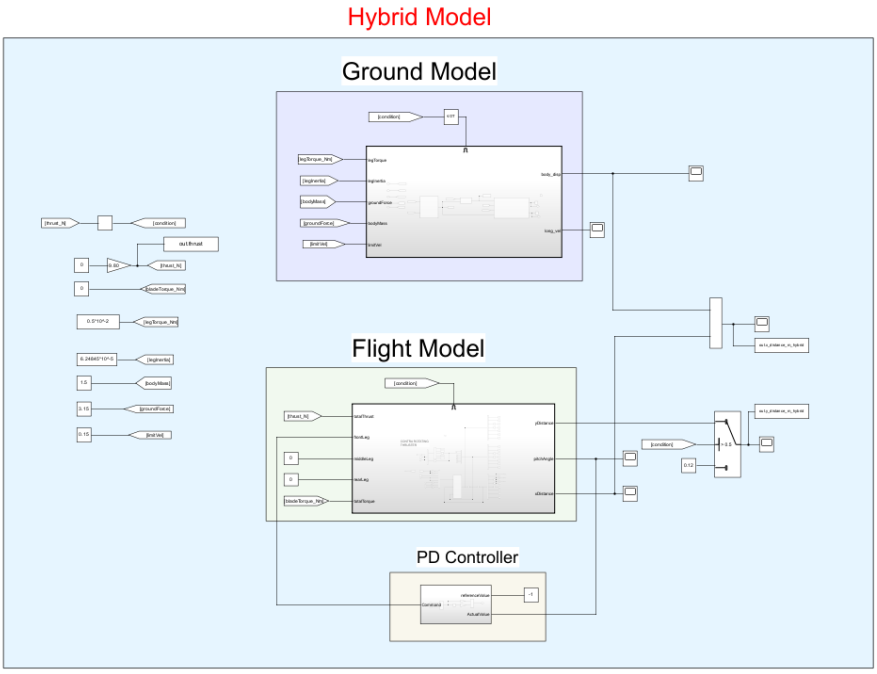

Figure 3.88. Hybrid Model Structure in SIMULINK

3.7. Conclusion

This section explains how the land and flight models to be used in mission simulations are made. Independent simulations were conducted to assess the suitability of two different models for mission simulations. In addition, various thrust options were tested, as this is a critical aspect of flight simulation. The first option tested was propellers, with the positioning of the propeller(s) being evaluated to determine the most appropriate option. Coaxial contra-rotating propellers were found to be the most suitable option for

the robot in mission simulation, based on these tests. However, either the propellers were insufficient to produce the required thrust, or they were too large to fit inside the robot. Consequently, electric ducted fan options were evaluated for coaxial contra-rotating thrust, and the desired results were achieved in terms of both dimension and thrust production. Afterward, battery options are presented for the electric ducted fan to produce this thrust. The flight time of these batteries working together with the electric ducted fan was calculated. In the cost analysis and dimensional section, a comprehensive evaluation was carried out to determine the most suitable setup. Following this selection, a hybrid model was developed, and a proportional-derivative (PD) controller was incorporated into the flight segment. The hybrid model and the chosen configuration established in this section will be employed in upcoming mission simulations.

4. SIMULATION RESULTS

4.1. Introduction

In this section, mission simulations will be performed with the selected setup. Mission simulations will take two different forms. The first task will be to cross a 5-meter water pound with a short flight. The second task will be to climb over a 7-meter vertical obstacle with a short flight. In the second task, the Rhex robot will stop before taking off for a short flight. Therefore, when it takes a short flight, it will move forward by changing the pitch angle to make a forward movement. The PD controller is integrated into the mathematical model to adjust this pitch angle. To do this, the robot will rotate in the z-axis direction with the torque input given to the front leg and the torque created in the front leg. As a result of these flights, it will be clear whether the short-flight Rhex robot designed for this thesis will succeed in the mathematical model's development environment.

4.2. Mission Simulation 1 (Water Pound)

In the first mission, the aim will be to cross a 5 meter wide water pound with a short flight. In order to achieve this crossing, the robot will activate the propulsion system while it is moving on the ground and the puddle will be crossed with the existing forward speed.

The first mission results of the hybrid model are given below. The first graph that is figure 4.1 shows the path it takes in the x direction.

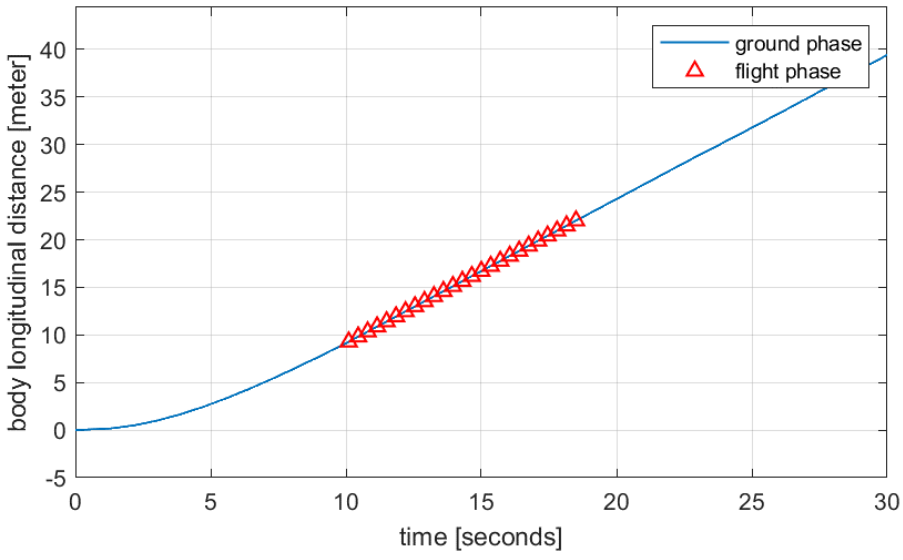

Figure 4.1. Body displacement in x-axis mission simulation 1

In figure 4.1, the robot remained in the air for approximately 8 seconds and covered a distance of 12 meters in this section. This is enough to cross 5 meters of water.

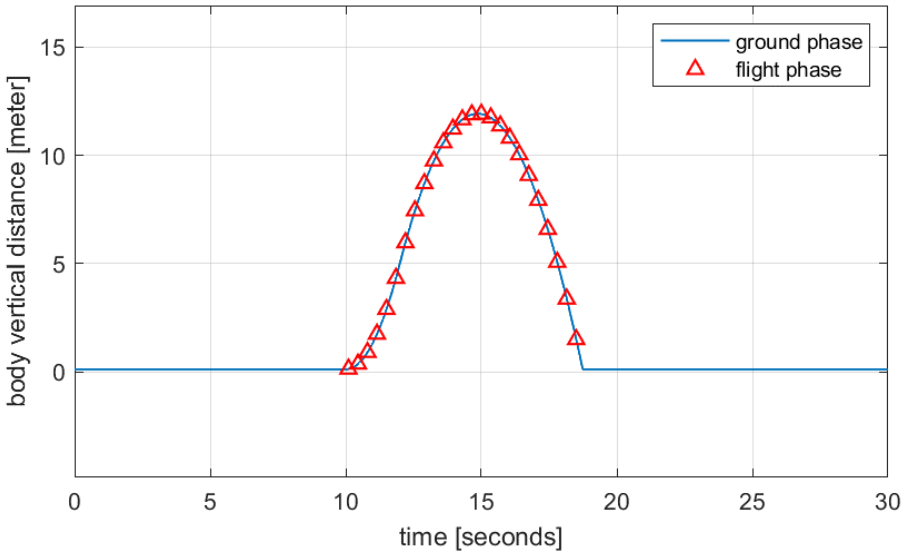

Figure 4.2. Body displacement in y-axis mission simulation 1

Figure 4.2 shows that the robot makes a short flight between 10 and 18 seconds. At its maximum point, it reached a height of more than 10 meters.

The distence taken in both y and x directions throughout the task is given in figure 4.3. According to this graph, the robot can cross 5 meters wide water pound with its short flight ability.

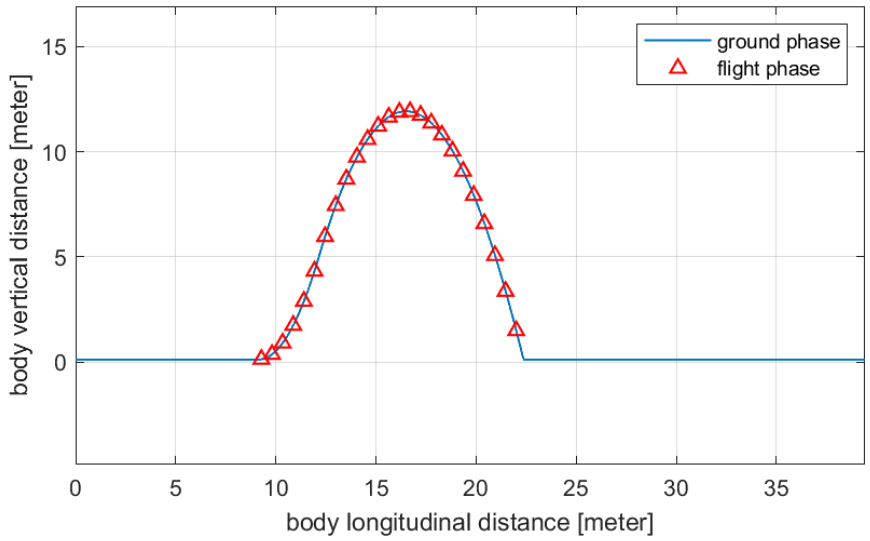

Figure 4.3. Total displacement during mission simulation 1

The thrust given to the robot throughout the simulation is given in figure 4.4

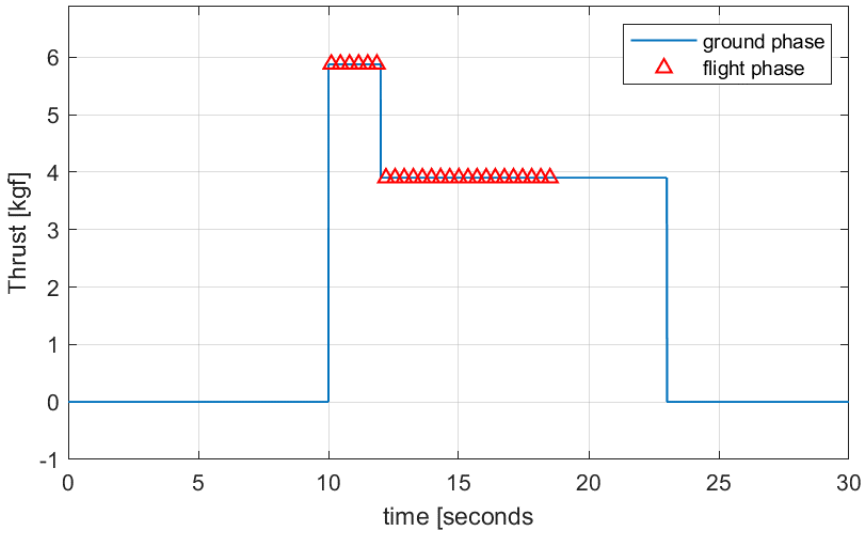

Figure 4.4. Thrust input during mission simulation 1

With the selected setup, the hybrid mathematical model has successfully completed the first task. In the second mission, Rhex robot will try to overcome a 7 meter long vertical obstacle.

4.3. Mission Simulation 2 (Obstacle)

In the second mission, the aim will be to climb a 7-meter-long vertical obstacle with a short flight. To ensure this transition, the Rhex robot will be in a standing position on the ground and after taking off, the pitch angle will be adjusted with the help of the controller. With the pitch angle change, the robot moving in the x direction will climb over the 7-meter obstacle.

The first figure that is figure 4.5 shows the path taken by the Rhex robot in the x direction. It seems that the forward path after take-off increases linearly with the change of pitch angle.

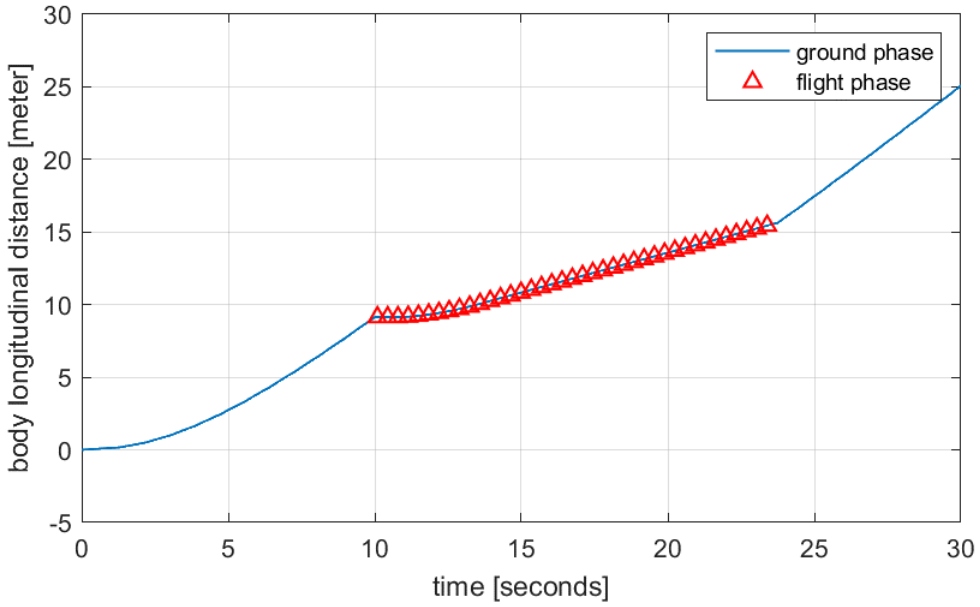

Figure 4.5. Body displacement in the x-axis mission simulation 2

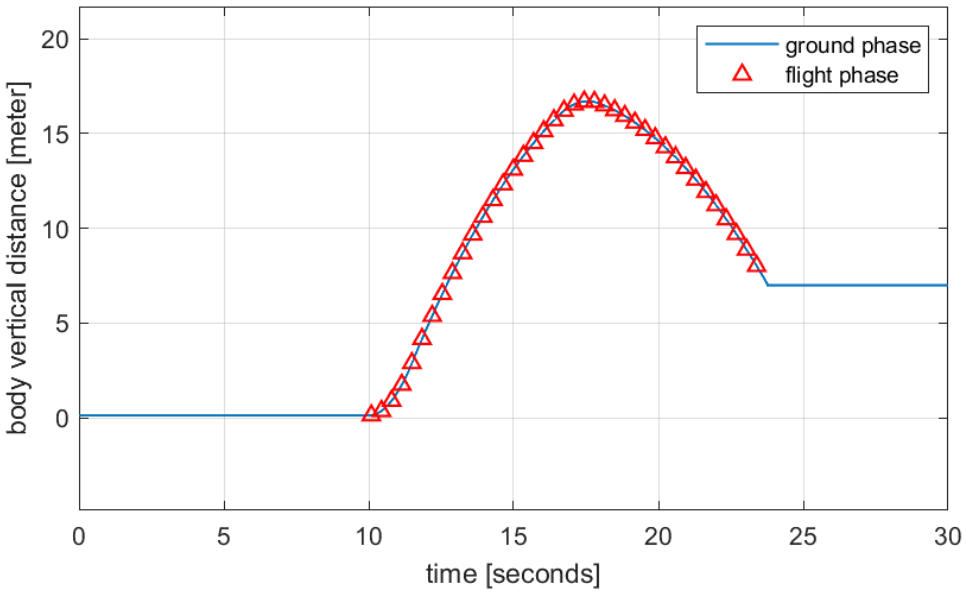

Figure 4.6. Body displacement in the y axis mission simulation 2

Figure 4.6 shows the path it took in the y direction during the second task. At the end of the flight phase, it is seen that it climbs above the 7-meter obstacle.

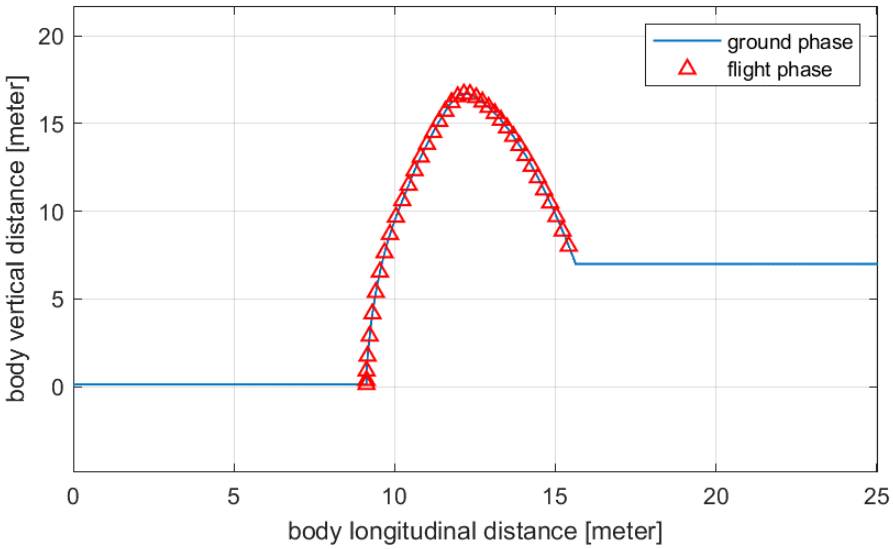

Figure 4.7. Total displacement during mission simulation 2

Figure 4.7 shows that when the Rhex robot starts flying, it does not travel in the x direction. Then, with the help of the controller, the Rhex robot moved in the x direction at the time of flight with the change in pitch angle. The pitch angle throughout the simulation is seen in figure 4.8.

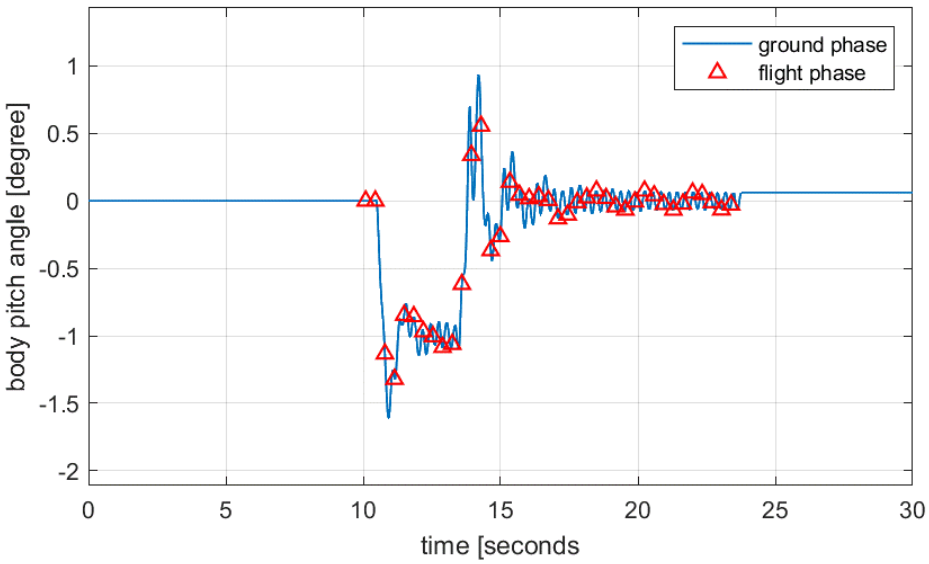

Figure 4.8. Body pitch angle during mission simulation 2

Finally, the thrust system input for the second mission is seen in Figure 4.9.

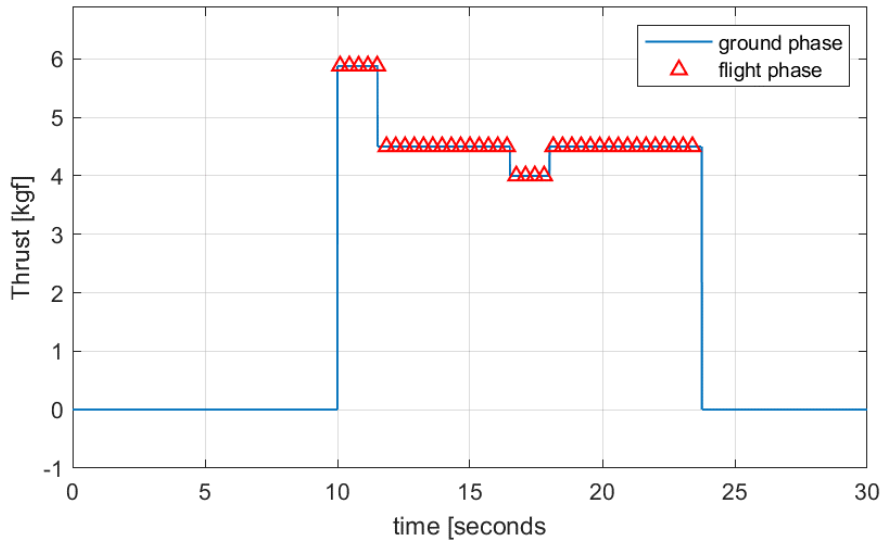

Figure 4.9. Thrust input during mission simulation 2

With the selected setup, the hybrid mathematical model has successfully completed the second task. Thus, the hybrid mathematical model successfully completed both tasks.

4.4. Conclusion

This section performed two specified tasks with the hybrid model with the selected setup. The first task is to cross this water pound, which is 5 meters wide, with a short flight by activating the propulsion system while the robot moves on the ground. The second task is to climb over a 7-meter-long vertical obstacle while it is not in motion by activating the propulsion system and changing the pitch angle with the help of the controller, allowing it to travel in the x direction. According to the results, the hybrid model prepared in this thesis has completed both tasks. The hybrid model is created by combining the flight model and ground model. The hybrid mathematical model successfully completed different types of tasks both in motion and stationary.

5. CONCLUSION

5.1. Conclusion

In this thesis, parametric design evaluation of a hybrid rhex robot was made. The hybrid rhex robot has a thruster for short flights. It also has c-type legs so it can locomate on the ground. In this thesis, these two types of motion were modeled and critical design parameters were investigated.

Rhex robot is a land robot with c type legs, produced for the purpose of traveling on land in difficult terrains and conditions. Although it can move successfully on many difficult surfaces, its mobility is limited in some more challenging conditions, such as ravines. In order to overcome these difficult conditions, a propulsion system was proposed to be on the rhex robot, allowing it to make short flights. With this short flight ability, it can continue its movement on many difficult surfaces or obstacles without any problems. In order to build this hybrid model, the ground model was created first. The ground model is based on the "spring loaded inverted pendulum" model. Thus, the land movement of the robot is provided mathematically. A flight model was developed to model the short flight phase. Along with the flight model, the dynamics of the robot in the flight phase were modeled and its movement during the flight was analyzed mathematically. The hybrid model is created by combining these two models. Thus, the mathematical model of the hybrid Rhex robot, which can move both on land and in the air, is presented.

With the emergence of the flight model, the most appropriate propulsion system was selected. For the selection of this propulsion system, normal propeller usage was first tested. Different sizes and different installation methods for propellers are discussed. The most appropriate installation method has been determined. This shape was found as "co-axial contra rotating". However, the propellers could not produce enough thrust to lift the robot the size of the robot used in the thesis. The propellers that produced sufficient thrust were much larger in size than the hybrid rhex robot. Therefore, the "electric ducted fan" system, which is a system that is smaller in size and can produce enough thrust, was tested with the flight model. As a result of the tests, it was seen that EDFs did not cause any problems in terms of both dimensionality and thrust production. Batteries were selected that could work properly with EDFs and would not cause any dimensional problems. By

comparing batteries and EDFs, the most suitable configuration was selected both in terms of dimension and energy.

Mission simulations were performed using the selected system configuration of the hybrid model. Two mission simulations were determined in the thesis. The first task was for the Rhex robot to cross a 5-meter-wide pond.. The second task was to overcome a 7-meter-high vertical obstacle. In the simulations, the hybrid robot successfully completed both tasks with the selected system configuration.

The main contribution of this thesis to the literature is the creation of a hybrid model by considering both the land and flight models together and the determination and selection of design parameters for the flight phase.

5.2. Future Works

The results of this thesis will form the basis for the development of a prototype for further investigation of enhancing the mobility of hybrid Rhex robot. Possible future inculude;

- Development of a 3D mathematical model which includes roll motion and coupled dynamics. Such a model will not only be able to simulate the hybrid Rhex robot more realistically but also will enable development of better controllers.
- A better terrain model to analyze the harsh conditions more reallistically, which would allow development of decision making algorithms to autonomously switch between land and air modes.
- Production of the prototype system.

REFERENCES

[1] O. Gültekin, MODELLING AND ANALYSIS OF LEGGED ROBOTS WITH TEMPORARY FLIGHT CAPABILITIES, Hacettepe University, 2023.

[2] U. Saranli, M. Buehler, D.E. Koditschek, RHex: A Simple and Highly Mobile Hexapod Robot, Http://Dx.Doi.Org/10.1177/02783640122067570. 20 (2001) 616–631. https://doi.org/10.1177/02783640122067570.

[3] D. Campbell, M. Buehler, Preliminary Bounding Experiments in a Dynamic Hexapod, Experimental Robotics VIII. (2003) 612–621. https://doi.org/10.1007/3-540-36268-1_56.

[4] E.Z. Moore, M. Buehler, Stable Stair Climbing in a Simple Hexapod Robot, n.d. www.cim.mcgill.ca/~arlweb.

[5] R. Altendorfer, N. Moore, H. Komsuo, ¯ Glu, M. Buehler, H.B. Brown, D. Mcmordie, U. Saranli, R. Full, D.E. Koditschek, RHex: A Biologically Inspired Hexapod Runner *, 2001. www.RHex.net.

[6] C. Georgiades, A. German, A. Hogue, H. Liu, C. Prahacs, A. Ripsman, R. Sim, L.A. Torres, P. Zhang, M. Buehler, G. Dudek, M. Jenkin, E. Milios, AQUA: An aquatic walking robot, 2004 IEEE/RSJ International Conference on Intelligent Robots and Systems (IROS). 4 (2004) 3525–3531. https://doi.org/10.1109/IROS.2004.1389962.

[7] C.J. Pratt, K.K. Leang, Dynamic underactuated flying-walking (DUCK) robot, Proc IEEE Int Conf Robot Autom. 2016-June (2016) 3267–3274. https://doi.org/10.1109/ICRA.2016.7487498.

[8] K. Peterson, R.S. Fearing, Experimental dynamics of wing assisted running for a bipedal ornithopter, (2011) 5080–5086. https://doi.org/10.1109/IROS.2011.6095041.

[9] K. Kawasaki, M. Zhao, K. Okada, M. Inaba, MUWA: Multi-field universal wheel for air-land vehicle with quad variable-pitch propellers, in: IEEE International Conference on Intelligent Robots and Systems, 2013: pp. 1880–1885. https://doi.org/10.1109/IROS.2013.6696605.

[10] C.J. Dudley, A.C. Woods, K.K. Leang, A micro spherical rolling and flying robot, in: IEEE International Conference on Intelligent Robots and Systems, Institute of Electrical and Electronics Engineers Inc., 2015: pp. 5863–5869. https://doi.org/10.1109/IROS.2015.7354210.

[11] D. Darrah, J. Eppler, W. Liu, W.A. Anemaat, Electric ducted fan design and testing for high performance uav integration, in: AIAA Scitech 2020 Forum, American Institute of Aeronautics and Astronautics Inc, AIAA, 2020: pp. 1–11. https://doi.org/10.2514/6.2020-0017.

[12] A. Ko, O.J. Ohanian, P. Gelhausen, Ducted Fan UAV modeling and simulation in preliminary design, Collection of Technical Papers - 2007 AIAA Modeling and Simulation Technologies Conference. 1 (2007) 161–180. https://doi.org/10.2514/6.2007-6375.

[13] Y. Moaad, J. Alaaeddine, K. Jawad, B.K. Tarik, B. Lekman, J. Hamza, H. Patrick, Design and optimization of a ducted fan VTOL MAV controlled by Electric Ducted Fans, (2019). https://doi.org/10.13009/EUCASS2019-108.

[14] S. Soyguder, H. Alli, Kinematic and dynamic analysis of a hexapod walking-running-bounding gaits robot and control actions, Computers and Electrical Engineering. 38 (2012) 444–458. https://doi.org/10.1016/j.compeleceng.2011.10.008.

[15] H. Dai, R. Tedrake, Optimizing robust limit cycles for legged locomotion on unknown terrain, in: Proceedings of the IEEE Conference on Decision and Control, Institute of Electrical and Electronics Engineers Inc., 2012: pp. 1207–1213. https://doi.org/10.1109/CDC.2012.6425971.

[16] Y. Ni, L. Li, J. Qiu, Y. Sun, G. Qin, Q. Han, A. Ji, A Novel Wheel-Legged Hexapod Robot, Biomimetics. 7 (2022). https://doi.org/10.3390/biomimetics7040146.

[17] J.Y. (Jo Y. Wong, Theory of ground vehicles, John Wiley, 2001.

[18] B.R. Munson, D.F. Young, T.H. Okiishi, Fundamentals of Fluid Mechanics, 6th ed., John Wiley and Sons, New York, 2009.

[19] Turnigy 2836 1000kv EMAX BLHeli 80A HY-1047 test data, (n.d.). https://database.tytorobotics.com/tests/5nk/turnigy-2836-1000kv-emax-blheli-80a-hy-1047 (accessed December 10, 2023).

[20] Artemis - U3 700KV - 12x4 Carbon test data, (n.d.). https://database.tytorobotics.com/tests/9rq9/artemis-u3-700kv-12x4-carbon (accessed December 10, 2023).

[21] 15-5 carbon prob u5 test data, (n.d.). https://database.tytorobotics.com/tests/7gnk/15-5-carbon-prob-u5 (accessed December 10, 2023).

[22] M. Thiele, M. Obster, M.H.- VFS, 8th Biennial, undefined 2019, Aerodynamic modeling of coaxial counter-rotating UAV propellers, Mediatum.Ub.Tum.DeM Thiele, M Obster, M HornungVFS, 8th Biennial Autonomous VTOL Technical Meeting, 2019•mediatum.Ub.Tum.De. (2019). https://mediatum.ub.tum.de/1473749 (accessed December 16, 2023).

[23] S. Deng, Z. Ren, Experimental study of a ducted contra-rotating lift fan for vertical/short takeoff and landing unmanned aerial vehicle application, Proc Inst Mech Eng G J Aerosp Eng. 232 (2018) 3108–3117. https://doi.org/10.1177/0954410017731441.

[24] Ducted Fan EDF Schubeler DS-68-AXI HDS 110mm + HET 800-68-685 motor - TURBINES RC, (n.d.). https://www.turbines-rc.com/en/schubeler/2758-ducted-fan-edf-schubeler-ds-68-axi-hds-110mm-het-800-68-685-motor.html (accessed December 10, 2023).

[25] Ducted Fan EDF Schubeler DS-51-AXI HDS V2015 90mm + HET 700-68-1200 motor (with mounting brackets) - TURBINES RC, (n.d.). https://www.turbines-rc.com/en/schubeler/1539-ducted-fan-edf-schubeler-ds-51-axi-hds-v2015-90mm-het-700-68-1200-motor-with-mounting-brackets.html (accessed December 10, 2023).

[26] EDF Ducted Fan Hacker Stream-Fan 100 / 1070kv - TURBINES RC, (n.d.). https://www.turbines-rc.com/en/hacker-stream-fan/2640-edf-ducted-fan-hacker-stream-fan-100-1070kv-4250320262381.html (accessed December 10, 2023).

[27] 2900mAh 18.5V 5S 35C Supersport Pro LiPo Battery, (n.d.). https://www.overlander.co.uk/lipo-batteries/18-5v-5s/2900mah-18-5v-5s-35c-supersport-pro-lipo-battery.html (accessed December 10, 2023).

[28] Gens ace G-Tech 2800mAh 22.2V 60C 6S1P Lipo Battery Pack with XT60 plug - Gens Ace, (n.d.). https://www.gensace.de/gens-ace-g-tech-2800mah-22-2v-60c-6s1p-lipo-battery-pack-with-xt60-plug.html (accessed December 10, 2023).

[29] Lipo 6s 5000 mAh 45C A2Pro Black Lithium XT60 - TURBINES RC, (n.d.). https://www.turbines-rc.com/en/all-lipos/935-lipo-6s-5000-mah-35c-a2pro-black-lithium-t-dean.html (accessed December 10, 2023).

[30] Schübeler Company, DS-51-AXI HDS_HET-700-68-1200kV_YGE90HV | Enhanced Reader, (n.d.). https://www.schubeler.com/?attachment_id=5516 (accessed December 28, 2023).

APPENDIX

APPENDIX A

$$0 = m_l\left(r\cos(\theta_m)\,\dot{\theta}_m{}^2 - \ddot{x}_b + rsin(\theta_m)\ddot{\theta}_m\right) - m_l\left(L_r\cos(\theta)\,\dot{\theta}^2 + \ddot{x}_b + L_r\sin(\theta)\,\ddot{\theta} - rsin(\theta+\theta_r)(\ddot{\theta}+\ddot{\theta}_r) - rcos(\theta+\theta_r)(\dot{\theta}+\dot{\theta}_r)^2\right) + \cos\left(\frac{\pi}{2}+\theta\right)(T_1+T_2) - M_b\ddot{x}_b + m_l\left(L_f\cos(\theta)\,\dot{\theta}^2 - \ddot{x}_b + L_f\sin(\theta)\,\ddot{\theta} + rsin\left(\theta+\theta_f\right)(\ddot{\theta}+\ddot{\theta}_f) + rcos\left(\theta+\theta_f\right)\left(\dot{\theta}+\dot{\theta}_f\right)^2\right)$$

$$0 = T_1\sin\left(\frac{\pi}{2}+\theta\right) + T_2\sin\left(\frac{\pi}{2}+\theta\right) - M_b g - F_D - 3gm_l - M_b\ddot{y}_b - m_l\left(\ddot{y}_b - rsin(\theta_m)\dot{\theta}_m{}^2 + rcos(\theta_m)\ddot{\theta}_m\right) - m_l\left(L_f\cos(\theta)\,\ddot{\theta} - L_f\sin(\theta)\,\dot{\theta}^2 + rcos\left(\theta+\theta_f\right)\left(\ddot{\theta}+\ddot{\theta}_f\right) - rsin\left(\theta+\theta_f\right)\left(\dot{\theta}+\dot{\theta}_f\right)^2 + \ddot{y}_b\right) - m_l\left(\ddot{y}_b + L_r\sin(\theta)\,\ddot{\theta} - rsin(\theta+\theta_r)\left(\dot{\theta}+\dot{\theta}_r\right)^2 + L_r\cos(\theta)\,\dot{\theta}^2 + L_r\sin(\theta)\,\dot{\theta}^2 + rcos(\theta+\theta_r)\left(\ddot{\theta}+\ddot{\theta}_r\right) - L_r\cos(\theta)\,\ddot{\theta}\right)$$

$$0 = T_f + T_m + T_r - I_b\ddot{\theta} - LT_1 + LT_2 - \frac{\left(L_r{}^2 m_l\dot{\theta}^2\right)}{2} - L_f{}^2 m_l\ddot{\theta} - L_r{}^2 m_l\ddot{\theta} + \frac{\left(L_r{}^2 m_l\ddot{\theta}\sin(2\theta)\right)}{2} - L_f g m_l\cos(\theta) - L_m g m_l\cos(\theta) + L_r g m_l\cos(\theta) - L_f m_l\ddot{y}_b\cos(\theta) - L_m m_l\ddot{y}_b\cos(\theta) + L_r m_l\ddot{y}_b\cos(\theta) + L_f m_l\ddot{x}_b\sin(\theta) - L_m m_l\ddot{x}_b\sin(\theta) - L_r m_l\ddot{x}_b\sin(\theta) + \frac{\left(L_r{}^2 m_l\dot{\theta}\cos(2\theta)\right)}{2} + L_m m_l r\dot{\theta}_m{}^2\sin(\theta+\theta_m) - L_m m_l r\ddot{\theta}_m\cos(\theta+\theta_m) + L_f m_l r\dot{\theta}^2\sin\left(\theta_f\right) - L_r m_l r\dot{\theta}^2\sin(\theta_r) + L_f m_l r\dot{\theta}_f{}^2\sin\left(\theta_f\right) - L_r m_l r\dot{\theta}_r{}^2\sin(\theta_r) - L_f m_l r\ddot{\theta}\cos\left(\theta_f\right) + L_r m_l r\ddot{\theta}\cos(\theta_r) - L_f m_l r\ddot{\theta}_f\cos\left(\theta_f\right) + L_r m_l r\ddot{\theta}_r\cos(\theta_r) - 2L_f m_l r\dot{\theta}\dot{\theta}_f\sin\left(\theta_f\right) + 2L_r m_l r\dot{\theta}\dot{\theta}_r\sin(\theta_r)$$

$$0 = \tau_1 + \tau_2 - I_{b,y}\ddot{\varphi}$$

$$0 = m_l r\ddot{x}_b \sin(\theta + \theta_f) - I_l\ddot{\theta} - I_l\ddot{\theta}_f - m_l r^2\ddot{\theta} - m_l r^2\ddot{\theta}_f$$
$$-gm_l r cos(\theta + \theta_f) - m_l r\ddot{y}_b cos(\theta + \theta_f) - \tau_f - L_f m_l r\dot{\theta}^2 \sin(\theta_f) -$$
$$L_f m_l r\ddot{\theta} \sin(\theta_f)$$

$$0 = m_l r\ddot{x}_b \sin(\theta + \theta_m) - I_l\ddot{\theta} - I_l\ddot{\theta}_m - gm_l r cos(\theta + \theta_m) -$$
$$m_l r^2\dot{\theta}_m \sin(\theta) - m_l r\ddot{y}_b cos(\theta + \theta_m) - \tau_m - m_l r^2\ddot{\theta}_m \cos(\theta)$$

$$0 = m_l r\ddot{x}_b \sin(\theta + \theta_r) - I_l\ddot{\theta} - I_l\ddot{\theta}_r - m_l r^2\ddot{\theta} - m_l r^2\ddot{\theta}_r$$
$$-gm_l r cos(\theta + \theta_r) - m_l r\ddot{y}_b cos(\theta + \theta_r) - \tau_r - \frac{(L_r m_l r\ddot{\theta} \sin(2\theta + \theta_r))}{2} -$$
$$\frac{(L_r m_l r\dot{\theta}^2 \cos(\theta_r))}{2} + L_r m_l r\dot{\theta}^2 \sin(\theta_r) - \frac{(L_r m_l r\dot{\theta}^2 \cos(2\theta + \theta_r))}{2} +$$
$$L_r m_l r\ddot{\theta} \cos(\theta_r) + \frac{(L_r m_l r\ddot{\theta} \sin(\theta_r))}{2}$$

APPENDIX B

Performance Chart of Selected Setup from manufacturer[30].

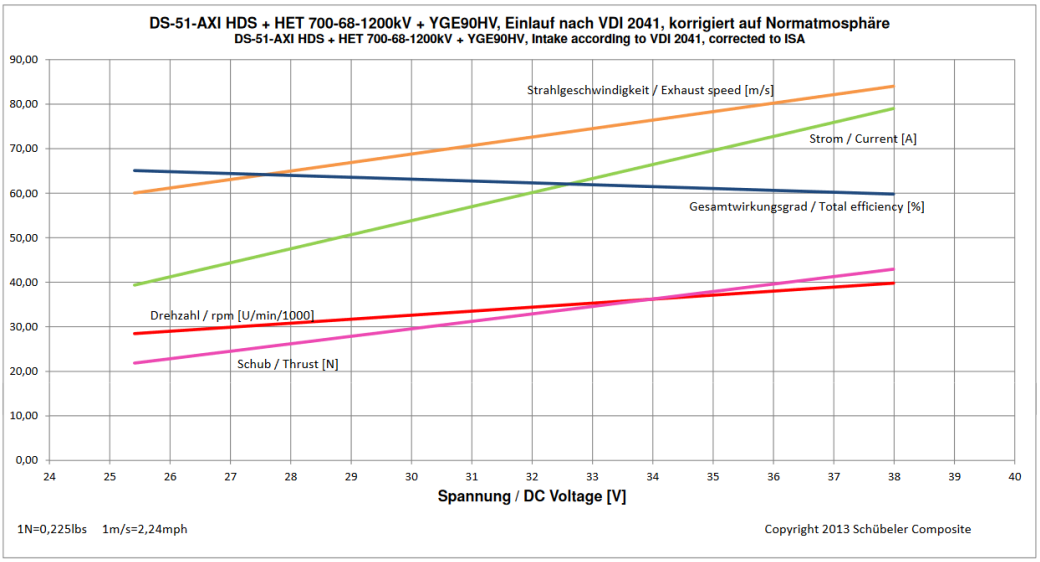

APPENDIX C

Inside of the controller block in hybrid model.